Summer 2009

The Use of Fourier Transform (FT) Surface-Enhanced Raman Scattering for Biochemical Analysis

Robert Butler Jeffers
Old Dominion University

THE USE OF FOURIER TRANSFORM (FT) SURFACE-ENHANCED RAMAN SCATTERING FOR BIOCHEMICAL ANALYSIS

by

Robert Butler Jeffers
B.S. May 1999, College of William and Mary

A Dissertation submitted to the Faculty of
Old Dominion University in Partial Fulfillment of the
Requirement for the Degree of

DOCTOR OF PHILOSOPHY

CHEMISTRY

OLD DOMINION UNIVERSITY
August 2009

Approved By:

John B. Cooper (Director)

Leslev H. Greene (Member)

Christopher J. Osgood (Member)

Patricia A. Pleban (Member)

ABSTRACT

THE USE OF FOURIER TRANSFORM (FT) SURFACE-ENHANCED RAMAN SCATTERING FOR BIOCHEMICAL ANALYSIS

Robert Butler Jeffers
Old Dominion University
Director: Dr. John B. Cooper

Surface-enhanced Raman scattering (SERS) is a powerful spectroscopic technique that has created exciting opportunities in the field of bioanalytical chemistry, where it combines ultrasensitive detection of biologically relevant molecules with vibrational spectroscopy. Due to the difficulties in preparing reproducible SERS active substrates, SERS has been mainly used as a qualitative tool. In order for SERS to be utilized as a viable tool for quantitative analysis, simple, facile SERS substrates which generate clean, highly reproducible signals must be developed. This dissertation deals with the evaluation of three different methods of SERS that led to the development of a novel substrate for the analysis of biological molecules.

In this dissertation, I demonstrated the generation of a SERS signal from pyridine adsorbed to the surface of a roughened silver electrode. The Raman signal was detected utilizing a remote fiber optic probe dispersive Raman instrument. The necessary parameters for generating the optimal SERS signal were established. The SERS spectrum of pyridine was successfully characterized.

The synthesis of silver colloid solutions for use as a SERS active substrate was demonstrated. Two different synthetic methods were utilized and the conditions for

optimal SERS signal strength were established. SERS signals from solutions of tryptophan were successfully generated and detected using an FT-Raman spectrometer.

In this dissertation, I report the successful chemical deposition of a thin silver film on the surface of a quartz/glass fiber filter for use as a SERS active substrate. The successful detection of the SERS signal of solutions of phenylalanine and tryptophan utilizing the silver-coated filters and a FT-Raman instrument was demonstrated. Significant progress was made to develop a quantifiable SERS method utilizing the silver-coated filters.

The silver-coated filter SERS method presented here is a novel and promising method for biochemical analysis. The demonstrated ability to detect amino acids and mixtures of amino acids can be further extended to the detection of similar biological molecules such as proteins, tumor markers, and nucleic acids. The use of a FT-Raman instrument combined with this new SERS method allows for a method with both high sensitivity and selectivity.

TABLE OF CONTENTS

Page

LIST OF TABLES

LIST OF FIGURES

CHAPTER I

INTRODUCTION

Laser spectroscopy is rapidly becoming an important tool in the clinical analysis of biological molecules. The use of lasers offers the possibility of a non-invasive approach that can be conducted in biological conditions. Raman Spectroscopy, in particular, has proven to be quite useful due to its high specificity and ability to identify structural information. Recent reviews of Raman Spectroscopy in the literature have demonstrated the power of Raman Spectroscopy in the study of proteins, amino acids, nucleic acid assemblies, tissue spectroscopy, and antigen-antibody interactions.[1,2] More recently, Surface-enhanced Raman Scattering (SERS) has become popular because of its increased sensitivity over normal Raman methods. There are many reviews in the literature that summarize the use of SERS to study biological molecules.[3-6]

One significant area of SERS research has been in the development of qualitative and quantitative techniques for the analysis of biological fluids. Current studies include the analysis of urine and blood.[7-13] These studies are necessary to improve the current analytical detection methods for important biomarkers contained in bodily fluids or tissues. Because of the increased sensitivity inherent in SERS, advances in this area could help in the early detection of disease as well as other abnormalities normally ascertained from the analysis of bodily fluids.

The text of this dissertation was modeled after *Applied Spectroscopy.*

The study of amino acids is especially important because it can be directly correlated to the study of proteins. Several papers exist in the literature that specifically use SERS in the study of amino acids.[14-20] These studies focused on the electrostatic interactions of the amino acids with the SERS substrate and the effect of steric hindrance of the molecules on the intensity of SERS. There is now a need to develop novel SERS techniques to analyze amino acids in solution. These techniques should demonstrate high sensitivity as well as the possibility of quantification. They should be reproducible and cost efficient for use in clinical situations.

The purpose of the research presented here is to demonstrate the development of a novel SERS technique for the analysis of amino acids in biological media. This technique presents an easy, specific, and sensitive method for the detection of amino acids. More importantly, the technique has demonstrated the possibility to be used in quantitative analysis. In the process of development, three methods of SERS detection were utilized along with two different types of Raman instrumentation. This dissertation will describe in detail the development of this novel technique along with all significant results and conclusions.

In Chapter II, an introduction to Raman Spectroscopy is given, including theoretical background, a description of the SERS effect, Raman instrumentation, and biological applications. Chapter III will provide a detailed description of all experimental methods. The results and subsequent discussion are given in Chapter IV, with a full conclusion in Chapter V.

CHAPTER II

RAMAN THEORY INTRODUCTION

Raman Theory

The Raman effect, first observed in 1928 by Raman and Krishnan, has proved itself to be a powerful technique for chemical analysis.[21] Essentially a light scattering phenomenon, its significance lies in its ability to uncover molecular vibrational information, especially low frequency vibrations. In recent history it has become a leading competitor with IR-absorption for qualitative chemical analysis. This is largely due to the advent of the laser, which provides monochromatic light that has increased the sensitivity of analysis. Other advances in detectors, photo multiplier tubes and charged coupling devices (CCD), optical filters, and spectrographs have also helped to make Raman spectroscopy more widely used. Fourier Transform (FT) Raman and dispersive Raman are the two most widely used methods of detection. In recent years surface-enhanced Raman scattering (SERS) has emerged as an important technique for enhancing the Raman signal. Now Raman spectroscopy is a common tool utilized in chemical, polymer, process controls, pharmaceutical, and biomedical industries.

To properly introduce the concept of Raman scattering, it is first necessary to examine the classical theory of light scattering from molecules. When electromagnetic radiation (monochromatic) is incident on a molecule, an oscillating dipole moment (μ) will be induced in the molecule.[22] Once induced, the molecule will re-emit or scatter light at the frequency of oscillation. Of course, the dipole moment will consist of many different frequency components. These components can be described by the following equation:

$$\mu(t) = \mu^{\circ}\cos(2\pi\nu_{sc}t) \qquad (1)$$

where ν_{sc} is the frequency of scattered light and μ° is the maximum induced dipole for a given frequency component.[22] If the magnitude of the electromagnetic field of the incident radiation ($\mathbf{E}_{in}$) is not too large, then the induced dipole moment can be better represented by:

$$\mu(t) = \alpha\mathbf{E}_{in}(t) \qquad (2)$$

where α is the polarizability (SI units: $C^2m^2J^{-1}$).[2] The polarizability can be defined as the ability of a molecular orbital to be deformed in the presence of an external electric field. As the volume of the molecular orbital increases so does the polarizability. The oscillating dipole will scatter light in all directions at the frequency of oscillation. If the frequency scattered is equal to the incident frequency this is called Rayleigh or elastic scattering. If they are not equal it is called Raman or inelastic scatter.

The electromagnetic field $\mathbf{E}_{sc}$ that is felt at a distance r from the molecule due to the induced dipole can be described by the Maxwell's equations:

$$|\mathbf{E}_{sc}(t)| = k\left(\frac{|\mu(t)|}{r\lambda_{sc}^2}\right)\sin\Phi \qquad (3)$$

where $k = \pi/\varepsilon_0$, Φ is the angle of scatter, λ_{sc} is the scattered wavelength.[22] The Rayleigh scattering intensity I_{sc} (W sr^{-1}) of the molecule can then be written as follows using the equation $I=Er^2$:

$$|I_{sc}(t)| = k'\left(\frac{|\mu(t)^2|}{\lambda_{sc}^4}\right)\sin^2\Phi \qquad (3a)$$

where $k'=k^2$. [22]

The above equation can be applied for isotropic molecules where the scattering intensity is independent of the molecules orientation. However, for anisotropic molecules this is not the case. When considering anisotropic molecules, the magnitude of the induced dipole will change as the orientation of the molecule changes. To account for the change in orientation, the polarizability of an anisotropic molecule can be represented as a symmetric matrix. This means that equation (2) can be re-written as follows:[22]

$$\mu = \underline{\alpha} \cdot \mathbf{E}_{in}$$

$$\begin{pmatrix} \mu_x \\ \mu_y \\ \mu_z \end{pmatrix} = \begin{bmatrix} \alpha_{xx} & \alpha_{xy} & \alpha_{xz} \\ \alpha_{yx} & \alpha_{yy} & \alpha_{yz} \\ \alpha_{zx} & \alpha_{zy} & \alpha_{zz} \end{bmatrix} \cdot \begin{pmatrix} E_x \\ E_y \\ E_z \end{pmatrix}$$

Therefore, when a stationary anisotropic molecule is exposed to linearly polarized light the induced dipole moment (μ) will not be aligned with $\mathbf{E}_{in}$. Thus the direction of polarization and the magnitude of $\mathbf{E}_{sc}$ will be different when compared with an isotropic molecule.

The polarizability of an anisotropic molecule can be represented visually as an ellipsoid. Because the polarizability matrix is symmetric it will possess three orthogonal eigenvectors and three corresponding eigenvalues, which are real numbers. The equation

of the ellipsoid will take the following form:[22]

$$\frac{x^2}{\alpha_{xx}^2}+\frac{y^2}{\alpha_{yy}^2}+\frac{z^2}{\alpha_{zz}^2}+\frac{2xy}{\alpha_{xy}^2}+\frac{2yz}{\alpha_{yz}^2}+\frac{2zx}{\alpha_{zx}^2}=1 \qquad (4)$$

The principal axes of the ellipsoid are aligned along the eigenvectors. It can then be inferred that this equation will depend on the position of the eigenvectors in reference to the coordinate axes. Therefore, if the molecule rotates relative to the frame of reference, the values of α will change along with the induced dipole. This means that the intensity of Rayleigh scattering will be dependent upon the position of the molecule. Also, the intensity will fluctuate if the molecule is allowed to rotate freely when exposed to the incident light. This will be true when sampling gases or liquids because these molecules are free to rotate. Equation (3) can still be used to predict the $\mathbf{E}_{sc}$ for anisotropic molecules but a time averaged value of μ must be used:

$$\overline{\mathbf{E}}_{sc}=k\left(\frac{\overline{\mu}}{r\lambda_{sc}^2}\right)\sin^2\Phi \qquad (5)$$

where Φ now refers to the angle of scatter from a point r from $\overline{\mu}$.[22] The intensity of scatter can then be described as follows:[22]

$$\mathbf{I}_{sc}(\Phi)=k'\left(\frac{\overline{\mu}^2}{\lambda_{sc}^4}\right)\sin^2\Phi \qquad (6)$$

This equation can be used to solve for the scattering intensity for any molecule whose position changes in reference to the incident light.

Ideally it would be better to describe the polarizability of an anisotropic molecule without being dependent on the position of the molecule. This is possible by using the eigenvalues of the polarizability matrix. The eigenvalues will always be constant regardless of the position of the molecule. It is now necessary to introduce two properties which are derived from the eigenvalues: the mean polarizability $\langle\alpha\rangle$ and the anisotropy γ^2

$$\langle\alpha\rangle = \frac{1}{3}(\alpha_1 + \alpha_2 + \alpha_3) \tag{7}$$

$$\gamma^2 = \frac{1}{2}\left[(\alpha_1 - \alpha_2)^2 + (\alpha_2 - \alpha_3)^2 + (\alpha_3 - \alpha_1)^2\right] \tag{8}$$

In this equation α_1, α_2, and α_3 are the three eigenvalues of α when the coordinate axes are aligned with the eigenvectors of the ellipsoid. This removes the off-diagonal elements of the polarizability.

From these new properties the average values of α_{ij} can be represented by the following equations:[22]

Off-diagonal elements, $\quad i \neq j \quad \bar{\alpha}_{ij}^2 = \frac{1}{15}\gamma^2$ (9)

Diagonal elements, $\quad i = j \quad \bar{\alpha}_{ii}^2 = \frac{1}{45}\left(45\langle\alpha\rangle^2 + 4\gamma^2\right)$ (10)

These can then be used to calculate the intensity of Rayleigh scatter. At $\theta = 90°$ only the scatter in the yz plane needs to be considered. The average induced dipole moment can then be calculated as follows using equation (4):[22]

$$\overline{\mu}_y = \overline{\alpha}_{xy}\overline{E}_x + \overline{\alpha}_{zy}\overline{E}_z$$

$$\overline{\mu}_z = \overline{\alpha}_{xz}\overline{E}_x + \overline{\alpha}_{zz}\overline{E}_z$$

The intensity of Rayleigh scatter at $\theta = 90°$ can then be expressed in terms of $\langle\alpha\rangle$ and γ as follows:[22]

$$I_{sc}^{p} = \frac{k'}{45}\left(\frac{45\langle\alpha\rangle^2 + 7\gamma^2}{\lambda_{in}^4}\right)E_{in}^{p} \qquad (11)$$

$$I_{sc}^{n} = \frac{k'}{45}\left(\frac{45\langle\alpha\rangle^2 + 13\gamma^2}{\lambda_{in}^4}\right)E_{in}^{n} \qquad (12)$$

When considering Raman scatter, it is helpful to rewrite equation (2) as follows:

$$\mu(t) = \alpha(t)\mathbf{E}_{in}(t) \qquad (13)$$

where the polarizability, α(t), is now time-dependent.[22] Both α and $\boldsymbol{E}_{in}$ can be described using harmonic functions and will therefore consist of a number of different frequency components. These different frequency components comprise the Rayleigh and Raman scatter.

It has already been shown that α will change when a molecule rotates. But it is also true that α changes when the molecule changes shape via vibrational motions. For the purpose of the discussion, only the vibrational effects will be considered. The time-dependent polarizability can be expressed in terms of the J vibrational modes of the molecule. This is accomplished by using a Taylor expansion about the equilibrium position of the atoms Q_{eq}:

$$\alpha_{ij}(t) = \alpha_{ij} + \sum_{k=1}^{J}\left(\frac{\partial \alpha_{ij}}{\partial Q_k}\right)_0 Q_k(t) + \frac{1}{2}\sum_{k=1}^{J}\left(\frac{\partial^2 \alpha_{ij}}{\partial Q_k^2}\right)_0 (Q_k(t))^2 + \cdots \quad (14)$$

where $Q_k\,(t)$ is the displacement from the equilibrium position for the k-th vibrational mode.[22] This displacement can be expressed as a harmonic oscillator by:

$$Q_k(t) = Q_k^0 \cos(2\pi \nu_k t) \quad (15)$$

where ν_k is the vibrational frequency of the k-th mode.[22]

Now an equation for the induced dipole moment can be derived by combining equations (13)-(15). This is done under the assumption that Q^0 is small, which allows all but the first two terms in equation (14) to be eliminated. The equation for the induced dipole moment looks like this:[22]

$$\mu(t) = \underline{\alpha}\mathbf{E}_0 \cos(2\pi \nu_{in} t) + \mathbf{E}_0 \cos(2\pi \nu_{in} t)\sum_{k=1}^{J} \underline{\alpha'}_k \cos(2\pi \nu_k)$$

where $$\underline{\alpha'_k} = \left(\frac{\partial \underline{\alpha}}{\partial Q_k}\right)_0, k = x, y, z$$

Simple trigonometry reveals that the induced dipole of a molecule may contain at the most 2J additional frequency components. The frequency components of the induced dipole can be expressed as follows:

$$\mu(t) = \sum_{k=-J}^{J} \mu_k^0 \cos(2\pi \nu_{sc} t) \qquad (16)$$

where $\mu_k{}^0$ is the maximum dipole moment for a given frequency.[22] When k = 0 this corresponds to Rayleigh scatter. When k ≠ 0 this corresponds to Raman scatter. Raman scatter consists of two types. When the scattered frequency is less than the incident frequency this is called Stokes Raman. When the scattered frequency is greater than the incident frequency this is called anti-Stokes Raman Scatter. When k < 0 this corresponds to Stokes Raman. When k > 0 this corresponds to anti-Stokes Raman.

Just as in Rayleigh scatter, the average polarizability can be expressed in terms of $\langle \alpha \rangle$ and γ. Using these two terms the average induced dipole moment and the intensity of Raman scatter can be expressed. Here is the expression for the average induced dipole moment for Raman scatter:[22]

$$\overline{\mu} = \frac{1}{2}\mu^0 = Q_k^0 \overline{\alpha}_k' \mathbf{E}_{in} \qquad (17)$$

The intensity of Raman scatter for the k-th vibrational mode is expressed as follows:[22]

$$I_r^p = \frac{k'}{45}\left(\frac{1}{2}Q_k^0\right)^2 \left(\frac{45\langle \alpha \rangle^2 + 7(\gamma')^2}{\lambda_r^4}\right) E_i^p \qquad (18)$$

$$I_r^n = \frac{k'}{45}\left(\frac{1}{2}Q_k^0\right)^2\left(\frac{45\langle\alpha\rangle^2 + 13(\gamma')^2}{\lambda_r^4}\right)E_i^n \qquad (19)$$

These equations for polarized and randomly polarized light apply to both Stokes and anti-Stokes Raman scatter.[22]

So far only the classical theory of Raman scatter has been discussed. There is, however, a problem with this theory. From equations (18) and (19) classical theory predicts that anti-Stokes scatter will be much stronger than Stokes scatter, but experimental evidence shows that this is not true. Therefore, quantum-mechanical theory was used to correct for this discrepancy.[22]

Quantum mechanics can be applied to Raman scatter by using perturbation theory. In this way, the incident light is treated as a perturbation of the eigenstates of the molecule. The perturbation of the molecule creates a time-dependent "virtual" state. The molecule can then relax to the initial state or a lower/higher energy state. Rayleigh scatter results in the molecule returning to the initial state. This means that the molecule has no net change in energy. In Raman scatter, the molecule will either gain or lose energy depending on whether the scatter is Stokes or anti-stokes. The creation of a virtual state and the different types of scatter is visualized in Figure 1.[22]

By using perturbation theory and the time-dependent Schrodinger equation, an expression for the polarizability of a molecule can be derived. If the molecule is in the stationary state ($|m\rangle$), the three eigenvalues of the polarizability matrix are as follows:

$$\alpha_i^m = \frac{2}{h}\sum_r \frac{\nu_{rm}(M_{rm})_i^2}{\nu_{rm}^2 - \nu_{in}^2} \qquad (20)$$

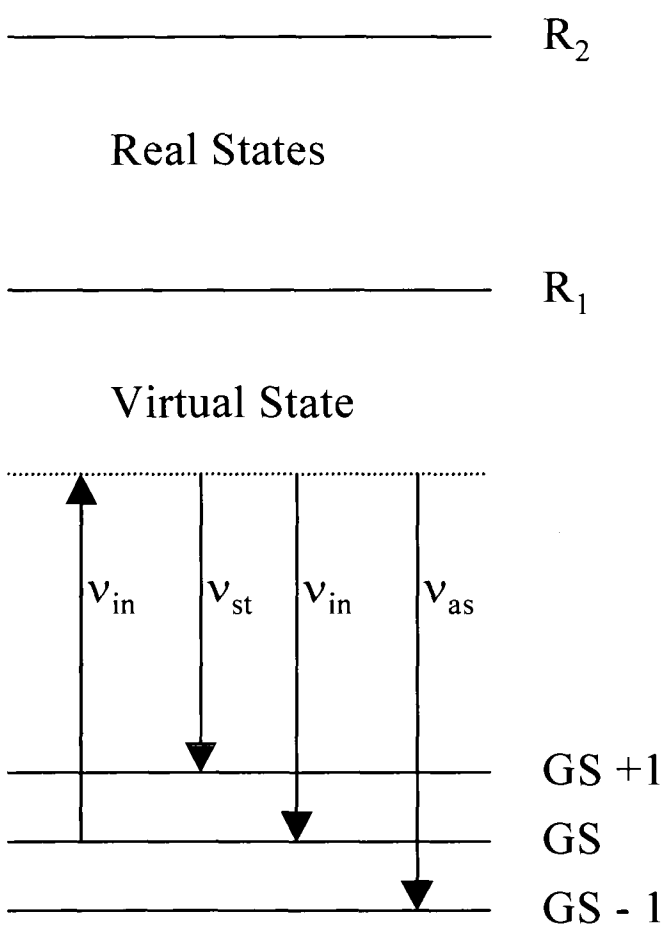

FIG. 1. Quantum mechanical image of light scattering.

where $|r\rangle$ corresponds to the unperturbed states of the molecule and $(M_{rm})_i$ represents the value of the transition dipole moment for the transition $|m\rangle \rightarrow |r\rangle$.[22]

It has already been shown that α^m is needed to determine the magnitude of μ for Rayleigh scatter at $\nu_{sc} = \nu_{in}$. It is then necessary to use quantum mechanics to describe the magnitude of μ for the additional frequency components due to Raman scatter. Using perturbation theory the maximum induced dipole for anti-Stokes scatter is as follows:[22]

$$\nu > \nu_{in} < E_m > E_n : \qquad \mu^0 = -\frac{1}{2h}\sum_r \left(\frac{M_{mr} M_{rn} E}{\nu_{nr} - \nu_{in}} + \frac{M_{rn} M_{mr} E}{\nu_{mr} + \nu_{in}} \right) \qquad (21)$$

and for Stokes scatter:[22]

$$\nu < \nu_{in}, E_m < E_n : \qquad \mu^0 = -\frac{1}{2h}\sum_r \left(\frac{M_{mr} M_{rn} E}{\nu_{nr} + \nu_{in}} + \frac{M_{rn} M_{mr} E}{\nu_{mr} - \nu_{in}} \right) \qquad (22)$$

These equations, while good theoretically, are not practical for determining Raman scattering intensity. The reason for this is that the equations contain terms that are unknown and the solutions require lengthy calculations.

A solution to this problem was proposed by George Placzek. He did this by developing a semi-classical polarizability theory. The first step in this theory is to derive an expression, which is analogous to equation (14). This equation looks like this:

$$\alpha_{mn}(t) = \langle n|\alpha|m\rangle + \sum_k (\alpha'_{mn})_k \langle n|Q_k|m\rangle \qquad (23)$$

which includes only the first two terms in the Taylor expansion and the summation includes all the k vibrational modes in the transition from m $\rightarrow$ n.[22] In the above equation the first term corresponds to Rayleigh scatter and will be zero unless m = n. The second term corresponds to Raman scatter and will vanish unless $n^k = m^k \pm 1$. This second term can be expressed as:

$n^k = m^k + 1$ (Stokes) $\quad \langle n|Q_k|m\rangle = \frac{1}{2}Q_k^0 = \sqrt{\frac{(m^k+1)h}{8\pi^2\mu_r\nu_k}}$

$n^k = m^k - 1$ (anti-Stokes) $\quad \langle |Q_k|m\rangle = \frac{1}{2}Q_k^0 = \sqrt{\frac{m_h^k}{8\pi^2\mu_r\nu_k}}$

where μ_k is the reduced mass and ν_k is the fundamental frequency.[22]

Previously it was shown that classical theory predicted that anti-Stokes scatter would be stronger than Stokes scatter. Of course this is not true experimentally; that is why quantum mechanical theories were introduced. How does quantum mechanics account for this problem? Well, it has been stated that Raman scatter results from a transition from two stationary states of a molecule. It is also known that vibrational energy is quantized and that the difference in energy between vibrational states is carried off by the scattered light. The probability of this scatter being Stokes or anti-stokes is equal according to classical theory. This is not true in quantum theory. Quantum mechanic predicts that anti-stokes Raman scatter will not occur when the molecule is in the lowest vibrational energy state. The probability that a molecule is in the lowest

vibrational states can be determined by the Boltzmann distribution for a harmonic oscillator. This is given by:

$$P(m^k = 0) = 1 - \exp\left[-\frac{h\nu_k}{kT}\right]$$

where k is Boltzmann's constant.[22] This equation predicts that at normal room temperature most of the molecules will be in the lowest vibrational state. This means that most of the Raman scatter detected will be Stokes. This is why Stokes scatter is stronger than anti-Stokes scatter.

Now it is possible to derive an expression for the magnitude of intensity from Raman scatter using Placzek's semi-classical theory. The following equation is for the Stokes Raman scatter of a molecule in the lowest vibrational state with linear polarized light and at a collection angle of 90°:[22]

$$I_{r,st}^{p} = \frac{k'}{45}\left(1 - \exp\left[-\frac{h\nu_k}{kT}\right]\right)\left(\frac{h}{8\pi^2\mu_r\nu_k}\right)\left(\frac{45\langle\alpha_k'\rangle^2 + 7(\gamma_k')^2}{\lambda_k^4}\right)E_{in}^{p} \qquad (24)$$

To close out this discussion on Raman theory, the concept of Raman scattering efficiency will be explained. A measure of the efficiency is needed to be able to compare Raman scatter with other phenomena such as Rayleigh scatter, fluorescence, and absorbance. The most common way to compare such processes is by using a cross-section (σ) or a differential cross-section ($d\sigma/d\omega$). The scattering cross-section is defined by taking the rate of photons being scattered (P_{sc}, units: W) by a molecule and dividing it

by the irradiance of incident light (E_{in}, units: Wm^{-2}). This gives you a scattering cross-section in m^2. The equation for this looks like this:[22]

$$\sigma_{sc} = \frac{P_{sc}}{E_{in}} \tag{25}$$

The rate of photons scattered can be calculated directly from the scatter intensity as follows:[22]

$$P_{sc} = 2\pi \int_0^{\pi} I_{sc}(\theta)\cos\theta d\theta \tag{26}$$

By substituting an appropriate expression for Isc in equation (26) and comparing with equation (25), an equation for the Raman scattering cross-section can be derived:[22]

$$\sigma_{sc} = k'\left(\frac{8\pi}{3}\right)\frac{\alpha^2}{\lambda_{in}^4} \tag{27}$$

Raman Instrumentation

Now that the theoretical basis for Raman scatter has been discussed, it is apparent that Raman scatter can be useful for both quantitative and qualitative chemical analysis. For this reason, Raman spectroscopy has become an important tool in many research labs around the world. In fact, as new instrument designs and novel techniques are developed, Raman spectroscopy is not confined only to analytical or organic chemistry but is now useful to many different scientific disciplines.

There are many different variations of Raman spectroscopic instruments. To discuss them all would not be beneficial. Only two types of Raman instruments were

used in this report, dispersive and Fourier transform. This discussion will be limited to these two instruments.

A typical dispersive Raman instrument is shown in Figure 2. The two definitive components of a dispersive instrument are the spectrograph and the array detector. Other components critical to the instrument are as follows: a laser, a fiber optic probe, optical filters, and optical lenses. The key advantage of a dispersive instrument is its affordability. Other advantages of the instrument are its ease of use, its rapid data acquisition, its stability, its calibration accuracy, its flexibility, and its ability to simultaneously image different wavelengths. Its biggest disadvantage is that it is highly susceptible to large fluorescent backgrounds. The reason for this is that most dispersive instruments use lasers in the visible wavelength and therefore strong fluorescent signals from the samples may over power the weak Raman signal.

The laser is, perhaps, the most critical component of any Raman instrument. The ability to excite a sample at a single narrow wavelength has literally changed Raman spectroscopy from being just an interesting theoretical phenomenon to an important analytical technique. When choosing a laser for a dispersive Raman instrument, the following characteristics are preferred: low cost, no excessive cooling requirements, no high power electrical requirements, and narrow, well defined incident wavelengths.[23] Lasers that meet these requirements fall into two categories: gas based and solid state. Gas-based lasers include helium-neon, helium-cadmium, and argon ion. These lasers typically have extremely narrow and well defined wavelengths. Two common solid state lasers are stabilized diode and Nd:YAG lasers. An advantage of using solid state lasers is that they tend to be electrically more efficient than gas lasers.[23] The most popular laser

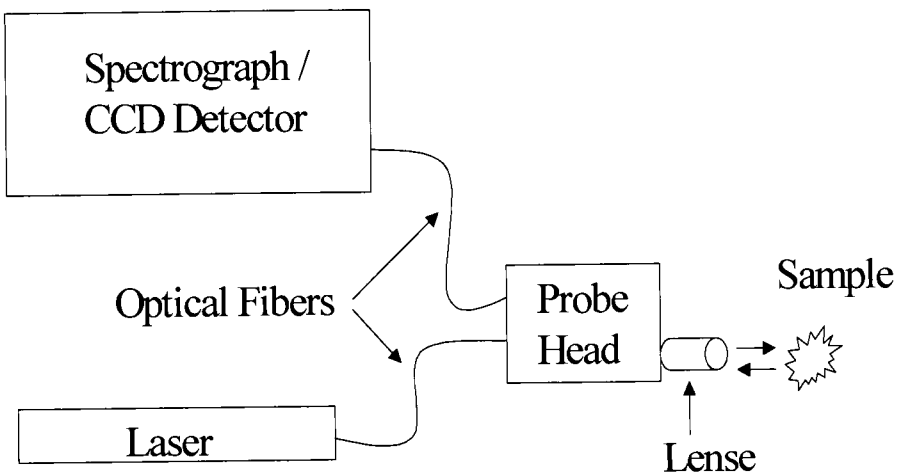

FIG. 2. Schematic of a typical dispersive Raman instrument with fiber optic probe and 180°collection geometry.

used in dispersive instruments is the helium-neon laser. These lasers are cheap, have a long lifetime, and provide a good Raman spectral region.

The use of fiber optic probes in dispersive Raman instruments has greatly increased the ease of sampling. These probes have allowed for the laser to be delivered to the sample over quite some distance and then collect the Raman signal and deliver it back to the spectrograph. This has allowed for a much greater mobility in sampling, creating a remote sensing ability. Optical fibers composed of a high refractive index core and a low refractive index cladding transmit light via total internal reflection at the interface between the core and cladding. Optical fibers are very efficient, losing little laser intensity over long path lengths. The core of an optical fiber is made from silica, which is a very weak Raman scatterer. The silica-induced Raman signal can become a problem when the optical fibers cover long distances.[24] This problem can easily be resolved by the use of optical filters to remove the silica signal.[24]

Another critical component of any dispersive Raman instrument is the optical filter. Optical filters are needed to eliminate any interfering signals from the analyte signal. The most common sources of interference are silica, sample fluorescence, and laser line reflection. The intensity of laser line reflection can be from 10^6 to 10^{10} times stronger than the Raman signal.[23] If this interference was not removed, the Raman signal would be lost. There are many different types of filters to choose from. The most common are holographic notch filters, chevron filters, interference filters, and zero dispersion spectrographs. Each filter has its advantages and disadvantages, but the most popular is the holographic notch filter. These filters provide good performance at a low cost and tend to be easy to use. They are produced for lasers ranging from 324 to 1500

nm wavelengths and have two different rejection bandwidths (±175 and ±350 cm^{-1}).[23] The key to any good filter is to maximize the attenuation of the laser wavelengths and to minimize the attenuation of the Raman wavelengths.

Optical lenses are important to any Raman instrument. Lenses serve two primary functions: first they are necessary to focus the laser on the sample to maximize the Raman scatter; second, they are used to collect the scattered light and focus it into the collection fiber or entrance slit of the spectrograph. A detailed discussion of lenses and collection optics is beyond the scope of this discussion.

Prior to spectrographs, Raman instruments could only monitor one Raman band of interest at a time. This meant that the majority of Raman scatter from the sample was lost along with the chemical information it contained. With the introduction of the spectrograph, multiple Raman bands could be monitored simultaneously. The spectrograph accomplished this by separating the collected Raman signal into individual wavelengths and image them onto a multi-element array detector.[23] The collected light from the Raman scatter is directed through an entrance slit and collimated onto a diffraction grating. The diffracted light, in its individual wavelengths, is then focused onto the exit plane. The most important characteristic of a spectrograph is its spectral resolution. This is a measure of the ability of the spectrograph to distinguish between two intense spectral lines. The spectral resolution is determined by the width of the entrance slit and the quality of the diffraction grating used. Spectrographs can be either one dimensional or two dimensional. The most common one-dimensional spectrograph is the Czerny-Turner spectrograph (Figure 3). These spectrographs separate light along only one axis of the exit plane.[23] Two-dimensional spectrographs can be used to increase

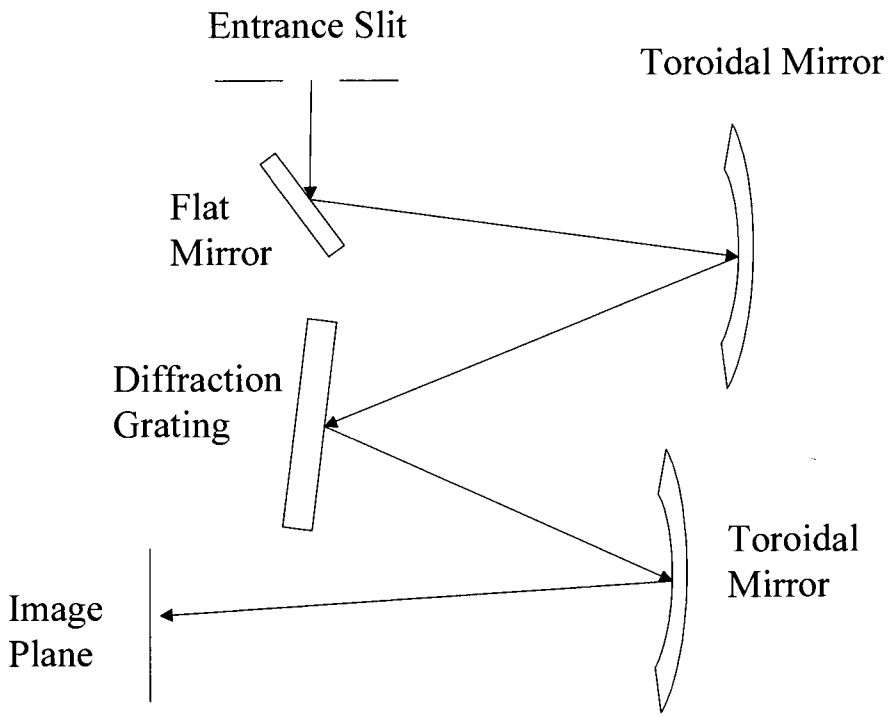

FIG. 3. Czerney-Turner spectrograph.

the spectral range by stacking different spectral segments on top of each other in the exit plane. This can be done without losing the spectral resolution.

The last component to be discussed is the array detector. The most common detector used in dispersive Raman instruments is the silicon charge-coupled device (CCD) detector. A CCD detector is composed of thousands of individual detector elements, pixels, and aligned into an array. Each pixel is actually a photosensitive capacitor.[23] When light is absorbed by the pixel a charge is produced by the photoelectric effect and stored in the capacitor. The charge produced is proportional to the number of photons that came in contact with the pixel. This charge is measured by moving it to a charge-sensing amplifier where it is digitized and then stored into a computer.[23] Like any detector, a CCD is affected by various sources of noise. The most dominant is shot noise. Shot noise is caused by the variable nature of light.[23] Other sources of noise include dark noise, spike noise, readout noise, and fixed pattern noise. Dark noise and fixed pattern noise are the next most prevalent sources of noise. Fixed pattern noise is caused by the minor differences in the sensitivity of pixels in the CCD. Dark noise comes from the detector itself and is the signal produced in the absence of light. Dark noise is highly temperature dependent and can be reduced dramatically at lower temperatures. When compared with other detectors such as a PMT or IPDA, the noise associated with the CCD is significantly low. The CCD is an ideal detector for a dispersive Raman instrument because it can create high signal-to-noise ratios in small amounts of time.[23]

Fourier Transform (FT) Raman instrumentation, although not commonly used, represents a promising alternative to dispersive Raman instrumentation. The primary disadvantage of FT Raman is its low sensitivity caused by the necessity of using high

noise solid-state detectors. However, this lack of sensitivity can be overcome by utilizing surface-enhanced Raman scattering techniques as demonstrated in the recent literature.[25-30] There are several advantages to using a FT Raman instrument. The FT instruments are commercially available with sample interfaces which provide turn-key operation. The use of a NIR excitation source (1064 nm) drastically reduces the background fluorescence along with the amount of laser-induced thermal damage. This makes the FT Raman ideal for use in biological systems. The use of an interferometer helps to reduce detector noise and allows for high spectral resolution. The main difference, other than the excitation source in instrumentation between an FT instrument and a dispersive instrument, is that the FT instrument uses an interferometer and single element detector instead of a spectrograph and CCD detector. The laser, interferometer, and detector will be discussed in the following paragraphs.

As already stated, the common laser used in FT Raman instruments is the Nd:YAG 1064 nm laser. The advantages of the 1064 nm laser have been stated above. A He-Ne 633 nm laser is also used along with the ND:YAG laser. He-Ne lasers are used as a frequency reference during data acquisition. They are also used to help align the laser onto the sample. The result of using a frequency reference is that the FT Raman instrument's frequency measurements are extremely precise.

The Michelson interferometer is used in FT Raman instruments in lieu of a spectrograph. A schematic of the interferometer is shown in Figure 4. The following is a brief description of how the interferometer works. Light is passed through a J-stop aperture and is directed to the beam splitter. When the laser hits the beam splitter it is partially reflected back to the source, partially reflected to the moving mirror, and

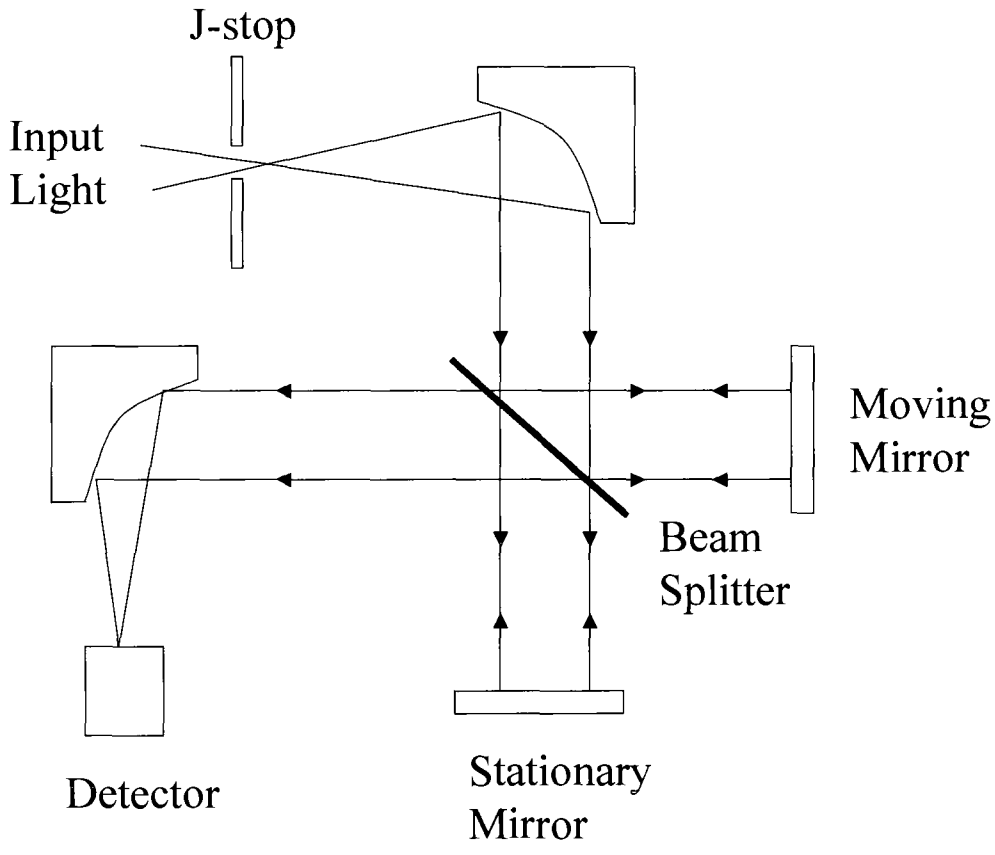

FIG. 4. Michelson interferometer.

partially transmitted to the stationary mirror. The moveable mirror moves at a constant velocity so that it introduces an optical path difference between the two beams that are initially in phase. The light from the moving mirror and stationary mirror is then directed back through the beam splitter where it is recombined and directed to the detector. When the two beams are combined an interference pattern is created. A plot of the interference pattern versus the optical path length difference is called an interferogram. The interferogram for one wavelength of light is just a cosine function plus a constant offset. An optical spectrum can be generated from an interferogram by using a cosine Fourier Transform. When using a laser with a wavelength longer than 1000nm, as is used in FT Raman, it is necessary to use a single-element detector. The two most common of these are the high purity p-type germanium detector and the InGaAs detector. These detectors tend to be very noisy but are known to have high quantum efficiencies. InGaAs detectors have good sensitivity at low temperature up to 3000 cm^{-1}.[23] At room temperature they can extend to 3400 cm^{-1} but will not be as sensitive.[23] Ge detectors can extend to 3400 cm^{-1} at low temperatures but are susceptible to cosmic rays that can cause intensity spikes.[23]

Surface-Enhanced Raman Scattering Theory

The Raman effect, although a powerful tool for chemical analysis, is limited by its extremely small cross-section as compared with fluorescence spectroscopy (12-14 orders of magnitude lower).[31] It was not until the advent of Surface-Enhanced Raman Scattering (SERS) that this limitation was overcome. The SERS phenomenon was first reported by a research group in 1974 when they observed an abnormally large Raman signal from pyridine that was adsorbed onto the surface of a roughened silver electrode.[32]

The increase in Raman signal has been attributed to the attachment of molecules to the surface of "atomically rough" metal surfaces. This effect has led to the enhancement of Raman signals by as much as 14 orders of magnitude and has enabled Raman spectroscopy to combine structural information with high sensitivity.[5,33-35]

Advances in the SERS technique has led to many exciting new applications for chemical and biological analysis. The high sensitivity and selectivity it provides along with the ability to gain information on molecular structure, surface processes, and interface reactions, has heightened its popularity. SERS signals have been reported using a variety of substrates including: metal electrodes, metal colloids, metal-coated nanospheres/nanoparticles, metal-coated silica substrates, metal coated filters, and silver membranes.[36-41] Gold and silver are the most common SERS active metals but SERS enhancements have also been reported using several transition metals including platinum, cobalt, iron, nickel, and palladium.[31] The SERS technique has become an invaluable tool for studying biological systems.[18-20,42-72] The use of near IR or visible lasers allows for non-invasive application of SERS under ambient conditions in an aqueous environment. Additionally, SERS measurements can be made with exceptionally low spatial and temporal resolutions. Spatial resolutions of about $1 \mu m^3$ have been reported along with temporal resolutions on the femtosecond scale.[5,73-75] This allows for the monitoring of biochemical processes in real time. SERS spectra have been acquired from amino acids, proteins, neurotransmitters, and nucleic acids.[5,6,18-20,42-72] SERS has been used to probe lipid chemistry, study membrane transport processes, immunoassay enzymes, and probe for DNA.[5,6,43,45,53,54,60,61,63,67] One study has even demonstrated the use of SERS to detect single adenine molecules.[5]

After the initial discovery of the SERS effect in the 1970's, it was determined that the enhancement was caused by the attachment of a molecule to a metallic surface. In normal Stokes Raman scattering, the power of the Raman signal $P^{RS}(\nu_S)$ is represented in the following equation:

$$P^{RS}(\nu_S) = N\sigma^{R}_{free} I(\nu_L) \tag{28}$$

where N is the number of molecules in the probed volume, σ^{R}_{free} is the Raman cross-section, and $I(\nu_L)$ is the excitation laser intensity.[3] To give an analogous equation for the SERS Stokes power, it is necessary to modify the equation to describe the effects of the metallic surface. Current theories describing the SERS effect suggest that there are actually two independent mechanisms contributing to the enhancement. These two mechanisms are the electromagnetic field enhancement and the chemical enhancement. Both of these effects need to be considered when describing the SERS signal. The following equation is a modified version of equation (28) that takes into account the two mechanisms:

$$P^{SERS}(\nu_S) = N'\sigma^{R}_{ads} \left|A(\nu_L)\right|^2 \left|A(\nu_S)\right|^2 I(\nu_L) \tag{29}$$

In this equation N' is the number of molecules in the SERS process, σ^{R}_{ads} is the Raman cross-section of the molecule absorbed to the metal surface, and $A(\nu_L)$ and $A(\nu_S)$ are the enhancement factors for the laser and the Raman-scattered field.[3]

To describe the electromagnetic field enhancement a simple example of a SERS signal generated from a single molecule adsorbed to the surface of a metal sphere will be used. The size of the sphere is small in relation to the wavelength of light. A molecule adsorbed to the sphere within a distance, d, is exposed to an electric field, E_m.

E_m comprises both the incoming field, E_0, and the dipole induced in the metal sphere, E_{sp}. The field enhancement factor, $A(\nu)$, can be represented by the following equation:

$$A(\nu) = \frac{E_M(\nu)}{E_0(\nu)} \approx \frac{\varepsilon - \varepsilon_0}{\varepsilon + 2\varepsilon_0}\left(\frac{r}{r+d}\right)^3 \tag{30}$$

where ε is the dielectric constant of the sphere, ε_0 is the dielectric constant of the surrounding medium, and r is the radius of the sphere.[3] This is just the ratio between the electric field that the molecule is exposed to and the incoming electric field. When ε is equal to $-2\varepsilon_0$, $A(\nu)$ is maximized. This condition occurs when the surface plasmons of the metal sphere are excited. From equation (29), the electromagnetic enhancement is represented by $|A(\nu_L)|^2|A(\nu_S)|^2$.[3] By substituting equation (30) into this expression an equation for the power of the electromagnetic field enhancement can be formed as follows:[3]

$$G_{em}(\nu_S) = |A(\nu_L)|^2|A(\nu_S)|^2 \approx \left|\frac{\varepsilon(\nu_L)-\varepsilon_0}{\varepsilon(\nu L)+2\varepsilon_0}\right|^2\left|\frac{\varepsilon(\nu_S)-\varepsilon_0}{\varepsilon(\nu_S)+2\varepsilon_0}\right|^2\left(\frac{r}{r+d}\right)^{12} \tag{31}$$

This equation shows the dependence of the electromagnetic SERS enhancement on the local field of the metallic surface. The enhancement increases as the fourth power of the local field. The enhancement is also stronger when the excitation source is in resonance with the surface plasmon. It is important to note that the electromagnetic enhancement does not require direct contact between the molecule and the metal but its strength will decrease dramatically with increasing distance.

The chemical enhancement SERS effect is not as well understood as the electromagnetic enhancement, but a number of theories have been suggested. One such

theory suggests that the enhancement is due to specific interactions between the adsorbed molecule and the metal. This interaction creates a molecule-metal complex, which generates an increased Raman cross-section of the adsorbed molecule when compared with a free molecule in solution.[3] Another theory suggests that a charge transfer between the metal and molecule occurs. Figure 5 shows a typical energy level diagram for a molecule-metal complex.[3] The normal molecular pathway is given in path (a). The charge transfer pathway is shown in paths (b) and (c). This charge transfer is a resonance Raman effect and occurs due to the highest occupied molecular orbital (HOMO) and the lowest unoccupied molecular orbital (LUMO) of the molecule being symmetric relative to the Fermi level of the metal. Another possible chemical enhancement effect is attributed to a proposed dynamical charge transfer. This occurs when a photon contacts the metal and excites an electron. The electron is then transferred from the metal to the LUMO of the molecule and back to the metal. The electron relaxes back to its initial state and generates a Stokes photon.[3]

The chemical SERS enhancement is relatively weak when compared with the electromagnetic enhancement, generating enhancement factors on the order of $10\text{-}10^2$. However, it has been suggested that charge transfer effects may be as much as 10^{14} times stronger than the normal Raman signal.[3]

Raman spectroscopy is unique because every molecule has its own characteristic spectra with differing frequency shifts and relative intensities. When comparing a Raman spectrum with a SERS spectrum for the same molecule, some differences may be observed. The enhancement of Raman modes from SERS can cause deviations in the

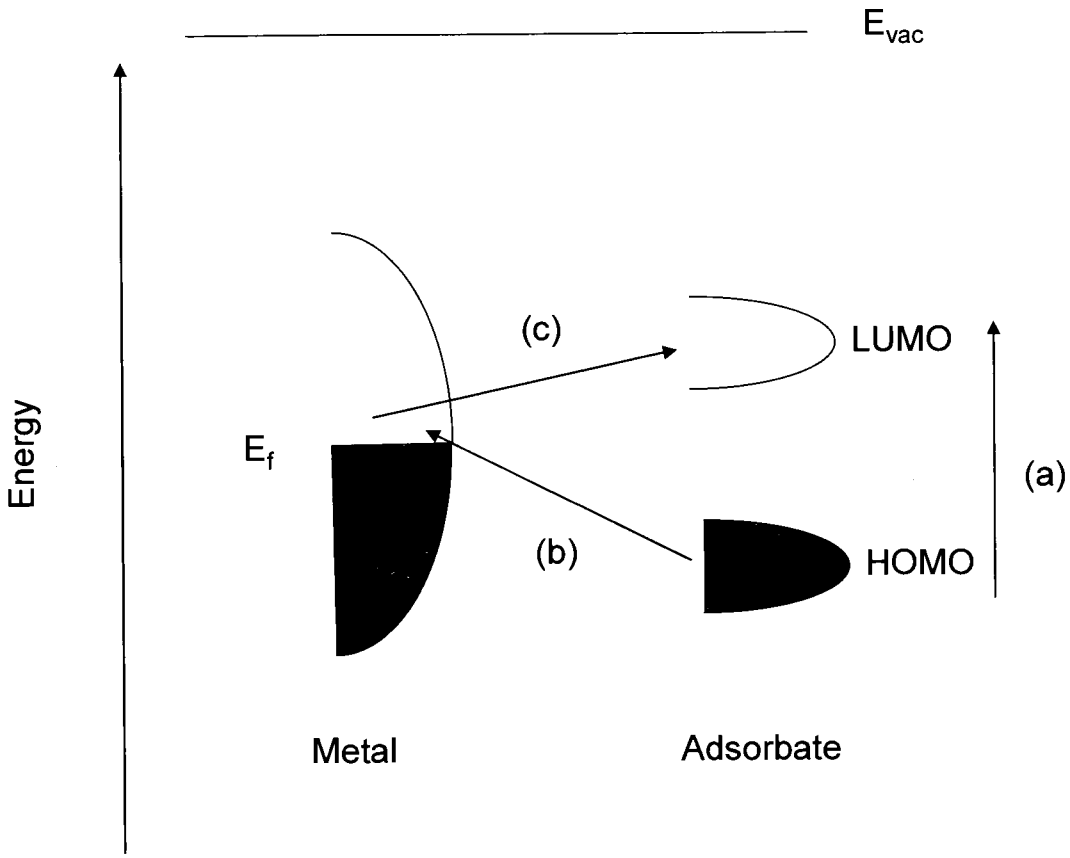

FIG. 5. Charge transfer mechanism.

relative intensities of the spectra. The interaction between the molecule and the metal may also cause shifts in the frequency of the Raman lines. However, these differences are usually small. This means that a SERS spectrum will still provide a unique spectrum for each molecule.

Applications of Raman/SERS Spectroscopy

Biological Raman Applications

In the last two decades, Raman and SERS spectroscopy have become important tools for studying biological systems. Several review articles have been published in recent years covering the topic.[1-6,36] Raman spectra have been acquired from amino acids, peptides purine and pyrimidine bases, proteins, neurotransmitters, DNA, RNA, porphyrins, chlorophyls, and enzymes. Many new applications have been developed. Recent examples of biological applications for both normal Raman and SERS will be discussed in the following paragraphs. These examples demonstrate the potential utility of Raman and SERS spectroscopy in the biomedical science field.

One particularly interesting application of Raman spectroscopy is in multicomponent blood analysis.[7-9] One research group reported the use of near-infrared (833nm) Raman to measure the concentrations of six analytes (glucose, cholesterol, triglyceride, BUN, total protein, and albumin) in serum and in whole blood.[9] Raman spectra were acquired using a dispersive Raman system with a NIR (830 nm) excitation source. Calibrations for each analyte were developed using partial least-squares cross validation. Concentration predictions were made with high accuracy on a 66 patient data set using 60-s spectra. The results of the study indicated that the concentration predictions were more accurate for the serum samples than for the whole blood samples.

However, the whole blood results did yield significant prediction accuracy and will improve once the data can be corrected for the effects of turbidity. The results of this study demonstrate a high potential for the development of a noninvasive technique for monitoring blood analyte concentrations.

Raman spectroscopy has also been applied to the study of biological tissues. Tissues, which are a cooperative assembly of different eukaryotic cells, contain a multitude of various biological molecules like lipids, proteins, DNA, and enzymes. These various molecules serve as markers to form a unique spectral fingerprint. Thus it is possible to correlate spectral changes with biochemical changes. Recent studies have been performed on tissues from the oral cavity, cervix, and the ovaries.[6] These studies focused on the spectral difference in normal cells as compared with malignant cells. It was found that in each of the tissue types chosen, a substantial difference in the spectra was observed between the normal and malignant cells. It was also shown that the spectral characteristics of the malignant cells would change depending on the stage of malignancy. The results of this study suggest the feasibility of developing in-vivo diagnostics for the early detection of cancer.

One last application of Raman spectroscopy is in the study of protein and nucleic acid assemblies.[1] Researchers have utilized the vibrational information contained in a typical Raman spectrum to deduce the three-dimensional structure, intermolecular interactions, and dynamics of a protein or nucleic acid molecule. Raman spectroscopy is now a viable alternative to X-ray diffraction and NMR in 3-D structure determination. One recent study utilized Raman spectroscopy in the study of protein/DNA recognition in gene regulatory complexes.[1] The use of Raman is preferred over the use of X-ray

diffraction or NMR because Raman is not limited by the availability of protein-bound and -unbound structures. The study examined the binding of several transcription activators to the DNA major groove. The reported results have demonstrated the sensitivity of the Raman signal to conformational reorganizations of the DNA when binding a protein. The Raman spectral perturbation can be correlated to the various stages of protein/DNA interaction.

Biological SERS Applications

A novel biological application of SERS reported recently is the detection of DNA and RNA using SERS activated nanoparticles.[76] Gold nanoparticle probes labeled with oligonucleotides and a Raman-active dye were captured by complimentary oligonucleotide molecules immobilized on a surface. The gold particles were then coated with silver to generate a SERS active substrate. The SERS spectrum of the Raman dye molecule was acquired confirming the presence of the target molecule. This process was carried out on six dissimilar DNA targets with six Raman labeled nanoparticle probes and two RNA targets with single nucleotide polymorphisms. The results of the study were highly favorable. The reported unoptimized DNA detection limit of this method is 20 femtomolar. The developed method proved also to adequately differentiate single nucleotide polymorphisms.

Recently, SERS has also been applied to the detection, identification, and quantification of neurotransmitters in brain fluid.[5] Under normal physiological conditions, the neurotransmitter concentrations are quite low and are undetectable with normal Raman instruments. The increased sensitivity of SERS has enabled detection at relevant physiological concentrations. One paper reported the SERS spectra of dopamine

and norepinephrine at concentrations ranging from micromolar to nanomolar.[5] Spectra were collected using integration times as low as 0.025 s using 100 mW NIR excitation. These concentrations and sample times are on the order of actual physiological neuronal events. Also significant were the clear differences between the spectra of dopamine and norepinephrine even though these molecules have almost nearly identical structures. This finding demonstrates the potential for SERS to have an increased selectivity over normal Raman. The normal Raman spectra of these two molecules are almost indistinguishable. The differences in spectra can be attributed to the small differences in the absorption behavior of these molecules. Quantitative information from mixtures of the two molecules was also reported.

The final biological application to be discussed is the utilization of SERS in immunoassays.[3] The fact that most immunoassays use multiple label molecules to detect multiple antigens makes SERS the ideal method to readout the assay. SERS can detect multiple labels because of its narrow Raman lines which allows for no spectroscopic overlap. Also, with SERS there is only one excitation source required and no quenching or photobleaching (normally associated with fluorescence techniques). A novel assay utilizing gold nanoparticles has recently been reported.[3] In this assay, antibodies immobilized on a gold surface capture antigens in solution. Gold nanoparticles with adsorbed specific antibody and Raman label are introduced and bind to the already captured antigen. Raman spectra are then collected with the gold nanoparticle acting as the SERS substrate. This assay design has been applied to several antigen/antibody systems.

Quantitative SERS Applications

We have already shown that SERS is a powerful tool for the selective detection of biological molecules at extremely low concentrations. However, until recently SERS has not been utilized as a quantitative analytical technique. The reason for this has been the difficulty in reproducing SERS enhancement processes, particularly the substrate preparation. In recent years, as the SERS enhancement process has become better understood, more and more quantitative SERS studies have been published.[11-13,18,77-85] One recent review article highlights this trend.[79] In the following paragraphs, several examples of SERS used in quantitative chemical analysis will be highlighted.

Adenine is an important biological species, particularly in cellular respiration, and has a strong Raman signal. A recent study demonstrated the concentration dependence of the SERS intensity of two different bands of the adenine spectrum.[84] SERS enhancements were generated from stable silver colloid solutions. The results show a clear linear dependence of the SERS intensity on the adenine concentration over the range between 1 x 10^{-7} M and 9 x 10^{-7} M. Large variations in the SERS intensity were observed for adenine concentrations above 1 x 10^{-6} M. This was attributed to changes in the adsorption geometry of the adenine as it saturated the colloid surface. The authors also noted that there was variation in the concentration dependence of the two different bands that were analyzed. This means that the distribution of the enhancement is not homogeneous over the Raman spectrum.

Creatine analysis in urine and serum is important for establishing proper renal function. A recent study demonstrated a novel SERS method for the quantitative determination of creatine in human serum.[12] The study utilized isotopically labeled

creatine as an internal standard along with complex multivariate data analysis. SERS enhancements were generated from silver colloid solutions. This method demonstrated the ability to quantify creatine at and below clinically relevant concentrations. Using a partial least squares regression model on 87 calibration spectra covering the full range of mole fractions of neat creatine, the prediction performance of the model was validated to within a standard deviation of less than 2% using independent reference samples. The results of measured serum creatine concentrations agreed with values obtained from gas chromatography/isotope dilution mass spectrometry to with in 3%.

Another recent study uses isotopic labels to detect and quantify proteins by SERS.[63] Silver colloids were used to generate SERS enhancements. In the study, isotopomeric rhodamine 6G (R6G) was used as a probe and was conjugated to several proteins (lysozyme and cytochrome c). Both proteins were successfully quantified from their SERS spectra. No interference was observed from the protein due to the overwhelming SERS enhancements of the R6G. The SERS spectra were proven to accurately reflect the relative molecular content of the protein solutions. Also, the technique was successfully applied to sodium dodecyl sulfate polyacrylamide gel electrophoresis (SDS-PAGE) gel analysis of each protein. This offers a novel practical approach to the separation and detection of biological mixtures.

The final study we will discuss compares SERS with fluorescence as an alternative method for quantitatively detecting labeled antibodies.[78] In the study, the same instrument and excitation source is used for both SERS and fluorescence measurements. Silver colloids were used to generate SERS enhancements. Nitric acid was used to aggregate the colloid. Tetramethylrhodamine-6-maleimide (TAMRAM) was the dye

used to label the antibodies. The authors pointed out that at high concentrations the fluorescence signal was superior to the SERS spectra, but at low concentrations the broad fluorescence band blends with the baseline and are difficult to discriminate from the background noise. The sharp SERS peaks at low concentrations, however, are easy to discriminate from the background, making it more effective than fluorescence. Concentration studies revealed good, straight-line behavior for both the SERS and fluorescence methods. From the concentration studies, the detection limit was determined for both methods. The detection limit for the SERS method, calculated as three times the standard deviation of the blank divided by the gradient, was lower (1.19×10^{-11} M) than the fluorescence method (3.46×10^{-10} M). The authors believe that this result suggests SERS can give greater sensitivity for antibody detection over fluorescence and, moreover, has the potential advantage of accomplishing multiple analyte detection.

CHAPTER III

EXPERIMENTAL PROCEDURES

Instrumentation

(A) Dispersive Raman System. A Solution 633 fiber-optic microRaman spectrometer (Detection Limit, Laramie, WY) was used for acquisition of SERS spectra. The spectrometer was equipped with a remote fiber optic probe head. The spectrometer and probe head are shown in Figure 6. The probe head consisted of a two, holographic notch filters (Kaiser), a mirror, a dichroic mirror, and an objective lens (8 mm focal length). A He-Ne laser (632.8 nm) was used as an excitation source. Maximum output laser power was 20 mW. The spectrometer was equipped with an air-cooled charge-coupled device (CCD) camera.

(B) FT-Raman System. A RAMAN 960 (Thermo Nicolet) FT-Raman spectrometer was used for the acquisition of all FT-SERS spectra. The RAMAN 960 utilizes a Spectra Physics Nd:YVO4 laser (1064 nm)) as an excitation source. Output laser power could be adjusted from 0.015 W to 5.0 W. A He-Ne (632.8nm, Melles Griot) was used as a reference source. Nominal He-Ne laser power was 2.0 mW. A Michelson interferometer and InGaAs (indium-galium arsenide) array detector were used to collect spectra.

Electrochemical Silver Electrode SERS of Pyridine

All SERS spectra were acquired using the 633 nm dispersive Raman system on solutions of 0.25 M Pyridine and 0.1 M KCl. All solutions were prepared using 18 MΩ milliQ water. Pyridine solutions were prepared by diluting 100 µl pyridine with 5 ml of

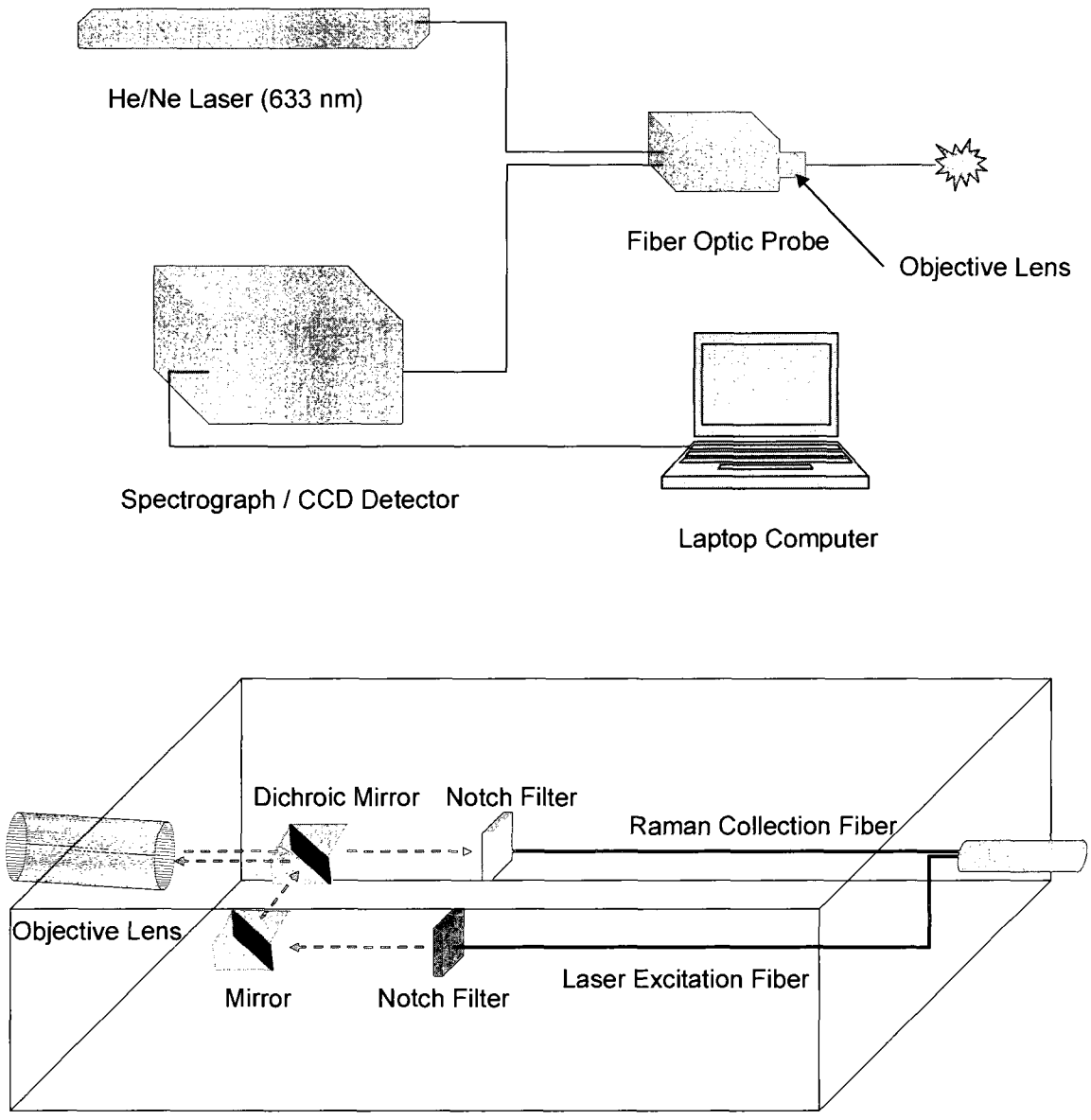

FIG. 6. Solution 633 fiber optic microRaman spectrometer with remote fiber optic probe.

0.1 M KCl solution. The pyridine solutions were pipetted into a glass cell. The Ag/AgCl reference electrode and platinum electrode were placed into the cell. Wet argon gas was bubbled through the cell for 5 minutes to remove any oxygen in the cell. The Ag electrode was inserted into the cell. The cell was then placed onto the sample holder. Each electrode was connected to the potentiostat. The Raman detector was turned on and allowed to cool down to -10°C. Once the temperature was reached the laser was turned on and focused onto the Ag electrode within the cell. Voltage was cycled through the electrodes and SERS spectra were acquired.

Optimization of the SERS Signal

A series of experiments were performed to determine the optimum parameters for acquiring SERS spectra using the silver electrode. The following parameters were considered most significant to achieving a maximum SERS signal: voltage scan rate, maximum forward potential, and maximum reverse potential. The experiments consisted of taking a SERS spectra of a pyridine solution at a given integration time, before and after 20 potential sweeps at a given scan rate, and max forward / reverse potential. Table I outlines the conditions under which the spectra were taken. Twenty consecutive scans were made for each scan rate with spectra taken before and after.

Colloid SERS

Chemical Preparation of Silver Colloid

Colloidal silver particles were prepared in aqueous solution following the procedure of Lee and Meissel.[86] A solution of $AgNO_3$ was prepared by dissolving 90 mg of $AgNO_3$ with 500 ml 18 MΩ milliQ water in a reaction flask. The reaction flask

TABLE I. Experimental Conditions for Electrochemical SERS Optimization.

Integration Time (s)	Scan Rate	Max Forward Potential (V)	Max Reverse Potential (V)
0.5s	50	-900	0
	100		
	200		
	300		
	500		
	1000		
	2000		
	5000		
0.5s	50	-900	100
	100		
	200		
	300		
	500		
	1000		
	2000		
	5000		
0.1s	50	-900	200
	100		
	200		
	300		
	500		
	1000		
	2000		
	5000		

TABLE I. Continued.

Integration Time (s)	Scan Rate	Max Forward Potential (V)	Max Reverse Potential (V)
	50		
	100		
	200		
0.5s	300	-900	300
	500		
	1000		
	2000		
	5000		
	50		
	100		
	200		
0.1s	300	-900	300
	500		
	1000		
	2000		
	5000		
	25000		
	20000		
	15000		
	10000		
0.1s	5000	-900	200
	2000		
	1000		
	500		
	100		
	50		

consisted of a 1000 ml three-neck round bottom flask with a thermometer, addition flask, and condenser attached. The reaction flask was placed on a heating mantle and the solution was brought to a boil (100°C). Once at a boil, 10 ml of a 1% sodium citrate solution was added drop wise through the addition flask. After a few minutes the solution changed from a clear solution to a greenish yellow. This signified the initiation of nanoparticle formation. Boiling was maintained for one hour after the initial color change. The solution was then removed from the heating mantle and allowed to cool down to room temperature. The solution was filtered through a 0.2 μm filter into a 1000 ml dark glass container. The solution was stored at 8°C and was used, as is, for all SERS experiments.

Colloids Prepared by Laser Ablation

Silver and gold nanoparticles were produced by laser ablation of a metal foil in an aqueous solution in accordance with known literature methods.[87-90] The metal foil was placed in the bottom of a beaker with 10 ml of 18 MΩ milliQ water. The output of a Nd:YAG pulsed laser at 10 Hz was directed to a mirror and focused onto the metal foil by a focusing lens. A schematic of the experimental apparatus is shown in Figure 7. Upon irradiation of the laser beam, the solution gradually changes to a yellowish-brown color. The irradiation of the metal foil continued for 15 minutes. The solution was then transferred into a glass vial and stored at 8°C and was used, as is, for all SERS experiments.

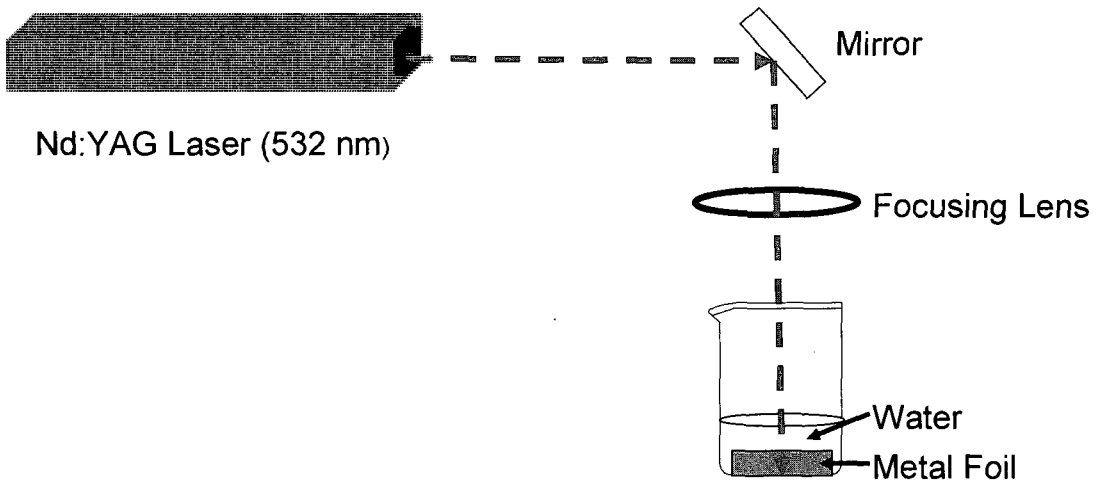

FIG. 7. Experimental apparatus for the generation of metal colloids via laser ablation.

Optimum Colloid Aggregation Conditions for SERS Generation

Five milliliter samples of tryptophan (7.5 mM) were prepared from a one molar stock solution of tryptophan and a stock solution of aqueous silver colloid (chemically prepared). Aggregation of the colloid was induced by adding either 100 mg of solid NaCl or 4 drops (~100 μl) of 1M aqueous NaCl. An aliquot of the aggregated solution was immediately transferred to a glass NMR tube and placed in the sample holder within the sample compartment of the RAMAN 960 FT-Raman spectrometer. The sample compartment was closed and the Nd:YVO4 laser was focused onto the colloid solution manually using the OMNIC Version 6.0a interface software. The laser power was set at 1.02 W. Once the laser was focused, SERS spectra were acquired using the OMNIC software set to take 64 scans with an 8.0 nm resolution.

Quantification of SERS Signal Using an Internal Standard

Five milliliter samples of tryptophan (7.5 mM) were prepared from a one molar stock solution of tryptophan and a stock solution of aqueous silver colloid (chemically prepared). Aggregation of the colloid was induced by adding 100 μl of 1M KNO_3. An aliquot of the aggregated solution was immediately transferred to a glass NMR tube and placed in the sample holder within the sample compartment of the RAMAN 960 FT-Raman spectrometer. The sample compartment was closed and the Nd:YVO4 laser was focused onto the colloid solution manually using the OMNIC Version 6.0a interface software. The laser power was set at 1.02 W. Once the laser was focused, SERS spectra were acquired using the OMNIC software set to take 64 scans with an 8.0 nm resolution.

Silver Deposition on Glass/Quartz Fiber Filters

Silver can be deposited on a glass silica surface by a reaction known as the "mirror" or "Tollen's" reaction. A thin silver layer was formed on the surface of glass/quartz fiber filters following the procedure of Batchelder et al.[91] Whatman GF/A glass microfiber filters, 25 mm diameter with a particle retention of 1.6 μm, and Whatman QM-A quartz microfiber filters, 25 mm diameter with a particle retention of 2.2 μm, were used in these experiments. All solutions used in this procedure were prepared using 18 MΩ milliQ water. Six milliliters of a 2% (w/w) silver nitrate solution was placed in a glass Petri dish. A 3.2% KOH solution was added drop by drop until a brown precipitate (Ag_2O) was formed. The solution was swirled to mix. To this solution a 30% (w/w) ammonia solution was added drop by drop until the precipitate was completely dissolved ($[Ag(NH_3)_2]^+$ was formed). Next, a 6% (w/w) silver nitrate solution was added drop by drop until the solution became yellowish brown. Three drops of 6%

ammonia was added and the solution became transparent. The Petri dish was swirled to ensure mixing. Six glass fiber filters were placed in the Petri dish and were completely immersed in the solution. The Petri dish was placed in a water bath set at 35 °C for 15 minutes to allow the solution to warm. In a separate glass vial, 2ml of a 35% (w/w) glucose solution was mixed together with 1 ml of methanol. The glucose methanol mixture was added to the Petri dish and mixed by swirling. The solution immediately became gray in color and turned completely black after a few minutes. The filters remained in the Petri dish for 30 minutes after which they were removed. Immediately after removing the filters were flushed with 1L of 18 MΩ milliQ water. The filters were left overnight to dry at room temperature. SEM images of the coated filters were acquired using a LEO 435 VP scanning electron microscope. No sample pre-treatment was required prior to obtaining SEM images.

SERS Spectra of Amino Acids Using Silver-Coated Filters

Amino acid solutions (10 mM) were prepared from one molar stock solutions and 18 MΩ milliQ water. 100 µl of the amino acid solution was pipetted directly onto the center of the coated side of a silver-coated quartz/glass fiber filter. The filter was then placed onto a sample holder which was inserted into the sample compartment of the Raman 960 FT-Raman spectrometer. Using the He-Ne laser, the sample position was adjusted manually so that the laser was focused directly onto the surface of the filter. The sample compartment was then closed. Using the computer interface software, Omnic Version 6.0a, the sample position was adjusted further to obtain the maximum Raman signal using the Nd:YVO4 laser set at 0.2 W. A Raman spectrum was then acquired from

the sample using the Omnic software interface. The instrument was set to acquire spectrum after 64 scans with a resolution of 8 nm and the laser power set at 0.2W.

SERS Spectra of Amino Acid Mixtures Using Silver-Coated Filters

Mixtures of phenylalanine and tryptophan (5mM) were prepared from one molar stock solutions of each amino acid and 18 MΩ milliQ water. SERS spectra of the mixtures were acquired from the silver-coated glass/quartz fiber filters as described previously.

Quantification of SERS Signal Generated from Silver-Coated Filters

Internal Standard. A one molar (1 M) stock solution of KNO_3 was prepared using solid KNO_3 and 18 MΩ milliQ water. Mixtures of phenylalanine and KNO_3 were prepared from stock solutions of 1 M phenylalanine and 1 M KNO_3 diluting with 18 MΩ milliQ water. SERS spectra of the mixtures were acquired from the silver-coated glass/quartz fiber filters as described previously.

Linear Calibration. A series of phenylalanine solutions at several known concentrations (0.01 – 5 ppm) were prepared from a one molar stock solution of phenylalanine and 18 MΩ milliQ water. Several SERS spectra were acquired from each concentration using silver-coated quartz/glass fiber filters as described previously. Each spectrum was exported into Microsoft Excel 2002 where all the spectra for each concentration were averaged together. The peak heights at 1001 cm^{-1}, 1031 cm^{-1}, and 1598 cm^{-1} were determined for each concentration and plotted using Excel. A linear fit to each plot was made using Excel.

CHAPTER IV

RESULTS AND DISCUSSION

Electrochemical SERS of Pyridine

The electrochemical method of SERS detection, first discovered by Jeanmaire and Van Duyne in the 1970's, is a highly sensitive technique for the chemical analysis of molecules adsorbed to the surface of metal electrodes.[92] Many applications of this method have been reported in the literature.[14,93-97] The SERS effect is typically observed from noble metal (Ag, Cu, Au, and Pt) electrodes. This method of SERS is particularly advantageous for the study of biological systems because measurements can be made in a controlled aqueous environment. Examples of this include the study of the adsorption characteristics of biological species such as imidazole, 6-mercaptopurine, glycine, threonine, and serine.[14,95,96] For this reason, the electrochemical method was used in our initial SERS study.

Our first set of experiments was designed to determine the optimal experimental conditions for generating the maximum SERS signal. A silver working electrode along with a platinum counter electrode and Ag/AgCl reference electrode were used in the electrochemical cell. This arrangement was selected for its ease of construction and its common use in the literature. Pyridine was selected as a test molecule for optimization experiments because of its large Raman cross-section and its high affinity for silver. A typical Raman spectrum of pyridine is shown in Figure 8. This spectrum was acquired from our Solution 633 fiber-optic microRaman spectrometer with remote fiber optic probe. The remote fiber optic probe allowed for sampling of the electrochemical cell

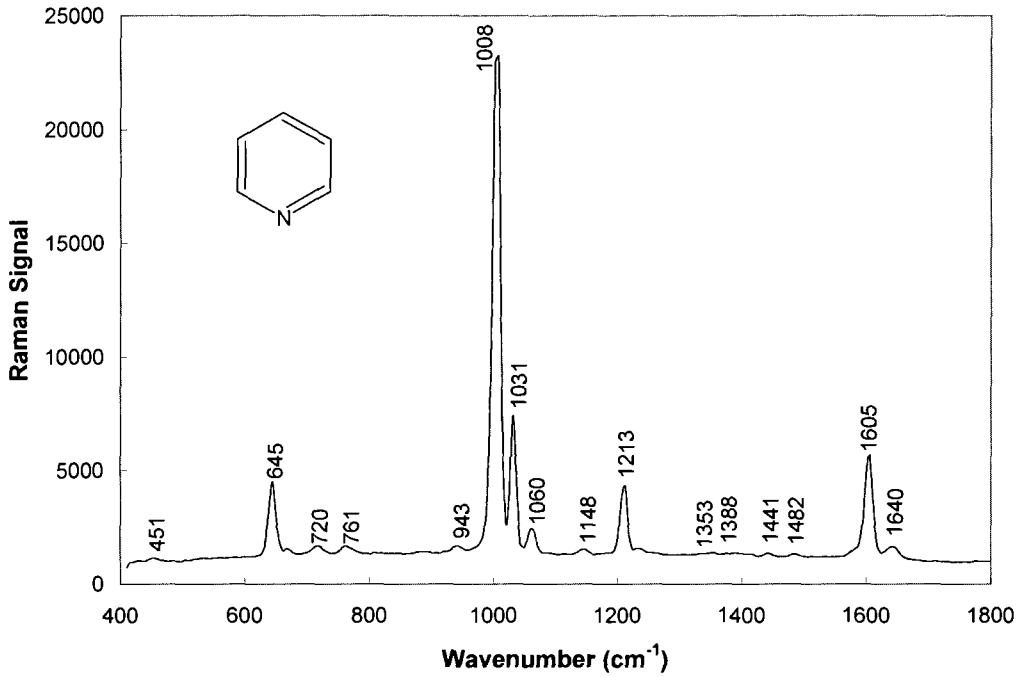

(a)

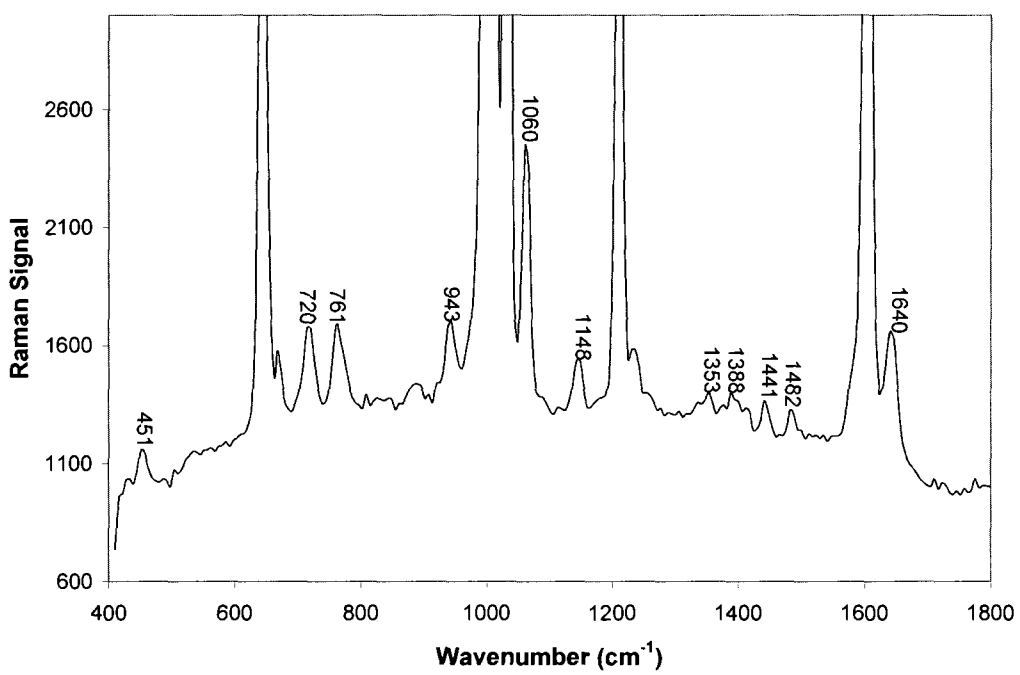

(b)

FIG. 8. (a) Raman spectrum of neat Pyridine solution. Spectrum obtained from Solution 633 fiber-optic microRaman spectrometer. Integration time was 1 sec. (b) Adjusted scale to show weaker peaks.

within a Faraday cage. The integration time of sampling was one second. Details of the spectrum and peak assignments are listed in Table II. The peak at 1008 cm^{-1} was the most intense and was used to evaluate the SERS measurements. From the spectrum of neat pyridine, we see that the peak Raman signal at 1008 cm^{-1} is 23,193 counts. This value was used as a baseline to determine the magnitude of SERS enhancement generated in our experiments.

To generate the maximum SERS signal from the silver surface, it is necessary to perform an oxidation-reduction cycle (ORC) on the electrode surface. This is accomplished by applying a potential sweep to the electrode. The parameters which govern the potential sweep will determine the rate of oxidation and reduction at the electrode surface. The oxidation and reduction rate is critical to creating the necessary surface morphology (roughness) for maximizing the SERS signal. A representative cyclic voltamogram is shown in Figure 9 (a). A corresponding SERS spectrum of pyridine acquired during our experiments is shown in Figures 9 (b) and 9 (c). Details of the spectrum and peak assignments as compared to the spectrum of neat pyridine are listed in Table III. The SERS spectrum of pyridine is almost identical to that of neat pyridine. Several of the peaks were shifted slightly for the SERS spectrum and only one peak was missing. The peak at 1640 cm^{-1} was not observed in the SERS spectrum.

Optimization experiments were conducted as described in Chapter III. The initial set of potential sweeps were made by varying the scan rate from 50 – 5000 mV/s while the max forward potential was -900 V and the max reverse potential was 0 V. Spectra were acquired before and after 20 sweeps at each scan rate and are shown in Figure 10.

TABLE II. Wavenumbers and Assignments for Neat Pyridine.

Raman Shift (cm^{-1})	Assignments[a]
451	ν16b
645	ν6b
720	ν11
761	ν10b
943	ν5
1008	ν1
1031	ν12
1060	ν18a
1148	ν15
1213	ν9a
1353	ν14
1388	-
1441	ν19b
1482	ν19a
1605	ν8a
1640	ν1 + ν6a

[a] Spectra assignments based on reference 99.

All spectra were taken with an integration time of 0.5s. The peak height at 989 nm was determined for each spectrum. A plot of peak height as a function of scan rate is given in Figure 11. The peak height before any potential sweeps were made was 1287. This value is equivalent to 128,700 when normalized to a neat solution of pyridine at 1s integration time. That represents an enhancement of the Raman signal of 5.3 times when compared to the maximum intensity attained from a normal Raman spectrum of a neat solution of pyridine. After the first 20 sweeps at 50 mV/s, the peak height actually decreases from the original value. Subsequent sweeps at increasing scan rates give similar results. This suggests that there was no reduction occurring at the electrode surface. Therefore, the morphology of the surface was not changing during the potential sweeps. Reduction of the surface is necessary to produce the required roughness suitable

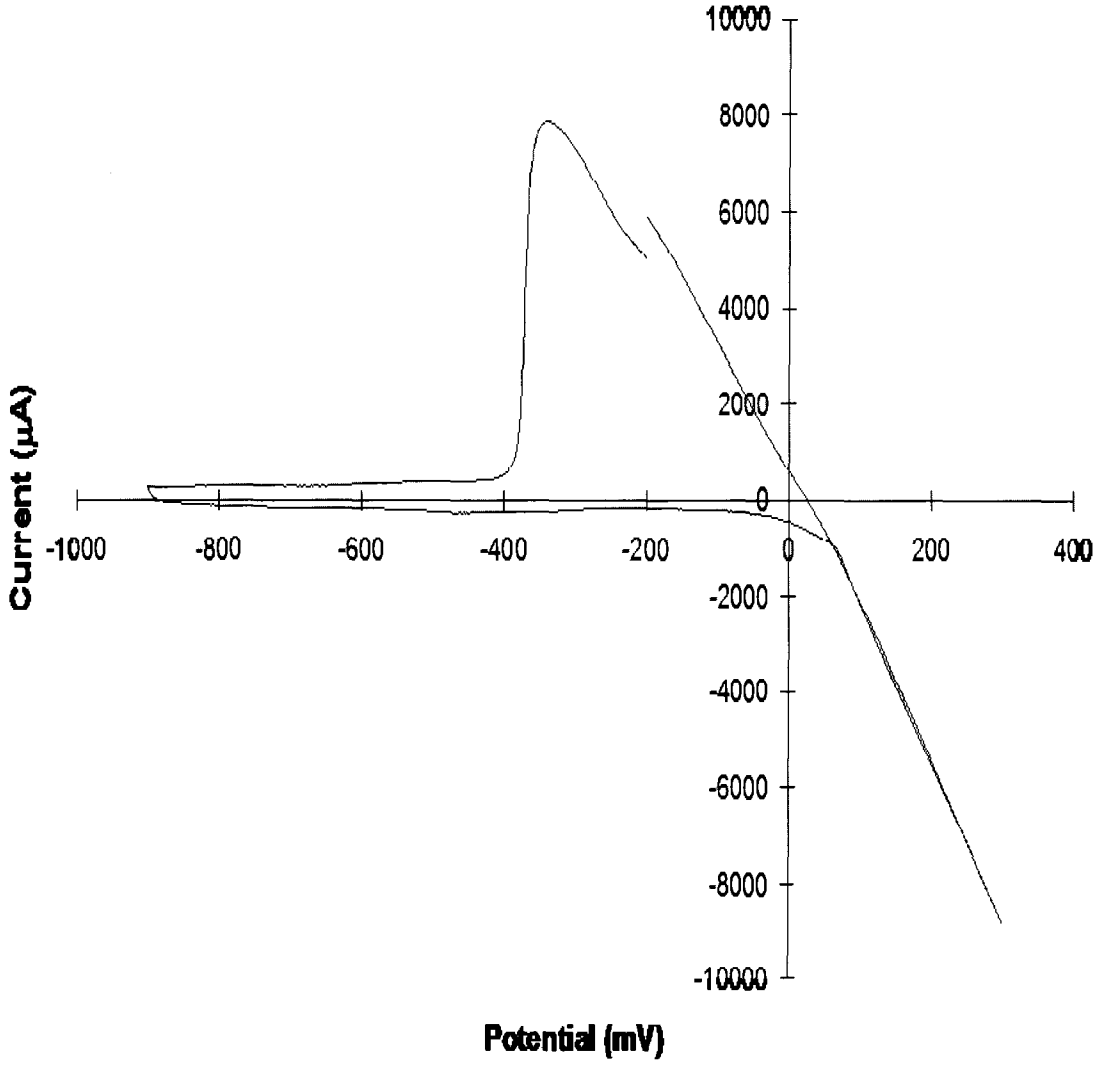

(a)

FIG. 9. (a) Typical cyclic voltamogram generated during experiments. Voltage scan rate was 500 mV/s.

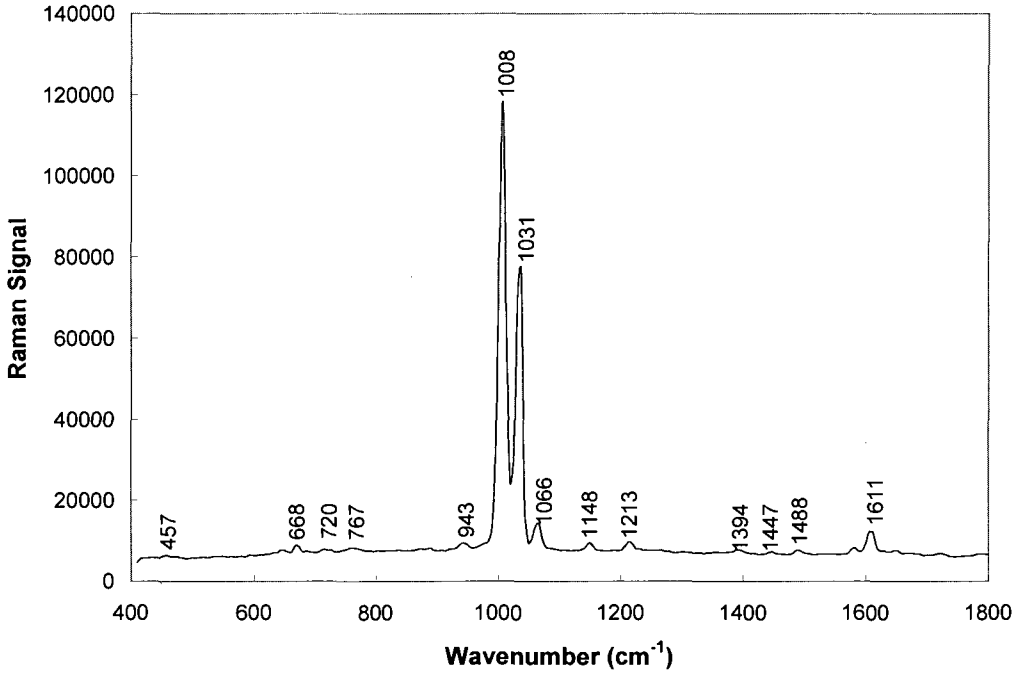

(b)

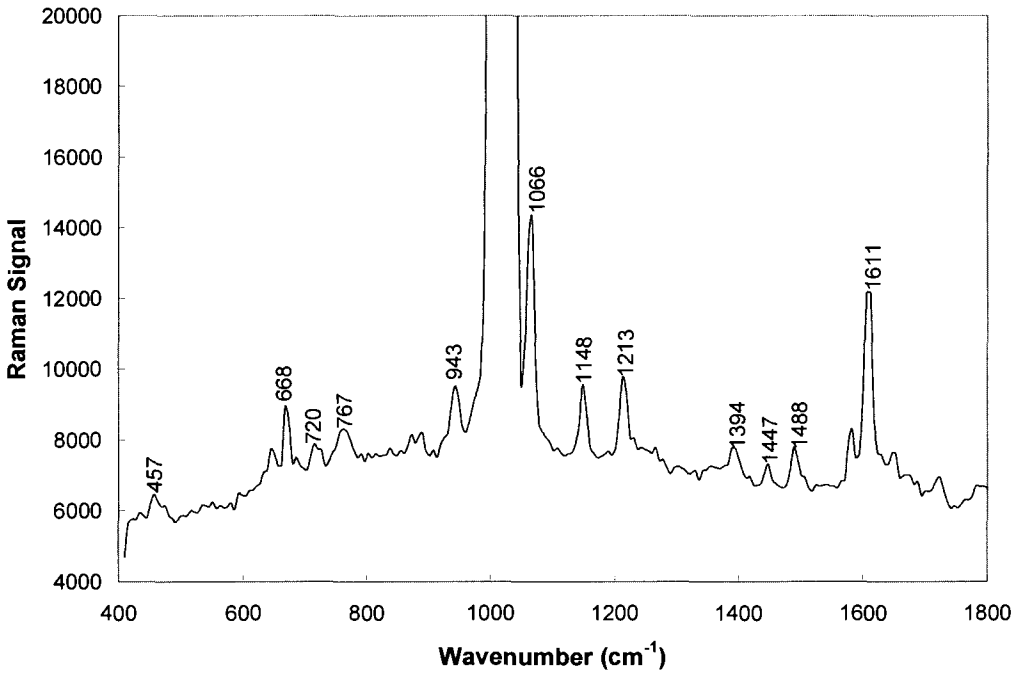

(c)

FIG. 9. (b) Corresponding SERS spectrum of pyridine. Integration time was 0.1s. (c) Adjusted scale to show weaker peaks.

TABLE III. Wavenumbers and Assignments for SERS Pyridine.

Raman Shift SERS Pyridine (cm^{-1})	Raman Shift Neat Pyridine (cm^{-1})	Assignments[a]
457	451	ν16b
668	645	ν6b
720	720	ν11
767	761	ν10b
943	943	ν5
1008	1008	ν1
1037	1031	ν12
1066	1060	ν18a
1148	1148	ν15
1213	1213	ν9a
-	1353	ν14
1394	1388	-
1447	1441	ν19b
1488	1482	ν19a
1611	1605	ν8a
-	1640	ν1 + ν6a

[a] Spectra assignments based on reference 99.

for SERS enhancement. The decrease in signal was most likely caused by the smoothing of the surface during oxidation. To ensure that reduction occurs, the maximum reverse potential of the sweep would have to be extended past 0 V.

When the maximum reverse potential was extended to 100 mV, a significant increase in the Raman signal was observed. The series of spectra at this potential are shown in Figure 12. The peak height was plotted as a function of scan rate and is shown in Figure 13. This plot shows that after the first 20 sweeps at 50 mV/s the Raman signal increases from 1287 to 15,386. Similar increases were observed from the other scan rates. The largest increase, 17,801, occurred at 1000 mV/s. This represents a 74 times enhancement over that of the normal Raman signal. Similarly, at a max reverse potential of 200 and 300 mV the enhancement of the Raman signal continued to increase. Figures

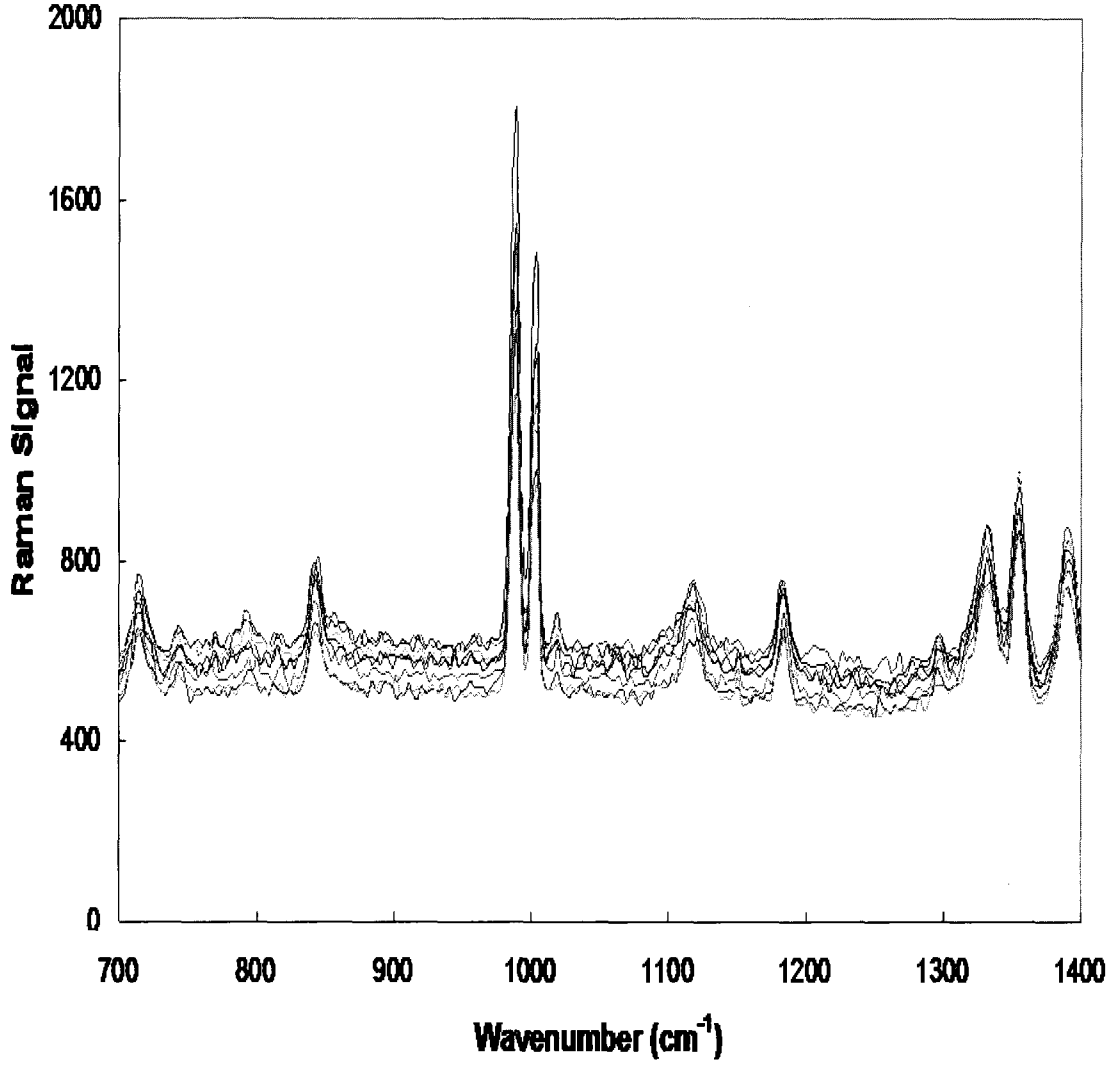

FIG. 10. Electrochemical silver electrode SERS spectra of pyridine at varying scan rates (50 – 5000 mV/s). Maximum forward potential was -900 mV and the maximum reverse potential was 0 mV.

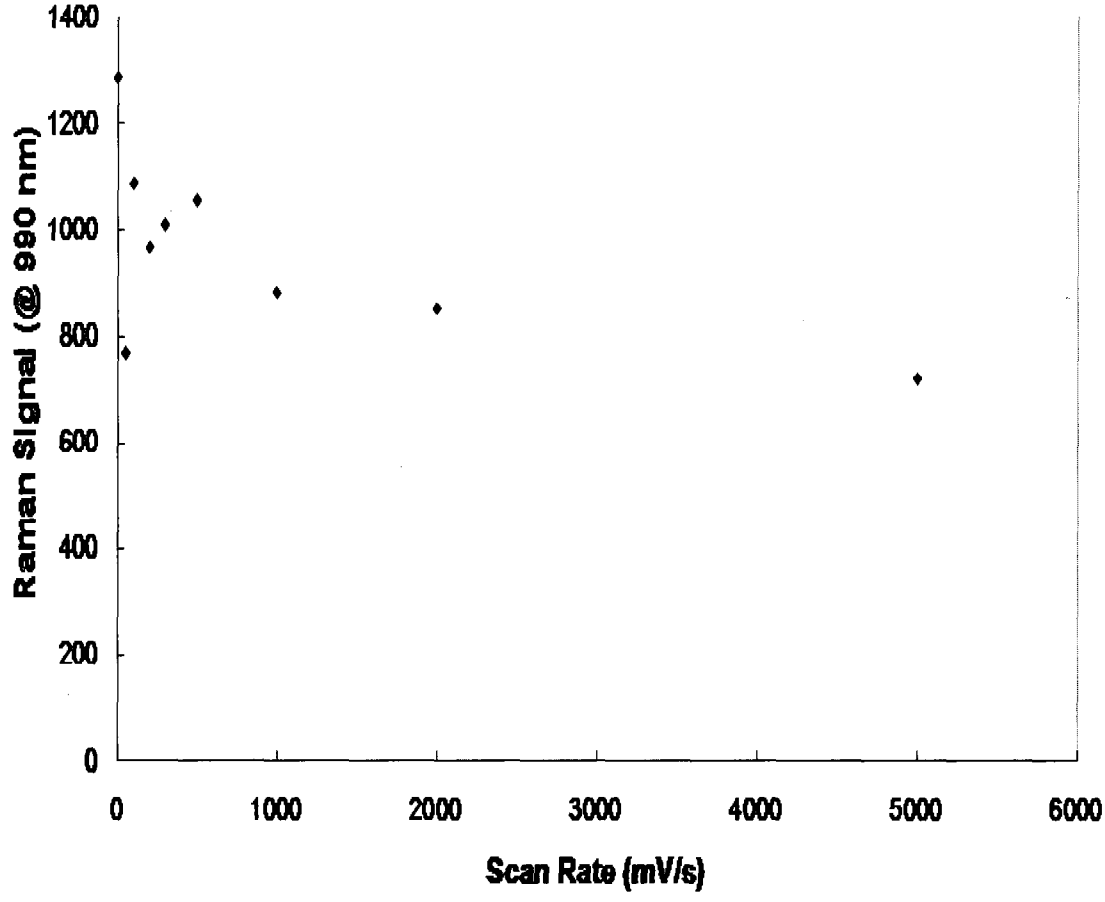

FIG. 11. Peak Raman signal versus scan rate for the electrochemical SERS spectra (max reverse potential 0 mV).

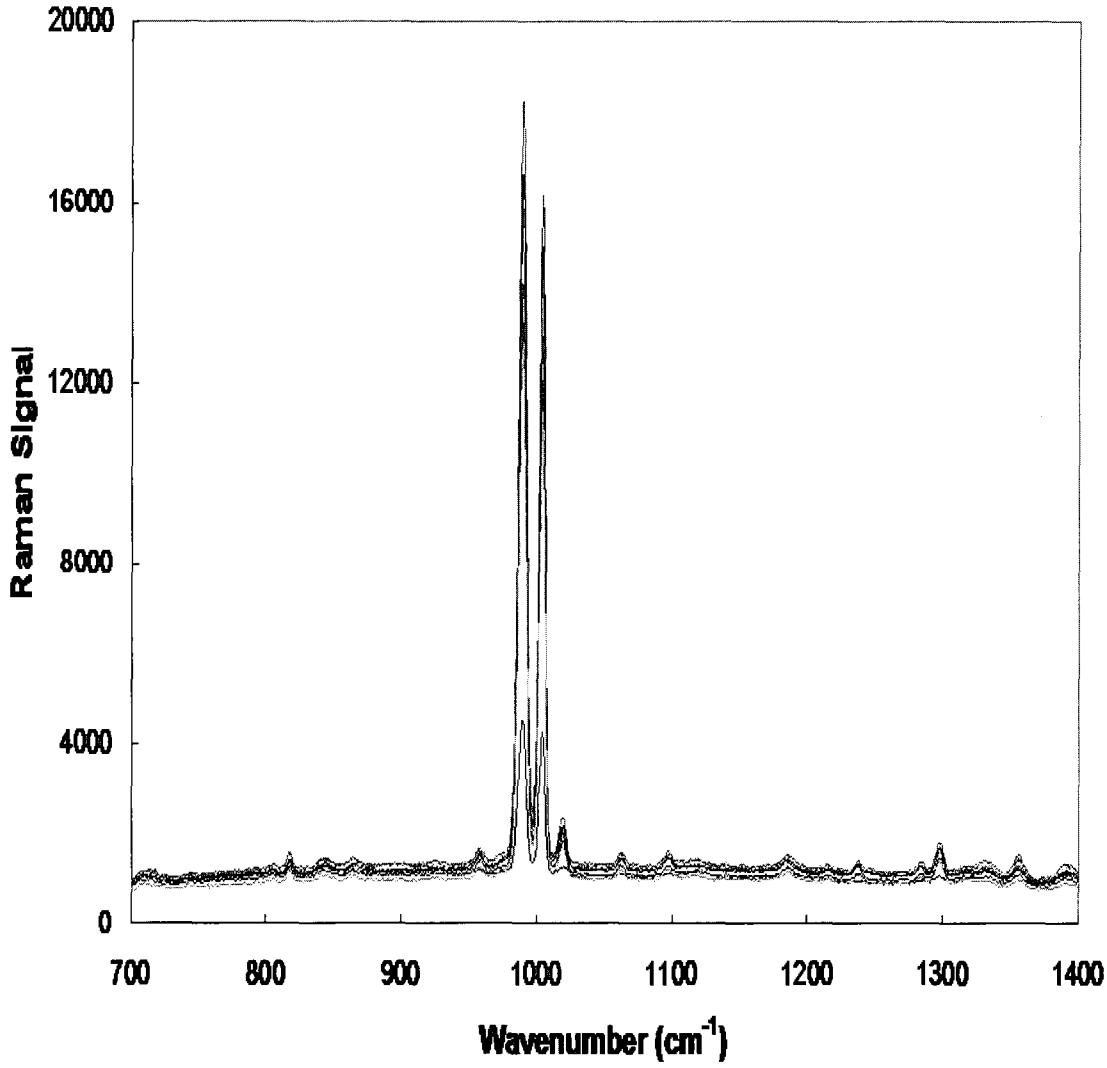

FIG. 12. Electrochemical silver electrode SERS spectra of pyridine at varying scan rates (50 – 5000 mV/s). Maximum forward potential was -900 mV and the maximum reverse potential was 100 mV.

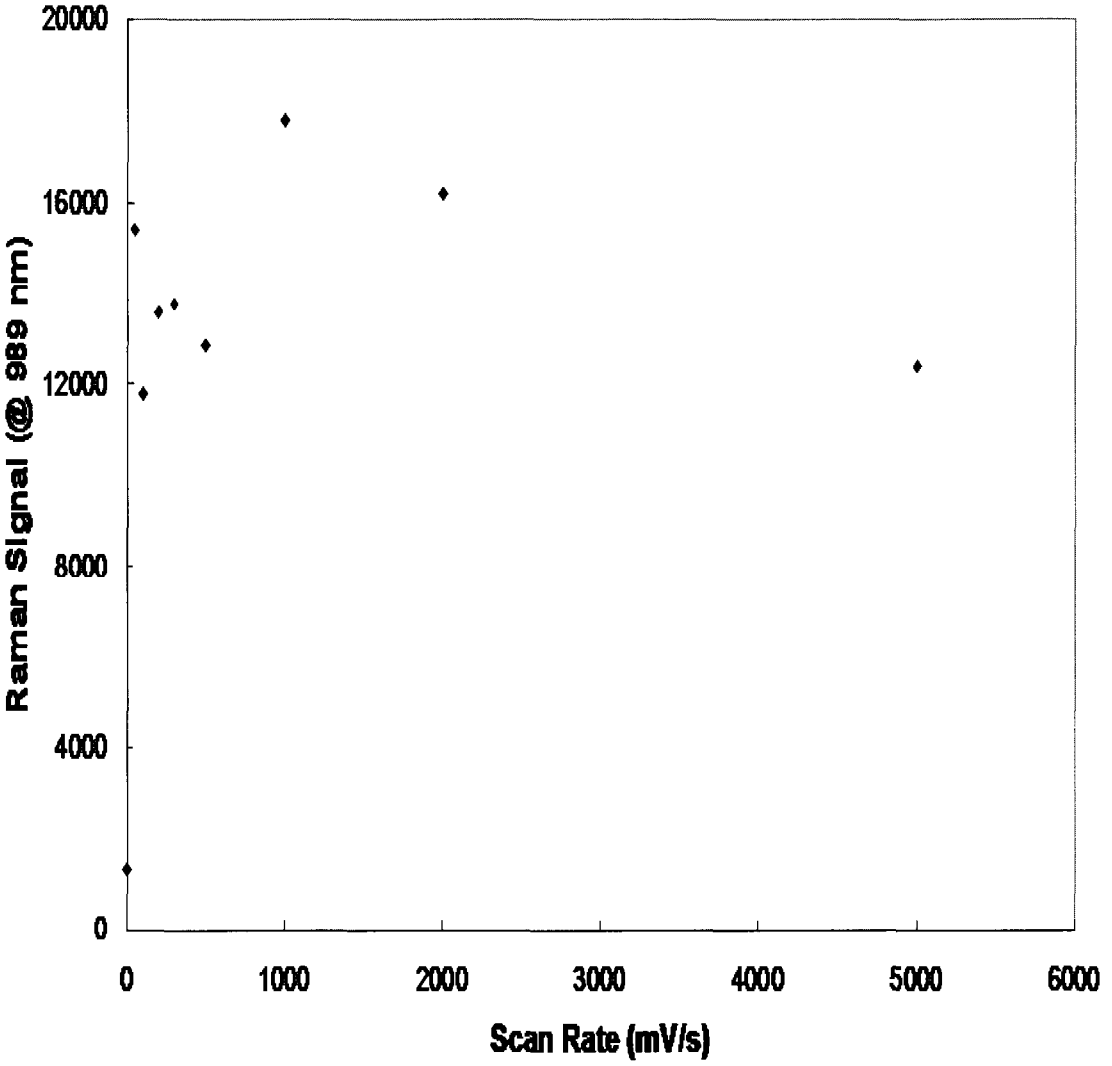

FIG. 13. Peak Raman signal versus scan rate for the electrochemical SERS spectra (max reverse potential 100 mV).

14 and 15 show the spectra acquired at 200 mV and 300 mV respectively. Figures 16 and 17 show the plots of peak height versus scan rate. The maximum Raman signal at 200 mV was 81,380 at 2000 mV/s, a 339 times enhancement. The maximum Raman signal at 300 mV was 112,980 at 50 mV/s, a 470 times enhancement. Also, at 300 mV, the Raman signal was shown to decrease with increasing scan rates. This result indicates that the optimal oxidation/reduction rate is achieved at lower scan rates. As the scan rate is increased, the oxidation/reduction rate on the electrode surface is also increased. This results in a smoother surface and therefore the SERS signal decreases. From this result, the optimum scan rate for the potential sweep is 50 mV/s.

A plot of the Raman signal versus maximum reverse potential at a scan rate of 50 mV/s, Figure 18, reveals a linear increase in Raman signal with increasing max reverse potential. When the maximum reverse potential was increased above 300 mV, no further enhancement of the Raman signal was observed. Therefore, a reverse potential of 300mV gave the maximum observed SERS signal. From these results the maximum observed Raman enhancement was observed after twenty potential sweeps with a max reverse potential of 300 mV, a max forward potential of -900 mV, and a scan rate of 50 mV/s.

It should be noted that each Raman spectra taken during the experiments was acquired at a potential of -200 mV. This was the beginning and ending potential for each sweep. It should also be noted that the Raman signal was continuously monitored during the sweeps. When watching the Raman signal during the sweep, we observed that the intensity of the SERS signal varied as the potential changed. In fact, the maximum SERS

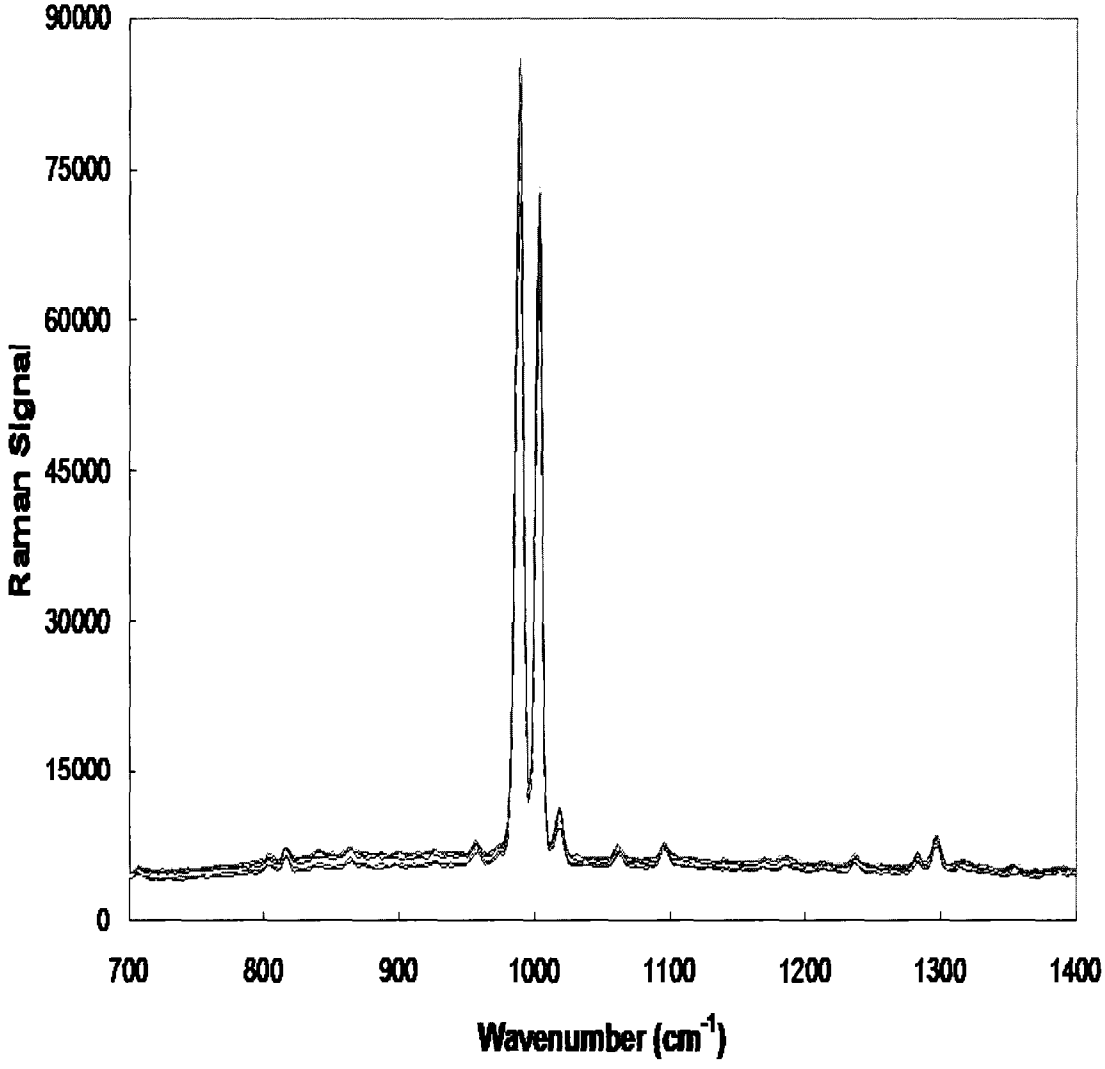

FIG. 14. Electrochemical silver electrode SERS spectra of pyridine at varying scan rates (50 – 5000 mV/s). Maximum forward potential was -900 mV and the maximum reverse potential was 200 mV.

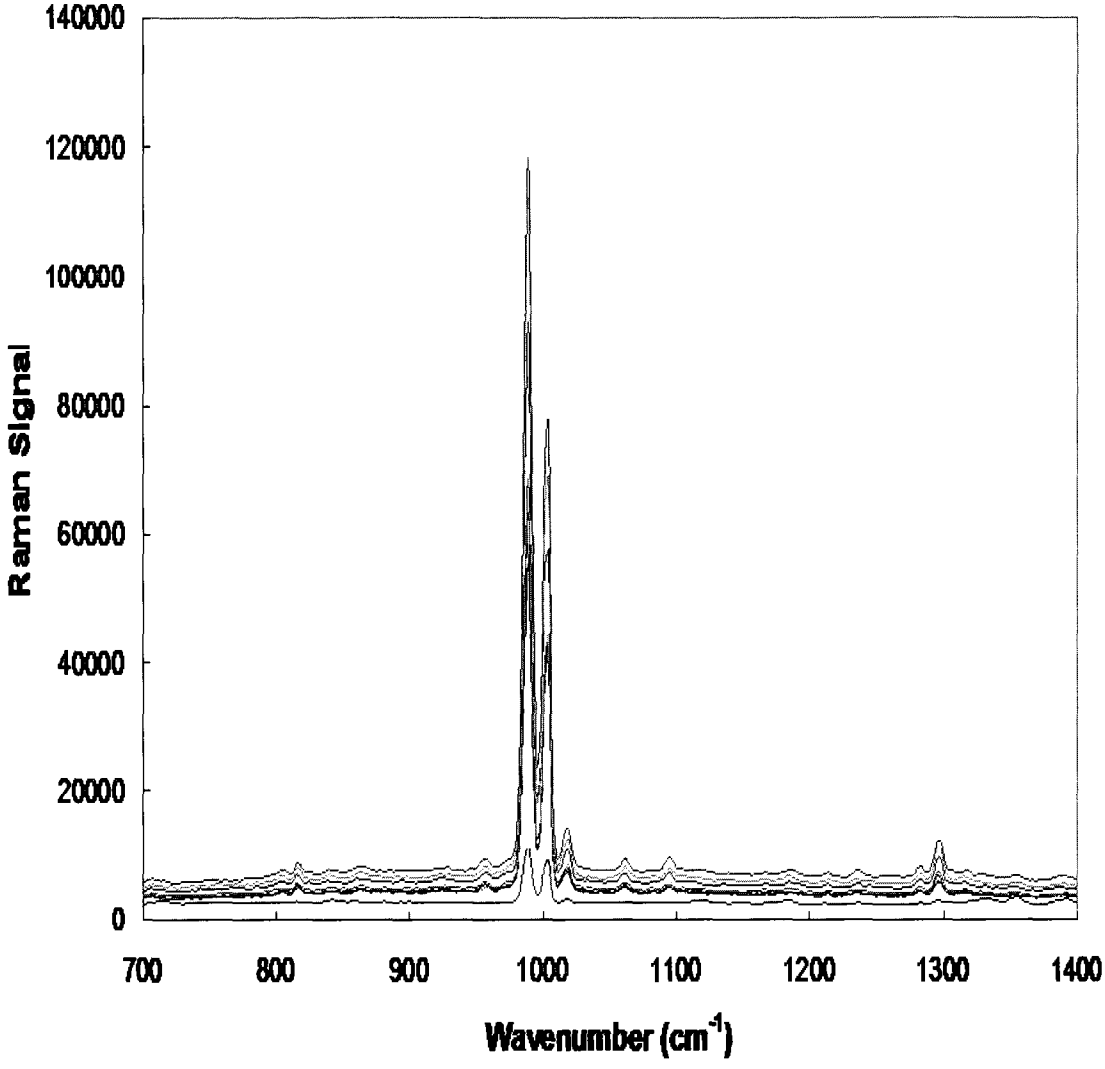

FIG. 15. Electrochemical silver electrode SERS spectra of pyridine at varying scan rates (50 – 5000 mV/s). Maximum forward potential was -900 mV and the maximum reverse potential was 300 mV.

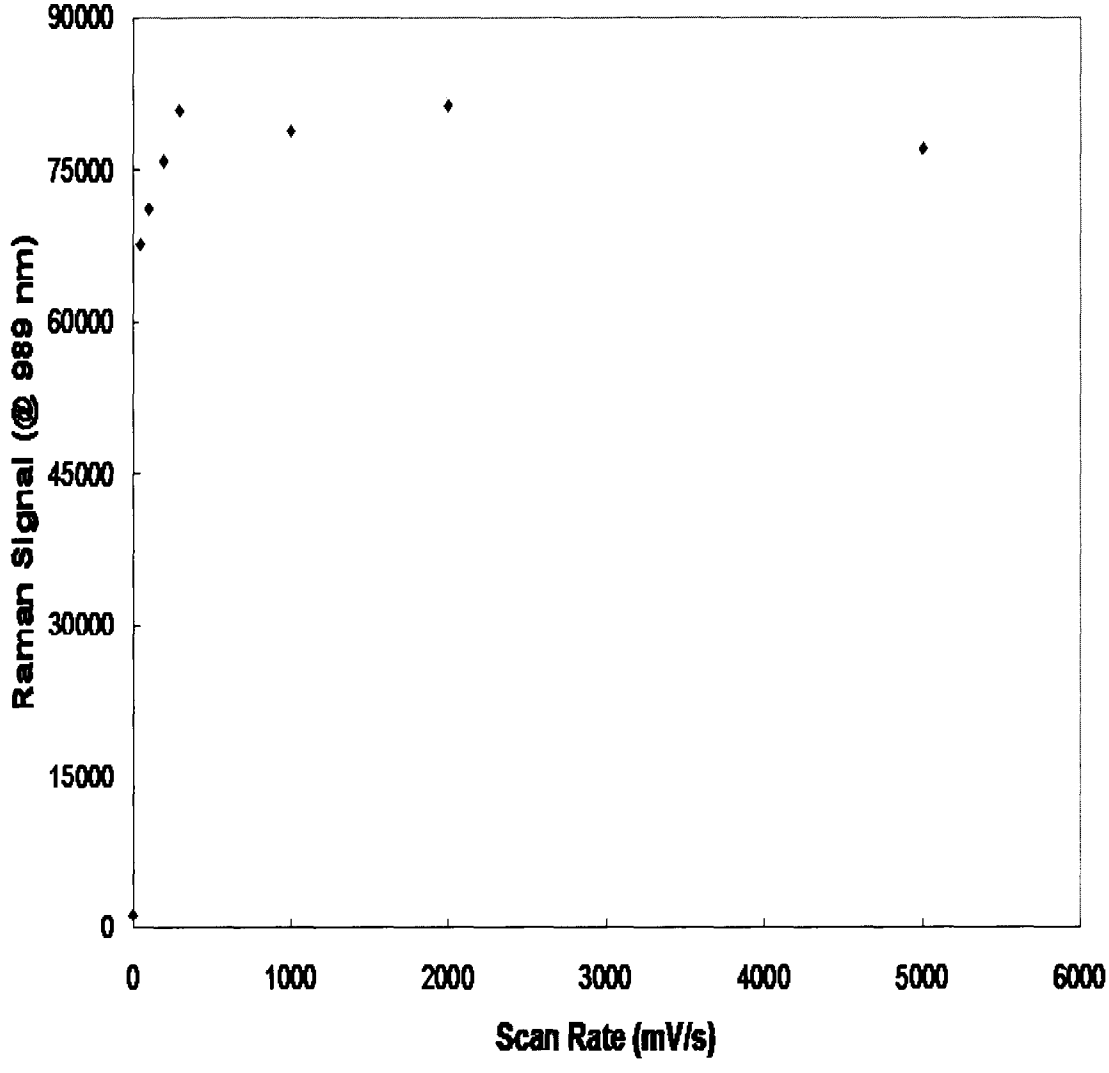

FIG. 16. Peak Raman signal versus scan rate for the electrochemical SERS spectra (max reverse potential 200 mV).

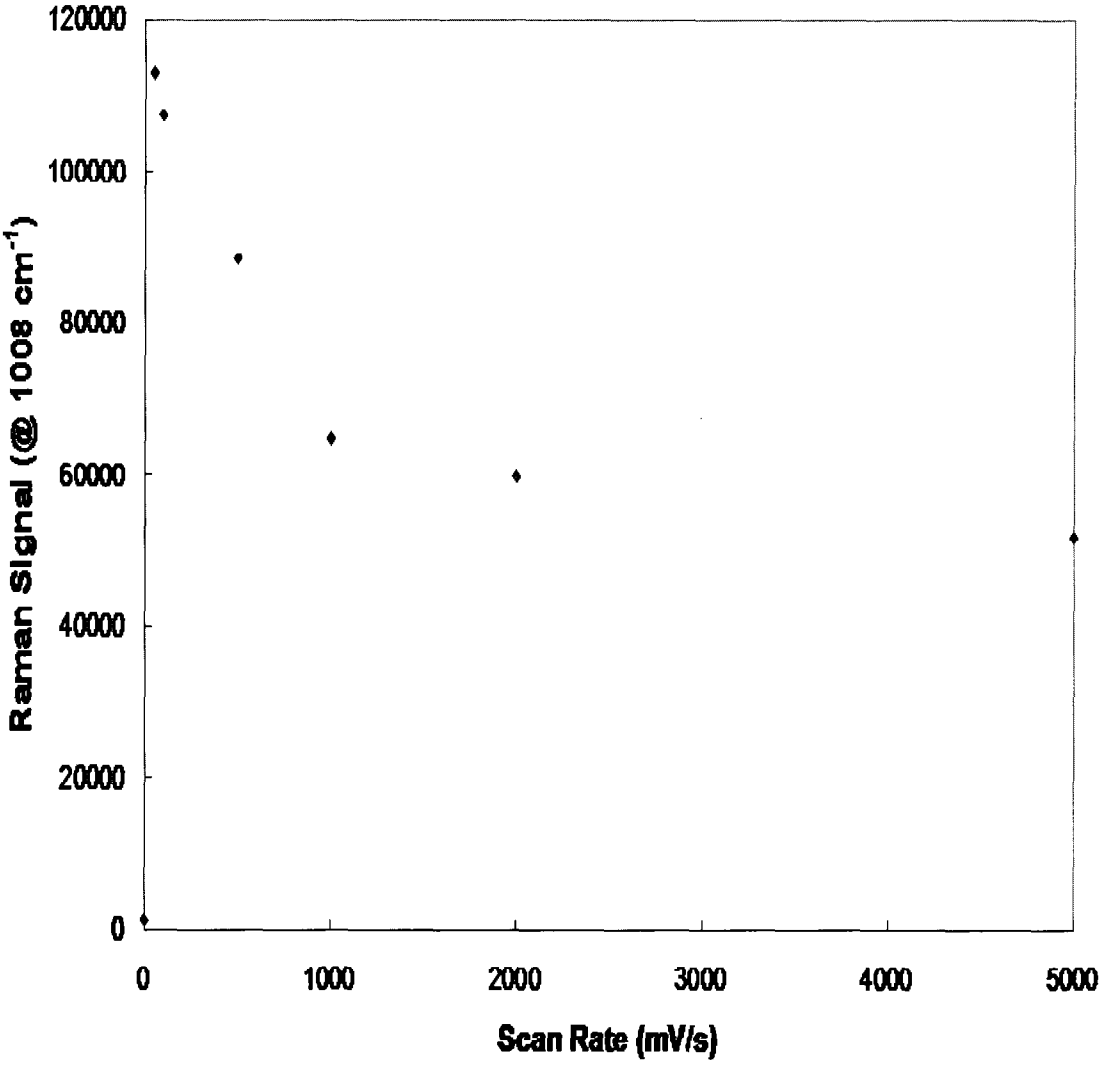

FIG. 17. Peak Raman signal versus scan rate for the electrochemical SERS spectra (max reverse potential 300 mV).

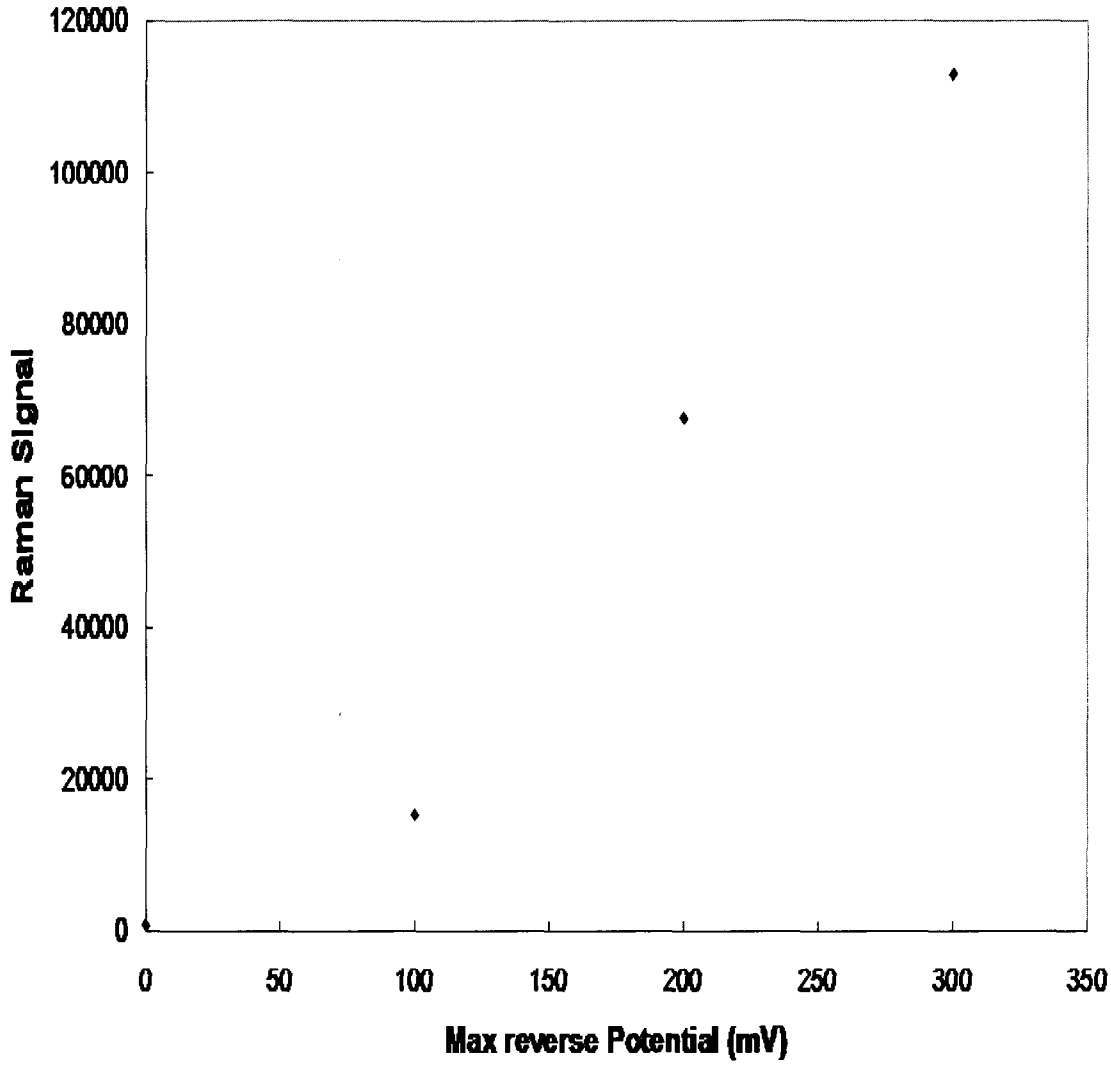

FIG. 18. Raman signal versus max reverse potential for Raman spectra obtained at a scan rate of 50 mV/s.

signal was found to occur at -700 mV. The variability of the SERS signal as the potential changed was due to the amount of pyridine absorbed to the electrode surface. At positive potentials the Raman signal was the lowest, meaning there was less pyridine absorbed to the electrode. As the potential became increasingly negative the amount of pyridine on the surface increased and, therefore, the Raman signal increased. At -700 mV the amount of pyridine absorbed reached a maximum and the Raman signal peaked at that point. Because of this, a Raman spectrum was acquired after twenty scans using the optimum parameters with the potential held at -700 mV. This spectrum is shown in Figure 19. The peak Raman signal at 986 nm was 327,675 which was the saturation point of the detector. This value is three times greater than the signal taken at -200 mV and is an enhancement of 1365 times. This is the maximum obtainable enhancement using the current detector.

Using the electrochemical method, we were able to observe a SERS signal from the adsorption of pyridine onto the surface of a roughened silver electrode. We were also able to optimize the oxidation-reduction cycle (ORC) parameters to maximize the magnitude of the SERS enhancement. During these experiments, the SERS enhancement of pyridine adsorbed to a silver electrode was characterized. This led to the demonstration of a significant SERS enhancement of pyridine. This method, however, was abandoned because it was determined to be impractical for the intended purposes of this dissertation. The use of a potentiostat and an electrochemical cell was considered to be too complicated for use outside of a research laboratory. In spite of that, the electrochemical method did serve as a quality introduction into the SERS phenomenon.

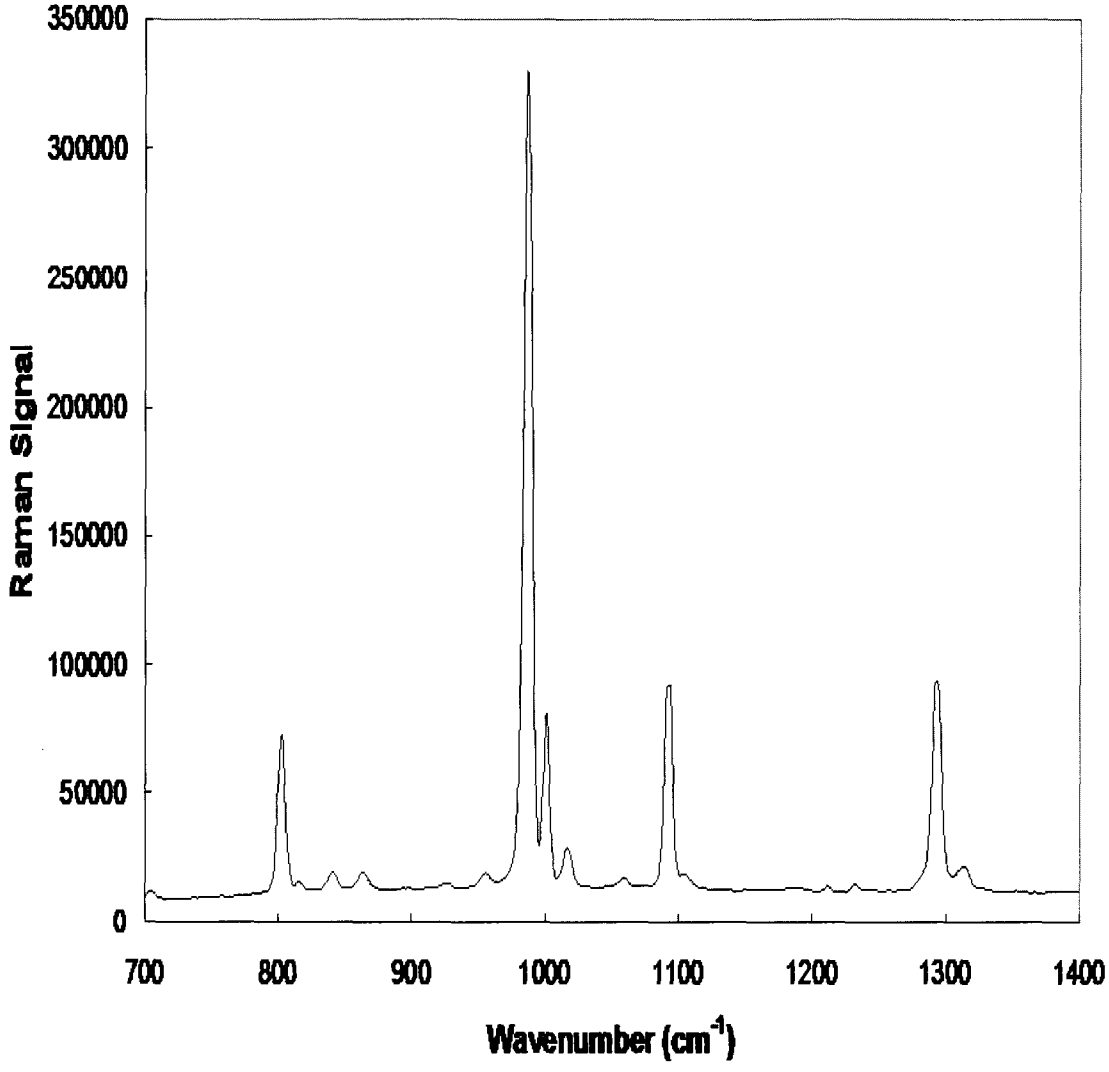

FIG. 19. Electrochemical SERS spectrum of pyridine obtained after 20 potential sweeps with a max forward potential of -900 mV, a max reverse potential of 300 mV, and a scan rate of 50 mV/s. The spectrum was obtained while holding the potential at -700 mV.

Silver Colloid SERS

Silver colloids are probably the most common substrate used to generate SERS enhancements.[10,15-17,98] Several metals, besides silver, have been used as SERS substrates. The two most common alternatives to silver are gold and copper. However, SERS enhancements have been observed from platinum, nickel, ruthenium, rhodium, palladium, cobalt, and iron.[99] Still, silver remains the most efficient SERS substrate primarily due to its strong surface plasmon resonance and its ability to adsorb many different molecules. That is why silver colloids were selected as an ideal SERS substrate for the analysis of amino acids. Another advantage to using silver colloids is that they are easy to prepare either chemically or via laser ablation and that they are compatible with biological systems.[86-90]

Colloids were prepared using two methods: chemical reduction of silver nitrate and the laser ablation of silver metal. Each method had its own inherent advantages and disadvantages. Chemically prepared colloids are easy to prepare and generate a large volume of fairly monodisperse particles. Particle size is also tunable by varying the rate of reduction.[86] The resulting particles are fairly stable and can be used for several months after preparation. The main disadvantage to chemically prepared colloids is that the reagents used in the reduction process will remain in the colloidal suspension and can cause an increase in the background Raman signal.[87] The primary advantage to laser-ablated colloids are that they have essentially no background Raman signal and will not interfere with the target SERS signal.[87] The drawbacks to this method of colloid preparation are that the process produces a small volume of particles and that the resulting particles are not stable. The lack of stability requires that the colloids be used as

soon as they are prepared. SERS experiments were performed using colloids generated via both methods.

For the colloid experiments, SERS spectra were acquired using a Raman 960 FT-Raman spectrometer (Thermo Nicolet). Traditionally, FT-Raman instruments are considered to be inferior to conventional Raman instruments because they are not as sensitive. However, there are several reasons why an FT-Raman instrument was used in lieu of a dispersive Raman instrument. FT-Raman bench top instruments are commercially available fully equipped and are made for ease of use. The use of a NIR excitation source (1064 nm) drastically reduces the background fluorescence along with the amount of laser-induced thermal damage. This makes the FT Raman ideal for analyzing biological systems. Also, the use of an interferometer helps to reduce detector noise and allows for high spectral resolution. Therefore, these advantages combined with the SERS enhancement can overshadow the lack of sensitivity attributed to the FT-Raman instrument.

Once prepared, the colloids were characterized by UV/Vis absorption. The resulting colloids from both methods were greenish yellow and had absorption maximum between 410-420 nm. For SERS experiments, the colloids were used as prepared with no special conditioning. Once prepared, SERS spectra were acquired from aqueous solutions of colloid and 7.5mm tryptophan. Four drops of 0.1M KNO_3 were used to initiate colloid aggregation. SERS spectra of tryptophan from both sets of colloids are shown in Figures 20 and 21. Details of the spectra and peak assignments are listed in Table IV. A spectrum of a 10 mM tryptophan solution in water with no silver colloid is

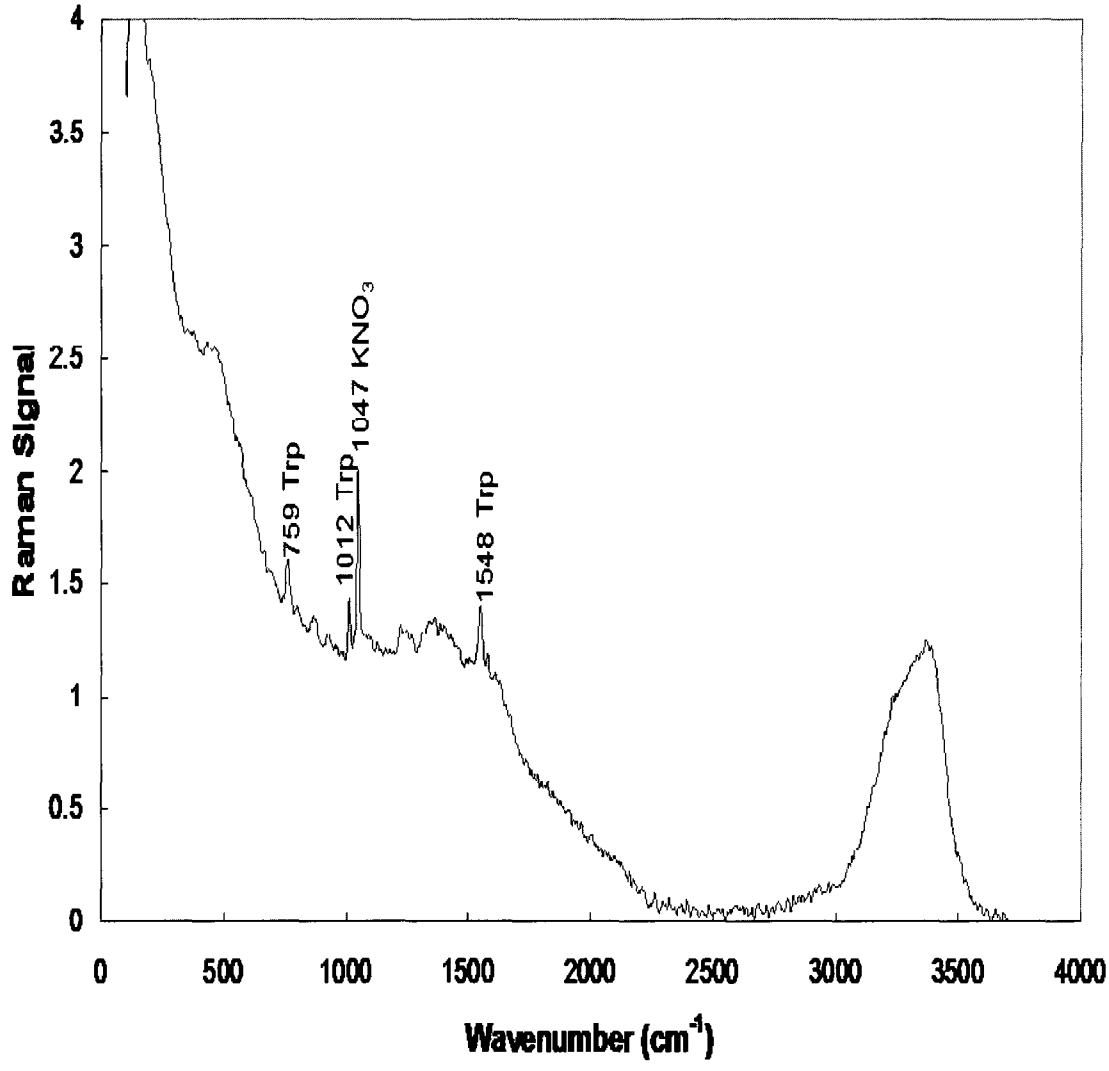

FIG. 20. SERS spectra of a 7.5 mM tryptophan solution using chemically prepared silver colloids.

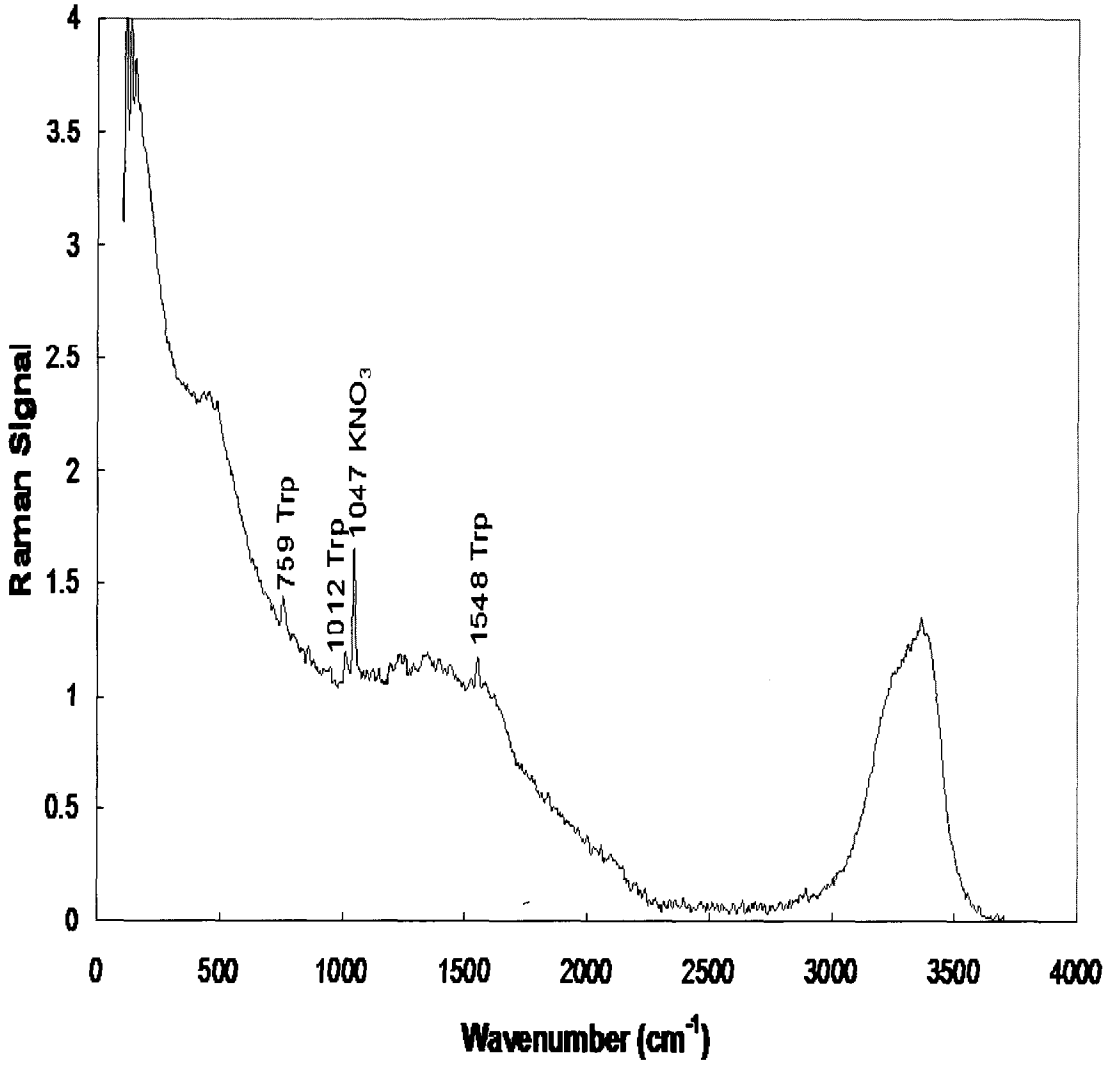

FIG. 21. SERS spectra of a 7.5 mM tryptophan solution using silver colloids prepared by laser ablation.

TABLE IV. Wavenumbers and Assignments for Tryptophan.

Raman Shift (cm^{-1})	Assignments[a]
759	Benzene and pyrrole ring breathing in-phase
1012	Benzene and pyrrole ring breathing out-of-phase
1047	KNO_3
1355	14pi benzene mode
1548	Totally symmetric naphthalene type stretching

[a] Spectra assignments based on reference 101.

given in Figure 22. In this spectrum there are no visible Raman peaks, only an increase in the background signal due to fluorescence of the tryptophan molecules. Raman peaks attributed to tryptophan at 759, 1012, 1355, and 1548 cm^{-1} are clearly visible in both Figures 20 and 21 verifying a SERS enhancement. The peak at 1047 cm-1 was attributed to the KNO_3 used to initiate aggregation. The quality of the SERS enhancement for both colloids was similar. Interestingly, there was no noticeable background Raman signal from the chemically-prepared colloid. For this reason and because they are easier to prepare in larger quantities, the chemically-prepared colloids were used in all subsequent experiments.

Initially, a series of experiments was conducted to determine the optimum conditions for aggregating the silver colloid. This was necessary because the magnitude of the SERS signal is highly dependent on the degree of colloid aggregation.[82] The first set of experiments utilized sodium chloride as the aggregating agent. This is perhaps the most commonly used compound for aggregation. SERS measurements were made on 5 ml samples of tryptophan (7.5 mM) prepared from stock solutions of aqueous silver

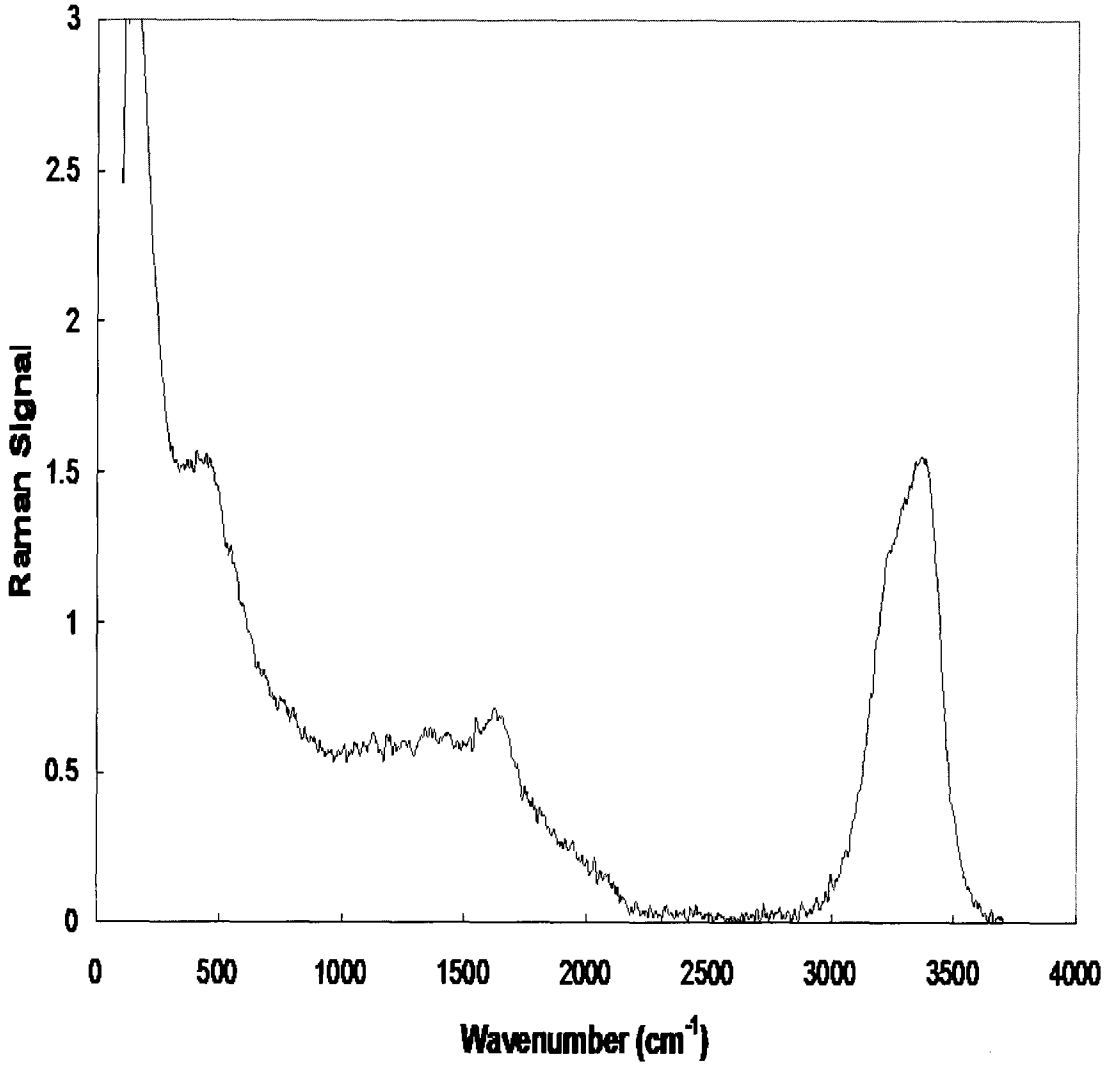

FIG. 22. Raman spectrum of a 10 mM tryptophan solution in water.

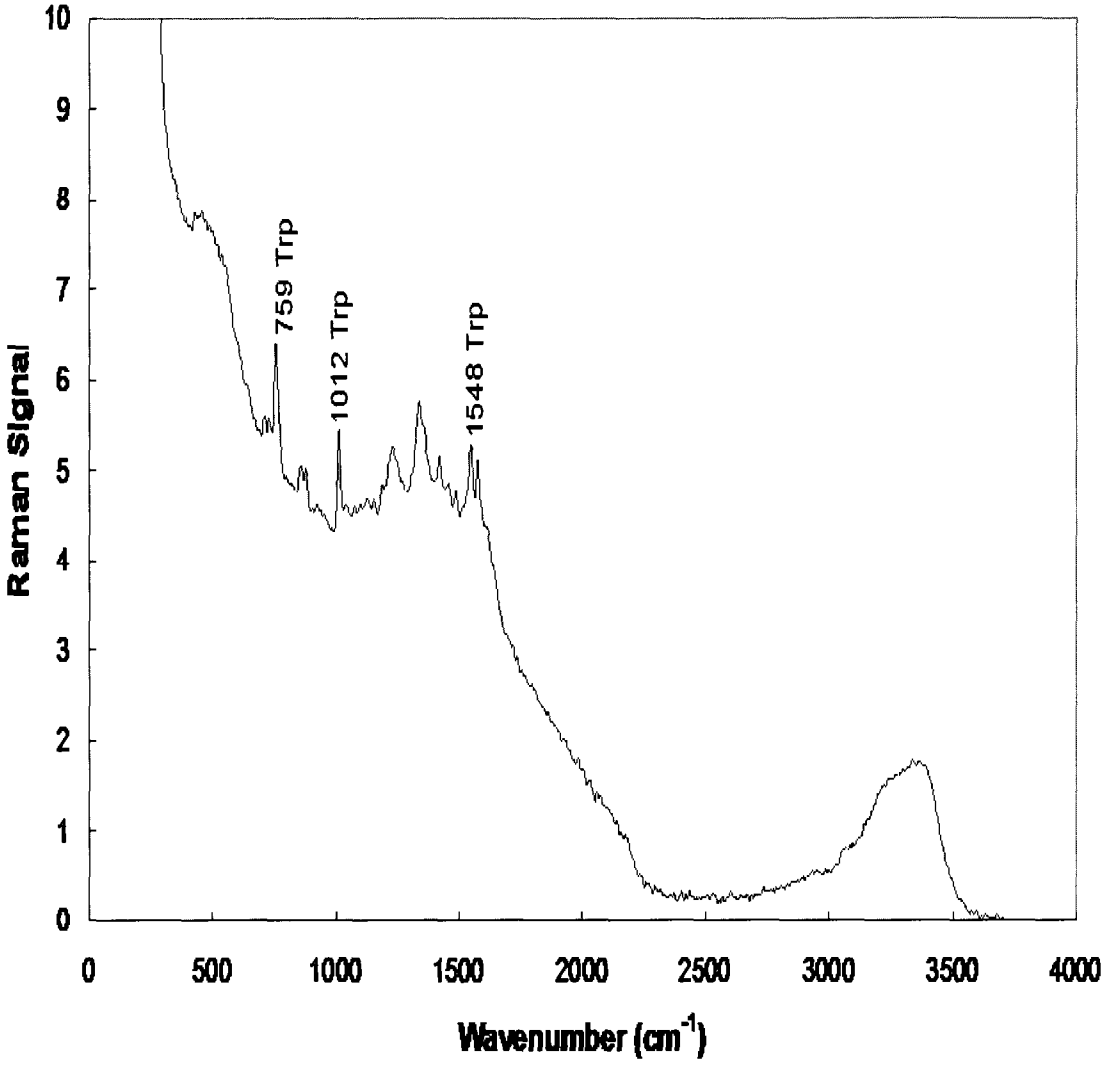

FIG. 23. SERS spectrum of 7.5 mM tryptophan solution from silver colloid aggregated with 4 drops of a 1M NaCl solution. The resulting concentration of NaCl was 0.02 M.

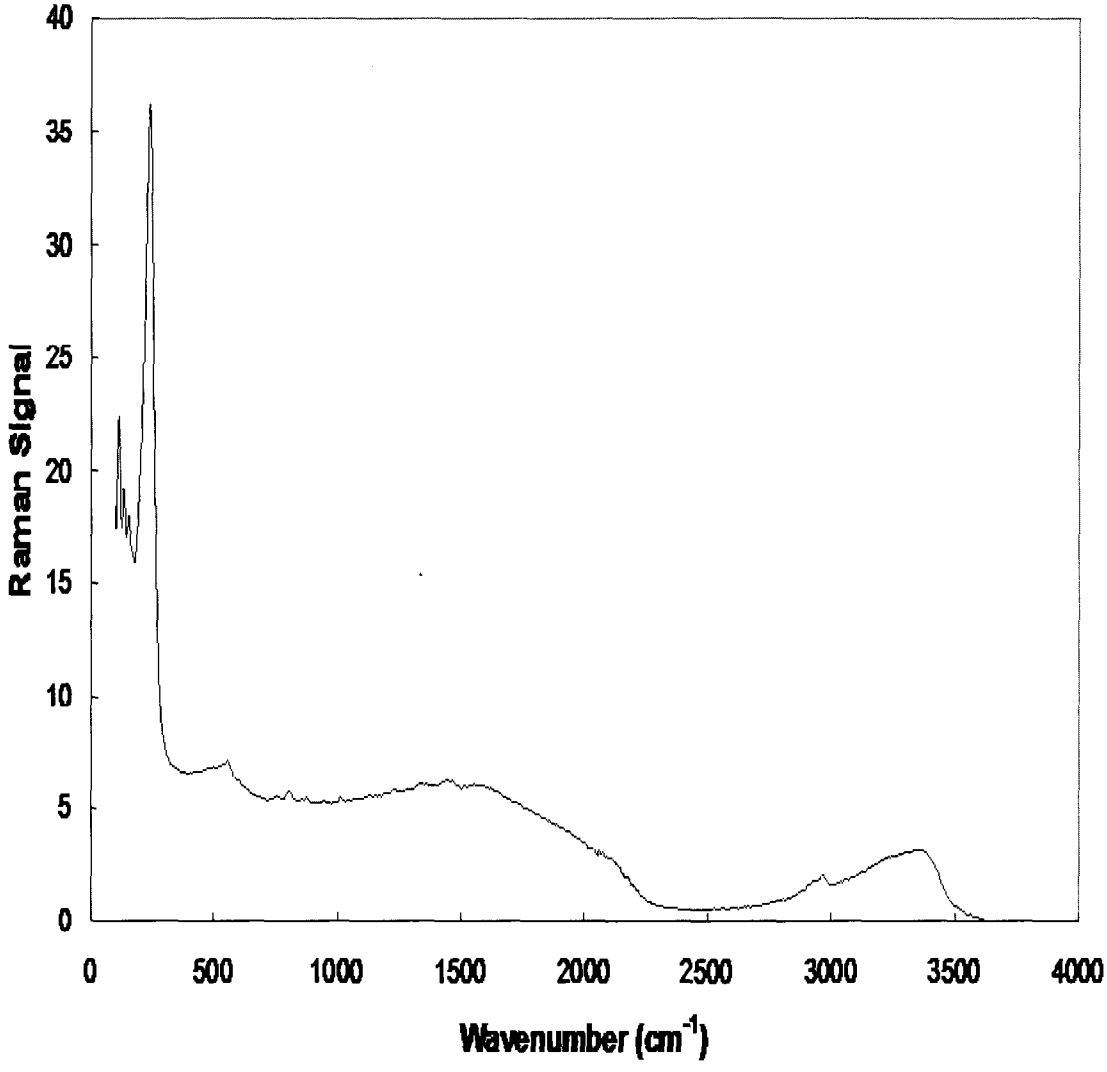

FIG. 24. SERS spectrum of 7.5 mM tryptophan solution from silver colloid aggregated with 100 mg of NaCl. The resulting concentration of NaCl was 0.34 M.

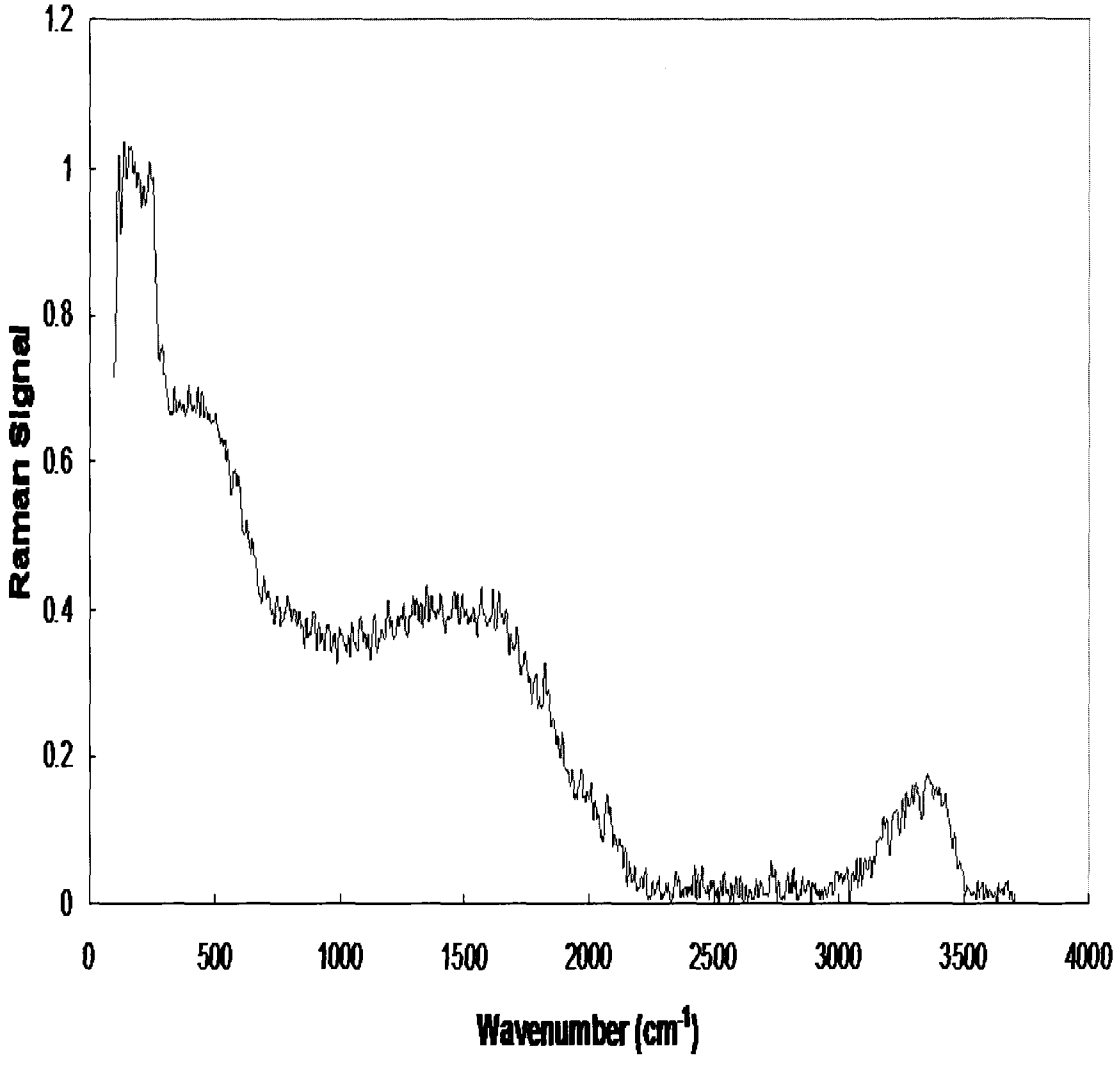

FIG. 25. SERS spectrum of a silver colloid solution aggregated by four drops of a 1 M NaCl solution.

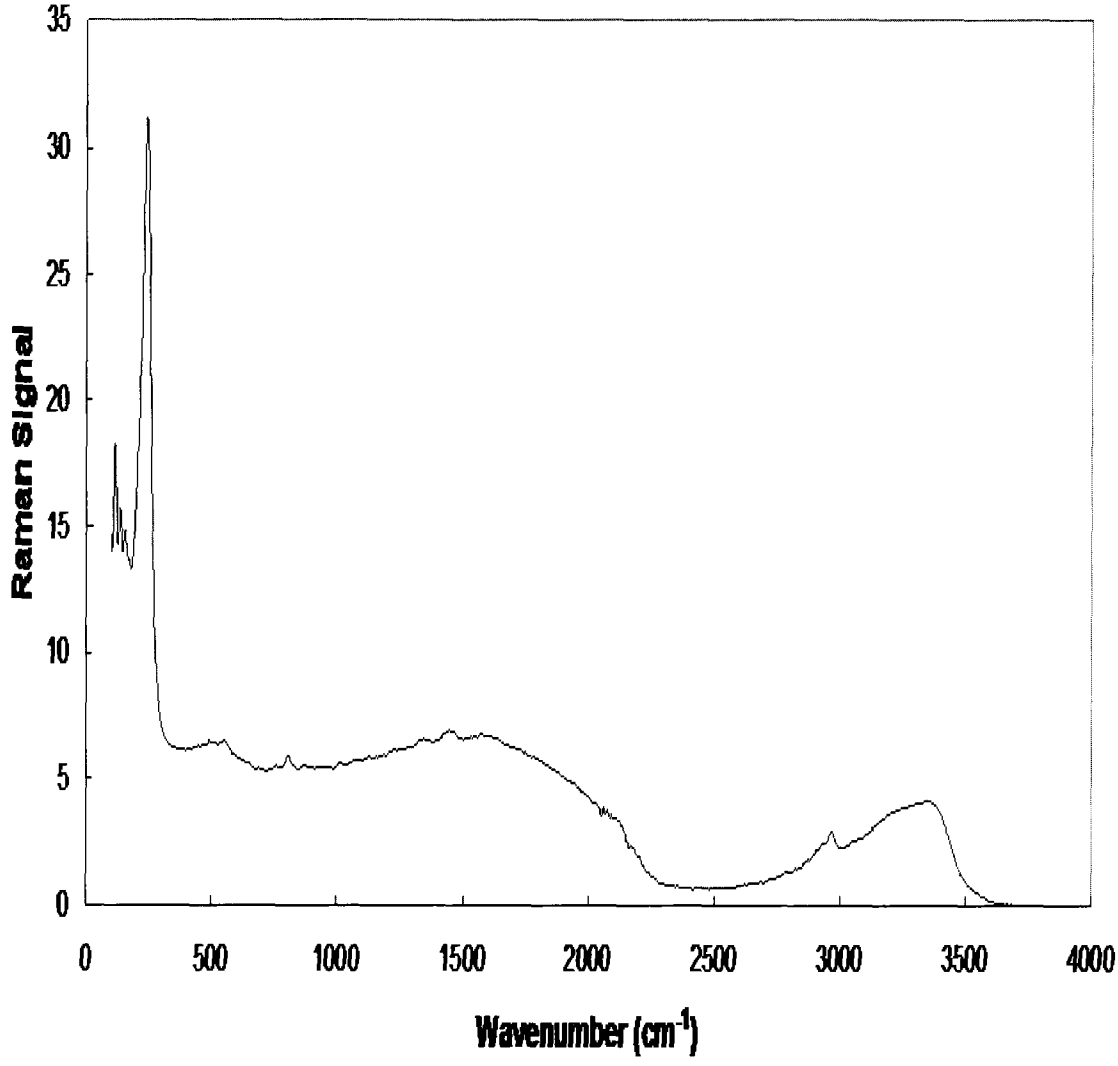

FIG. 26. SERS spectrum of a silver colloid solution aggregated by 100 mg of NaCl.

colloid. Aggregation of the colloid was induced by either adding 100 mg of solid NaCl to the samples or by adding four drops (~100 μl) of 1M aqueous NaCl. The resulting NaCl concentration in the sample for each method of aggregation was 0.34 M and 0.02 M, respectively. A spectrum from both methods is given in Figures 23 and 24. As a control, SERS measurements were also made on 5 ml samples consisting only of aqueous silver colloid and 100 mg NaCl or 4 drops of 1 M NaCl (Figures 25 and 26). Looking at the spectra of both the control and tryptophan sample with 100 mg NaCl in Figure 24 and Figure 26, no distinct Raman peaks are apparent. The distinguishing feature of the spectra is a highly intense and broad signal which occurs between 2000 and 500 cm^{-1}. This broad and intense signal can be attributed to formation of large silver aggregates which generated a large amount of Rayleigh scattering at all wavelengths. The intensity of Rayleigh scattering is orders of magnitude greater than Raman scattering and will therefore overshadow any detectable Raman signal. The size of the silver aggregates is a function of the ionic strength of the solution. In this case the ionic strength was too high due to the concentration of NaCl and large aggregates were formed. When only 4 drops of 1M NaCl was used to induce aggregation, the large background Raman signal was eliminated. This is evident in Figure 25. Aggregation at this concentration of NaCl was adequate to generate a SERS signal from the tryptophan molecules, as seen in Figure 23. This concentration of NaCl was used to initiate colloid aggregation in all subsequent experiments.

Once the ability to consistently generate SERS spectra from tryptophan was established using the silver-colloid solutions, experiments were conducted to quantify the concentration of tryptophan in the sample. Quantification of SERS signal using silver

colloids proves to be quite difficult due to the irreproducible nature of generating aggregated colloids. One way to overcome this problem is to include an internal standard at a known concentration in the sample; thus the Raman signal from the analyte can be compared with the signal from the internal standard. The ratio of the two, theoretically, would not be dependent on the variability of the aggregation process. Therefore, reproducible values could be acquired from analyte samples allowing for quantification.

Potassium nitrate was selected as an internal standard for our experiments. Potassium nitrate was an ideal candidate for use as an internal standard because it generates a strong Raman signal at 1050 cm^{-1} that would not interfere with any signal from the amino acids (Figure 27.). Also, potassium nitrate could function as an aggregating agent eliminating the need to use NaCl.

SERS spectra of 7.5 mM tryptophan with 0.2 M and 0.02M KNO3 were acquired. The resulting spectra are shown in Figures 28 (a) and 28 (b), respectively. In both spectra, the tryptophan peaks at 759, 1012, and 1548 cm^{-1} and the KNO_3 peak at 1047 cm^{-1} are clearly visible. Also, the KNO_3 peak is plainly distinguishable from the tryptophan peaks. This result demonstrates the ability of KNO_3 to be used as an internal standard.

A set of experiments was designed to establish the optimum concentration of KNO_3 to be used for quantification. However, after some consideration, the silver-colloid method of SERS detection was abandoned. The primary reason for this decision was the promise of developing a more practical method for SERS detection. The colloid method of SERS detection was considered impractical because of the need to induce colloid aggregation, which requires a multi-step sample preparation. Also, the timing of

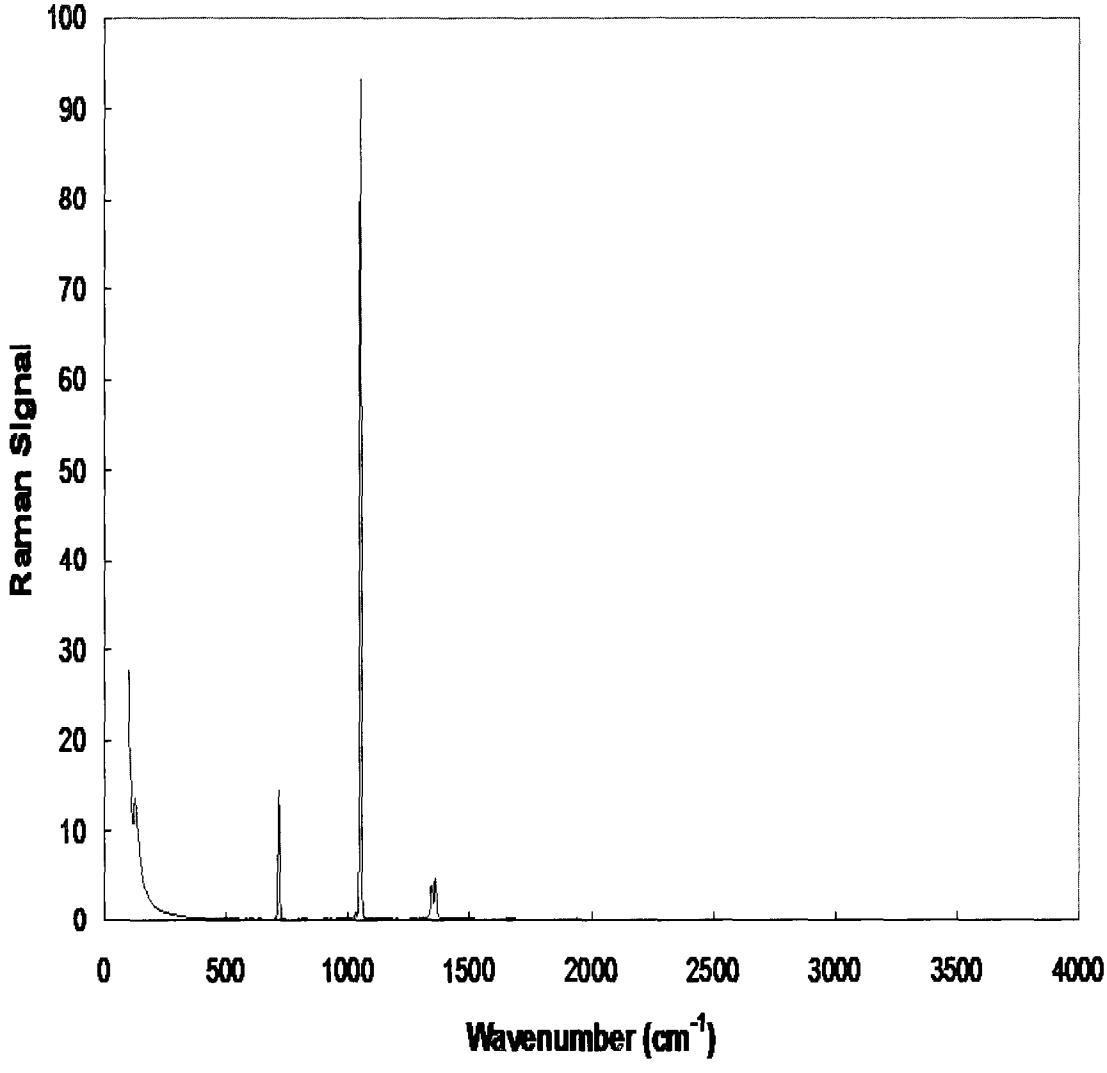

FIG. 27. FTIR Raman spectrum of solid potassium nitrate (KNO_3).

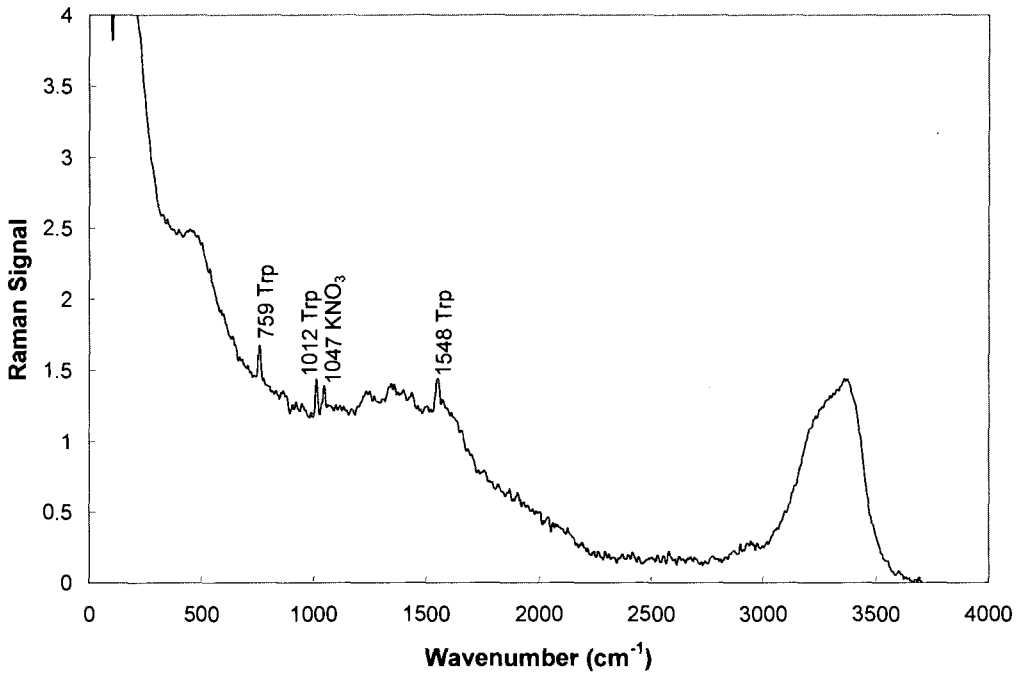

(a)

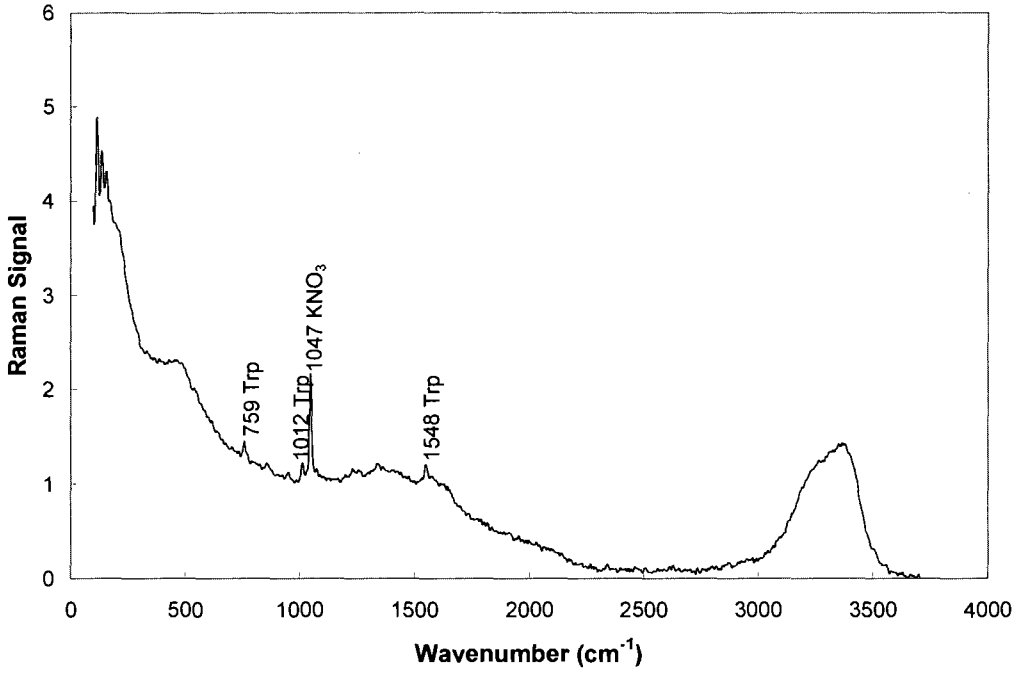

(b)

FIG. 28. SERS spectra of a silver colloid solution with (a) 7.5 mM tryptophan + 0.20 M KNO_3 and (b) 7.5 mM tryptophan + 0.02 M KNO_3.

SERS measurements after aggregation is critical and requires great precision in order to generate consistent signals. For these reasons the focus of our research shifted to developing a simple and novel method for SERS detection.

SERS on Silver-Coated Quartz/Glass Fiber Filters

While attempting to develop a practical method for SERS analysis of biological molecules, two things were considered. First, the method should require little or no sample preparation. Second, the method should be compatible with current commercially available instrumentation. With this in mind, a novel substrate was developed which allowed for the direct SERS measurement of unknown biological samples. The substrate consisted of a thin film of silver deposited on a quartz fiber filter. The silver was deposited onto the filter utilizing the "mirror reaction".[91] This simple method for silver deposition has previously been used to prepare silver surfaces on glass slides and silicon chips for SERS detection.[91] The quartz fiber filter was selected as the surface for deposition because it was porous and could easily absorb a liquid sample. Also, the roughness of the silver film would be amplified due to the fibrous nature of the filter. Using this substrate, the sample to be analyzed could be directly transferred to the filter surface and immediately placed in a Raman instrument for SERS measurements.

The first step in developing the new substrate was to demonstrate the ability to generate a SERS-active surface on the quartz fiber filter using the "mirror reaction". The reduction of ($[Ag(NH_3)_2]^+$) by glucose in the presence of the quartz fiber filters was carried out at a temperature of 35 °C for 30 minutes. The filters were then immediately flushed with 1L of 18 MΩ milliQ water and air dried overnight at room temperature. SEM micrographs of the coated filters prepared under the above conditions are shown in

Figure 29. As can be seen from the image, the entire surface of each fiber was covered with silver. There was some noticeable aggregation or clumping of particles but the overall coating of the fibers appears fairly regular. The utility of the filter as a SERS-active substrate was demonstrated by measuring the Raman spectra from a 100 µl sample of a 10mM phenylalanine solution adsorbed to the filter surface. SERS measurements were made using a Raman 960 FT-Raman spectrometer (Thermo Nicolet). A representative SERS spectrum of phenylalanine acquired from a silver-coated filter is given in Figure 30. Details of the spectrum and peak assignments are listed in Table V.

Once the ability to generate SERS signals from phenylalanine was demonstrated, experiments were conducted to determine the filters ability to detect tryptophan. Tryptophan is one of the aromatic amino acids and is extremely fluorescent which makes it difficult to be detected by traditional Raman methods. Tryptophan has a pI value of 5.89. SERS measurements were acquired from 100 µl samples of 10mM tryptophan solutions. A typical tryptophan spectrum can be seen in Figure 31. Details of the spectrum and peak assignments are listed in Table VI. As expected there is a strong background fluorescent signal but a distinct SERS fingerprint can be clearly seen. This result is comparable to the tryptophan spectra acquired from the silver-colloid solutions.

The next set of experiments consisted of acquiring SERS spectra from equal mixtures of phenylalanine and tryptophan. The objective of the experiments was to determine if both amino acids could be differentiated from one another from a single SERS spectrum. SERS spectra were acquired from aqueous solutions of 5mM tryptophan and 5 mM phenylalanine. A representative spectrum is given in Figure 32. From this spectrum it is apparent that the dominating features are due to the tryptophan

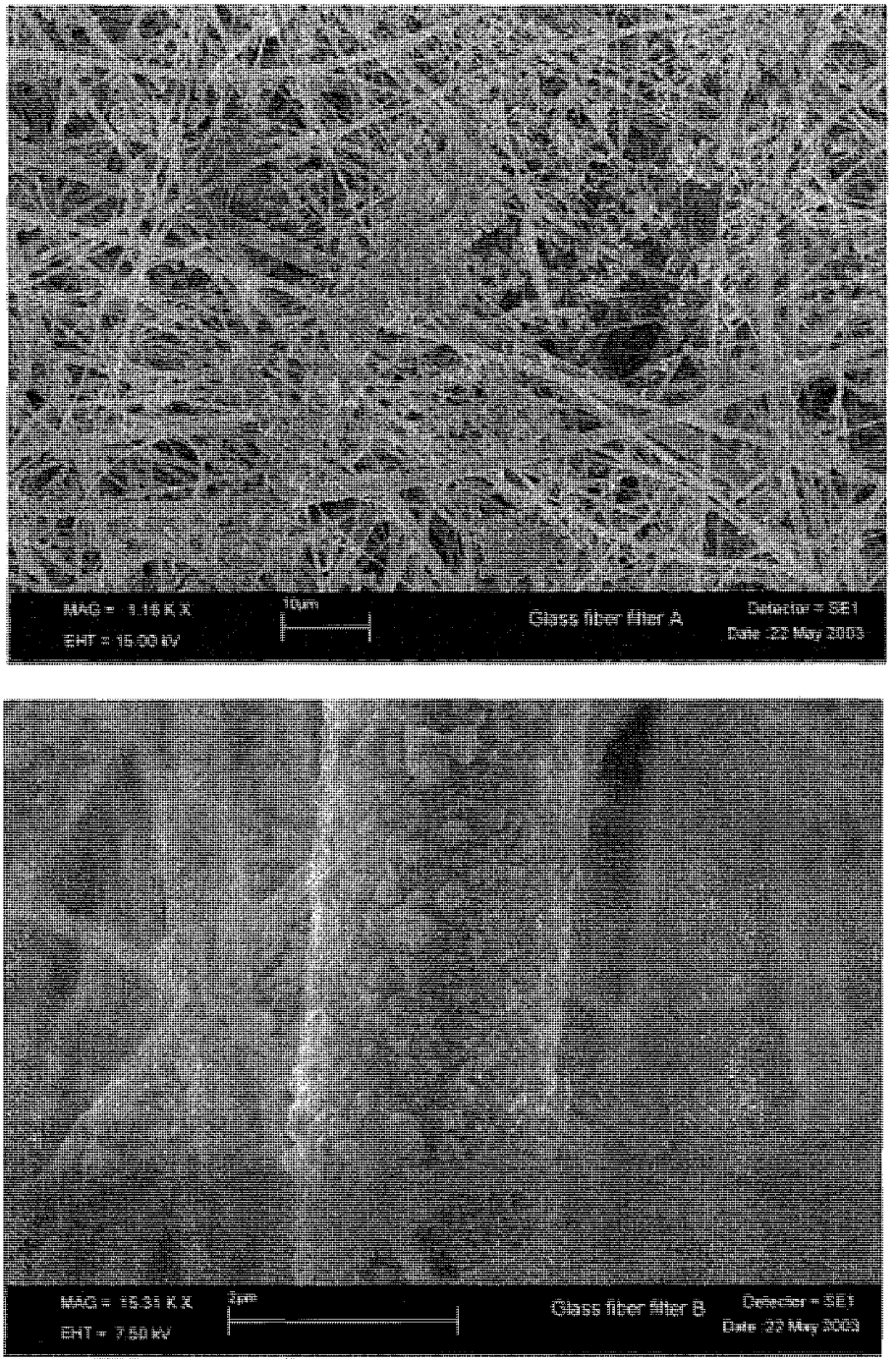

FIG. 29. Scanning electron micrographs of a silver-coated glass fiber filter (25 mm Whatman GF/A) prepared using the "mirror" reaction. The reaction was conducted at a temperature of 35 °C for 30 minutes.

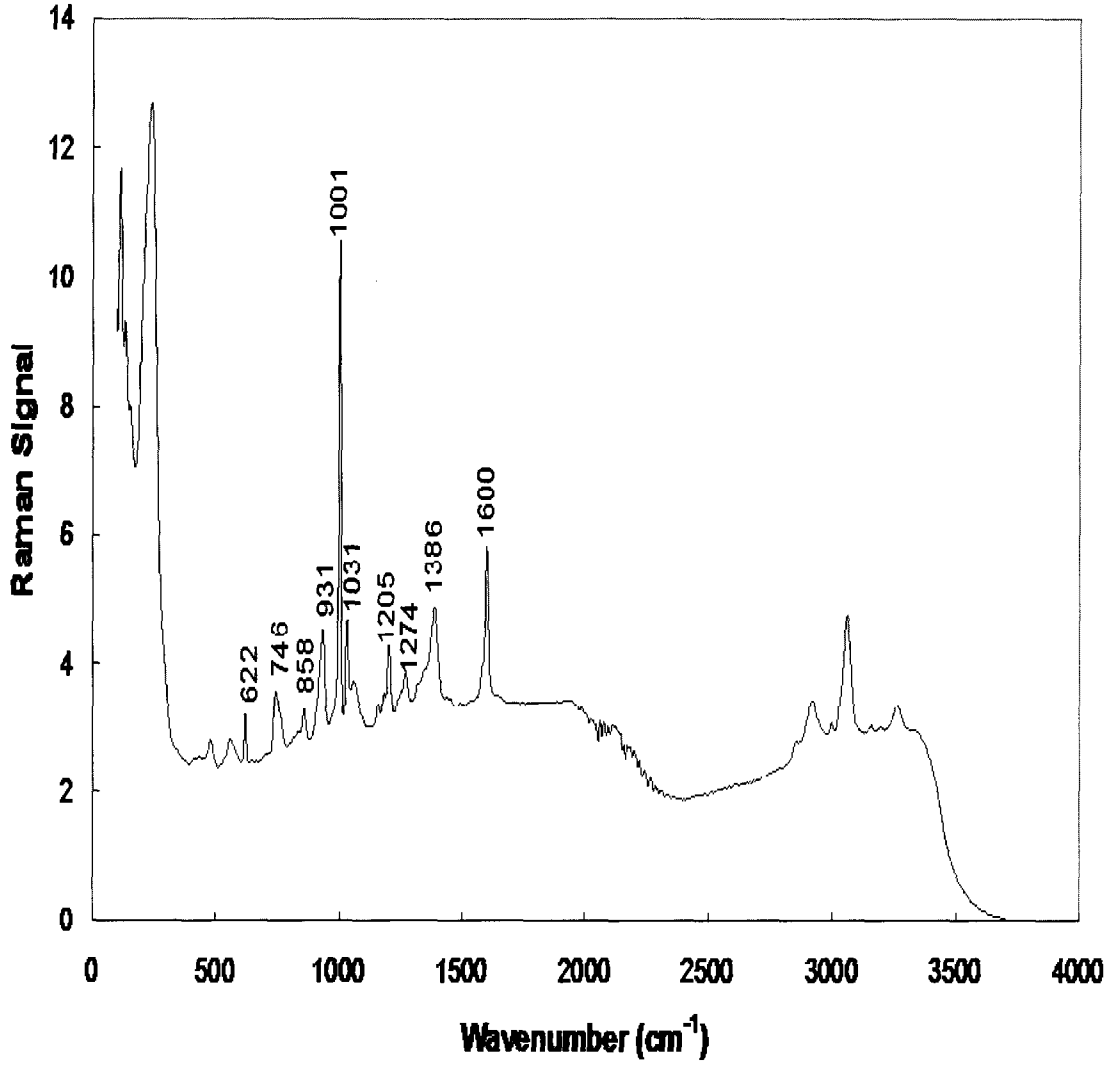

FIG. 30. SERS spectrum of a 10 mM phenylalanine solution (100 μl) adsorbed onto the surface of a quartz fiber filter (25 mmWhatman QM-A).

TABLE V. Wavenumbers and Assignments for Phenylalanine.

Raman Shift (cm^{-1})	Assignments[a]
622	ν6b inplane ring deformation
746	ν1 symmetric ring breathing
858	-
931	C-COO^- - stretching
1001	ν12 symmetric ring stretch
1031	ν18a inplane CH bending
1205	ν7a phenyl-C stretch
1274	-
1386	C-COO^- - symmetric stretching
1600	ν8a inplane ring stretching

[a] Spectra assignments based on reference 100.

molecules. The large fluorescence background and the peaks at 750, 1350 and 1548 cm-1 are indicative of tryptophan. However, two phenylalanine peaks are clearly visible at 1001 and 1031 cm^{-1}. These two peaks displace the tryptophan peak at 1012 cm^{-1}. One other phenylalanine peak is slightly visible at around 1600 cm^{-1}. This result confirms the ability to identify two individual amino acids in a mixture using the silver-coated filters. Even with the strong background fluorescence from the tryptophan, the phenylalanine was still detectable.

During the course of our SERS experiments, an important observation was made. If multiple SERS measurements were made consecutively on the same filter, in the same location on the filter's surface, the SERS signal would gradually increase over time until the detector became saturated. The signal increase was attributed to the heat generated from the continuous exposure of the filter to the NIR source. An example of this is shown in Figure 33. This would present a serious problem when trying to quantify the SERS measurement because a single concentration of amino acid could result in variable

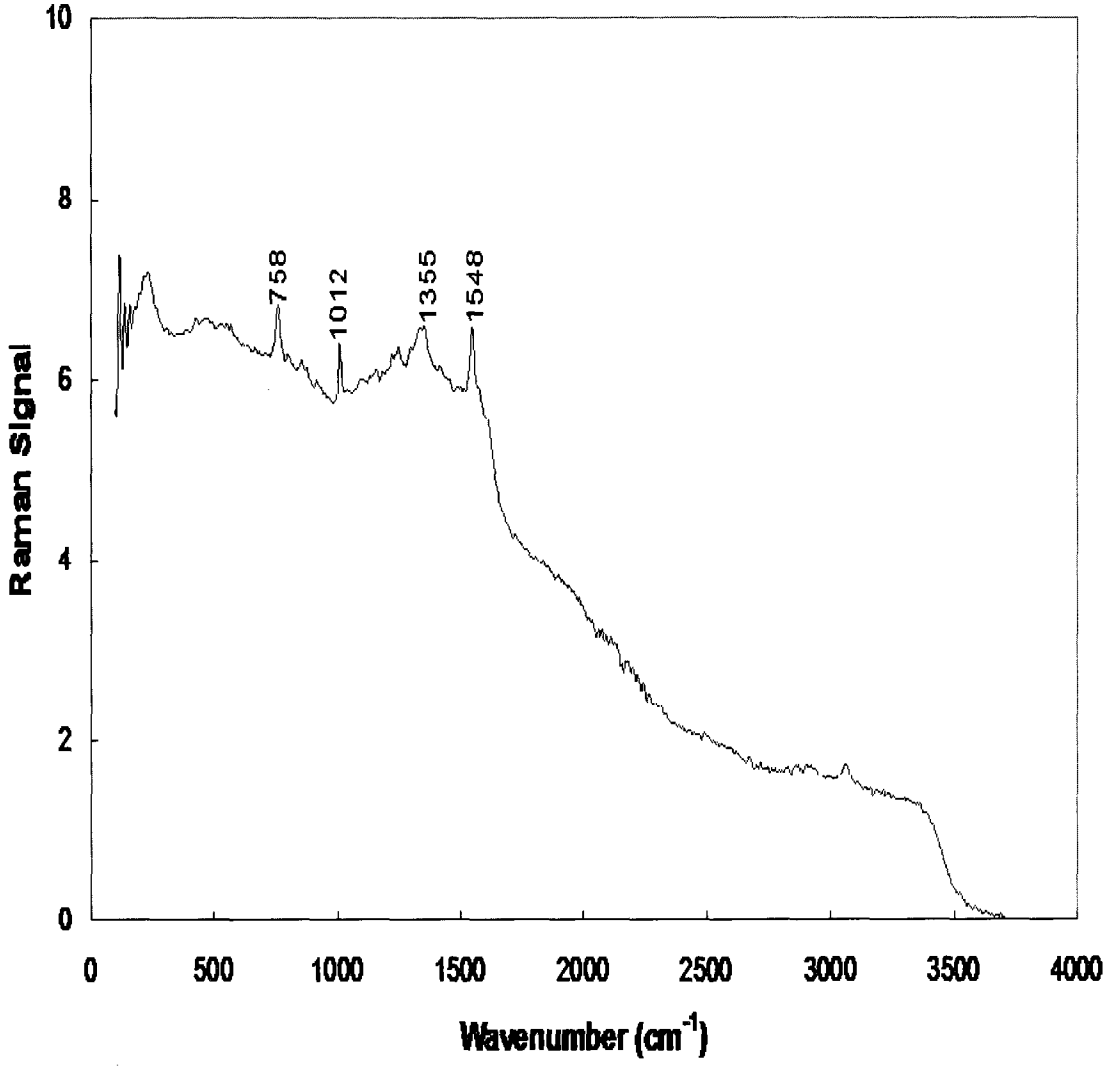

FIG. 31. SERS spectrum of a 10mM tryptophan solution (100 μl) adsorbed onto the surface of a silver-coated glass fiber filter (25 mm Whatman GF/A).

TABLE VI. Wavenumbers and Assignments for Tryptophan.

Raman Shift (cm^{-1})	Assignments[a]
759	Benzene and pyrrole ring breathing in-phase
1012	Benzene and pyrrole ring breathing out-of-phase
1355	14pi benzene mode
1548	Totally symmetric naphthalene type stretching

[a] Spectra assignments based on reference 101.

signal values depending on how long it was exposed to the laser. To prevent this from happening, a standardized procedure for acquiring SERS spectra from the filters was developed. A sample volume of 100 μl transferred via pipette directly onto the center of the coated side of the filter was used as a standard volume for each measurement. This volume allowed for adequate wetting of the filter without it becoming saturated. Once the sample was completely absorbed into the filter and no visible liquid was observed on the surface, the filter was placed directly onto the sample holder and inserted into the sample compartment. At this point the laser was immediately focused onto the filter surface and spectra were acquired. The Raman 960 FT-Raman spectrometer was set to acquire a single spectrum after 64 scans with a resolution of 8 nm with the laser power set at 0.2W. Using these settings, it took 2 minutes to acquire a single spectrum. This protocol was followed for all subsequent SERS measurements.

The most difficult task for the development of any SERS technique is to quantify the SERS signal. The ability to combine quantitative analysis with the already powerful qualitative analysis would make any SERS technique an extremely valuable tool in analytical chemistry. The first attempts to quantify the SERS signal generated from the

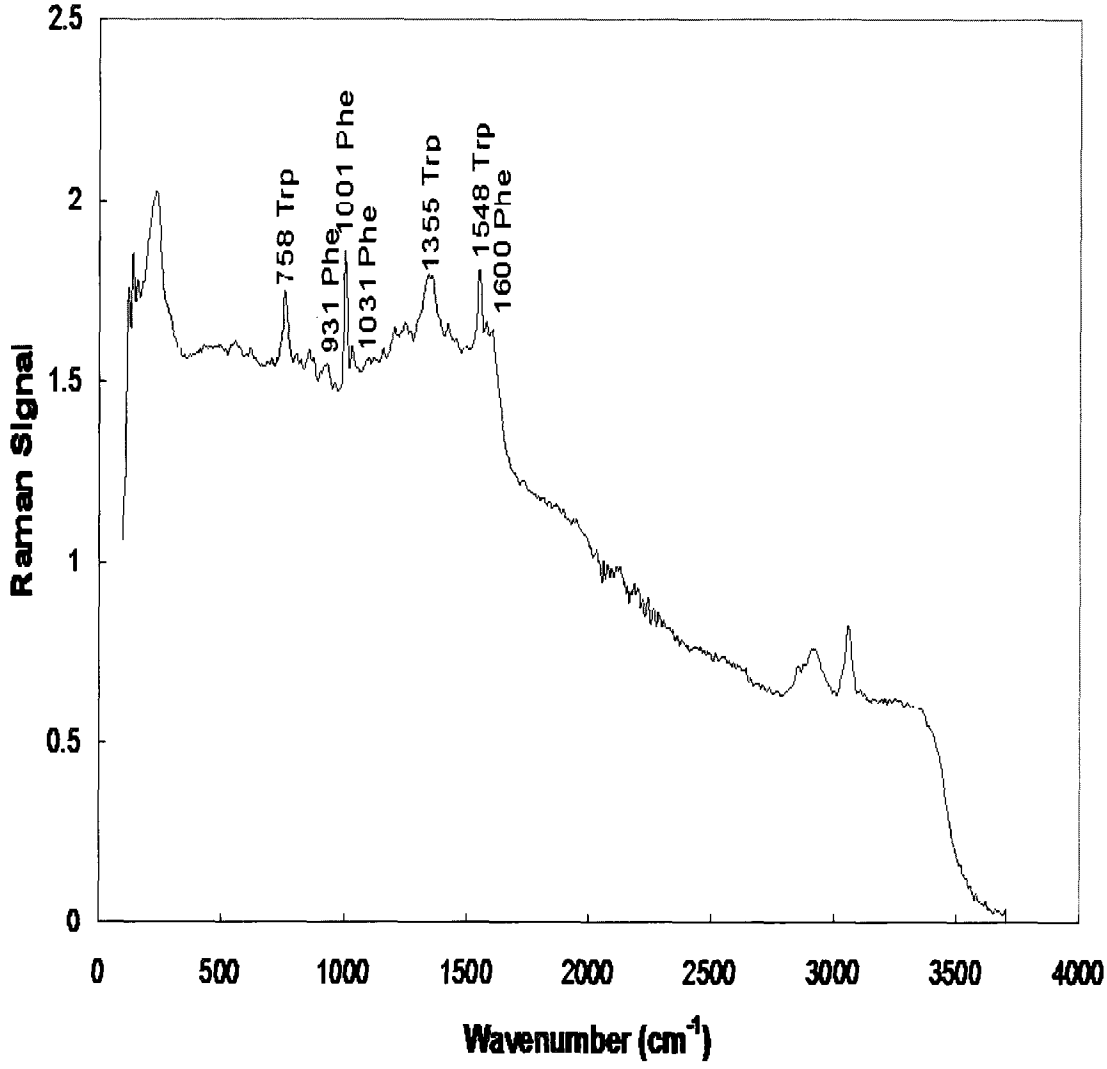

FIG. 32. SERS spectrum of a 5mM phenylalanine + 5mM tryptophan mixture (100 μl) adsorbed onto the surface of a silver-coated glass fiber filter (25 mm Whatman GF/A).

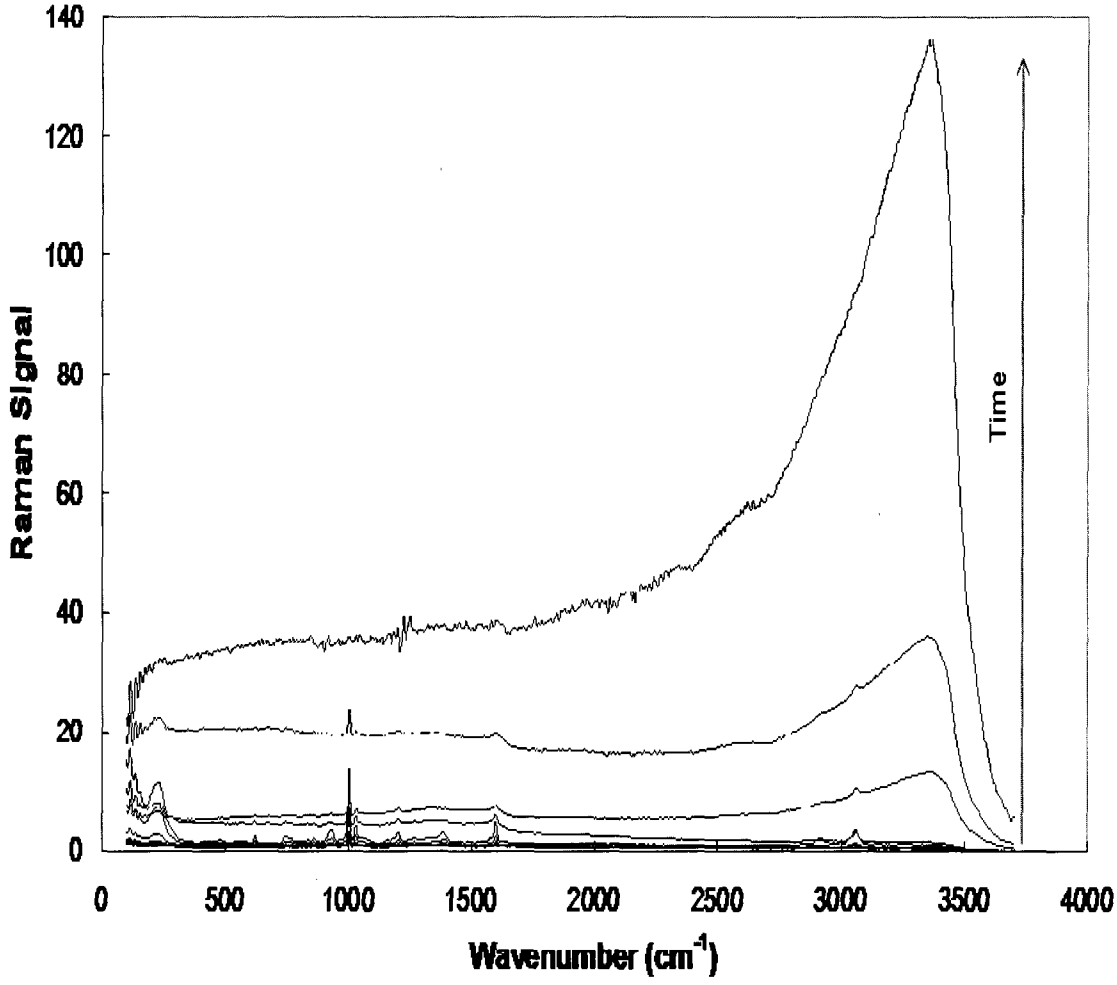

FIG. 33. Sequential spectra of a 10 mM phenylalanine solution (100 μl) adsorbed onto the surface of a silver-coated glass fiber filter (25 mm Whatman GF/A) with continuous laser exposure at a power of 0.2 W for 32 minutes. Spectra were acquired every two minutes.

silver-coated quartz/glass fiber filters involved the use of an internal standard. Potassium nitrate was selected to be used as an internal standard for the initial testing. Its peak wavelength at 1047 cm^{-1} is strong and should not interfere with any of the amino acid peaks. Phenylalanine was chosen as the amino acid to be used in the testing. Figures 34-37 show the SERS spectra of mixtures of phenylalanine and KNO_3. At the low phenylalanine concentrations, the KNO_3 peak at 1047 cm^{-1} is noticeably larger then the phenylalanine peak at 1001 cm^{-1}. As the phenylalanine concentration is increased the peak at 1001 cm^{-1} becomes more dominant. A plot of the ratio of the phenylalanine peak at 1001 cm^{-1} with the KNO_3 peak at 1047 cm^{-1} versus phenylalanine concentration is given in Figure 38. A linear regression of the data is displayed on the plot, along with the equation of the line and the R^2 value. This result was promising and demonstrated the proof of concept for using KNO_3 as an internal standard to quantify the phenylalanine SERS signal. However, a plot of the phenylalanine peak height at 1001 cm^{-1} versus phenylalanine concentration revealed a greater linearity then the previous plot. This plot is given in Figure 39. This led us to believe that quantification of the SERS signal could be possible without the use of an internal standard.

Experiments were conducted to test the reproducibility of the previous results. The experiments were designed to analyze the intensity of the SERS signal at a specific wavenumber for a given set of amino acid concentrations. In this way, we could determine if there was a linear dependence of the SERS signal on the amino acid concentration and develop a calibration curve for the filters. Phenylalanine was the amino acid used for all quantification experiments.

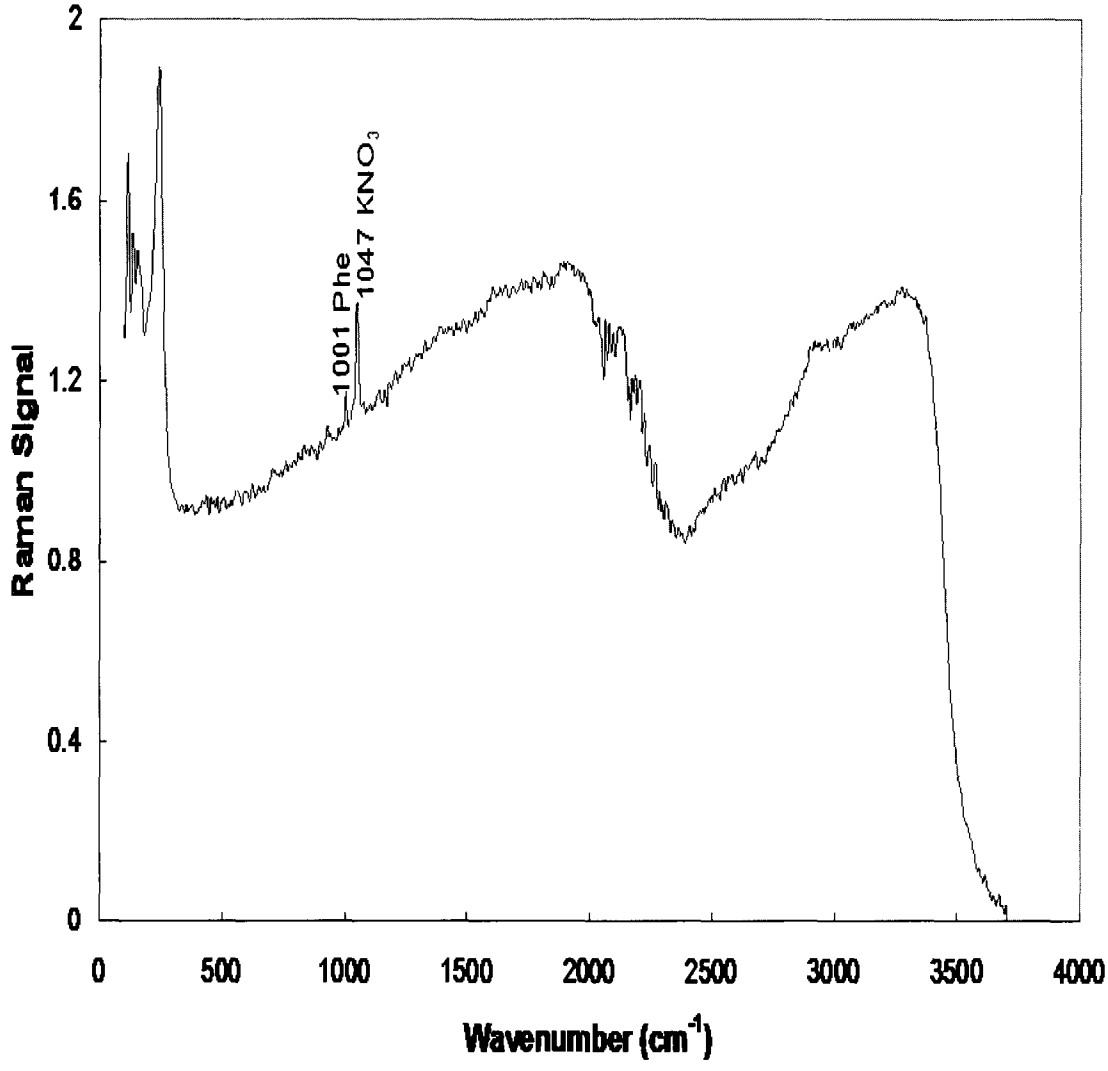

FIG. 34. Average of three SERS spectra of a 0.5 mM phenylalanine + 0.25 M KNO_3 solution (100 µl) adsorbed onto the surface of a silver-coated glass fiber filter (25 mm Whatman GF/A).

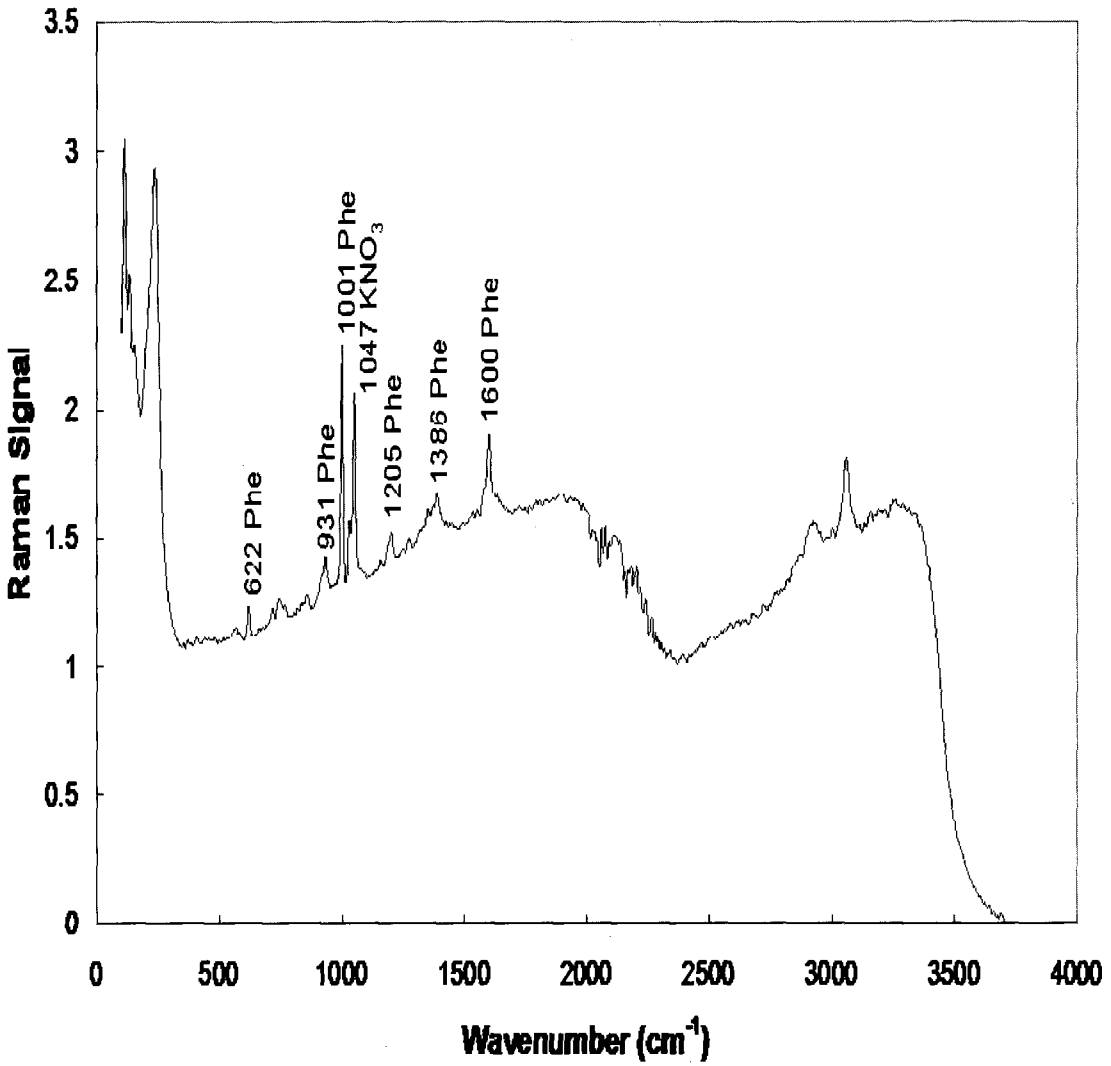

FIG. 35. Average of three SERS spectra of a 1mM phenylalanine + 0.25 M KNO_3 solution (100 μl) adsorbed onto the surface of a silver-coated glass fiber filter (25 mm Whatman GF/A).

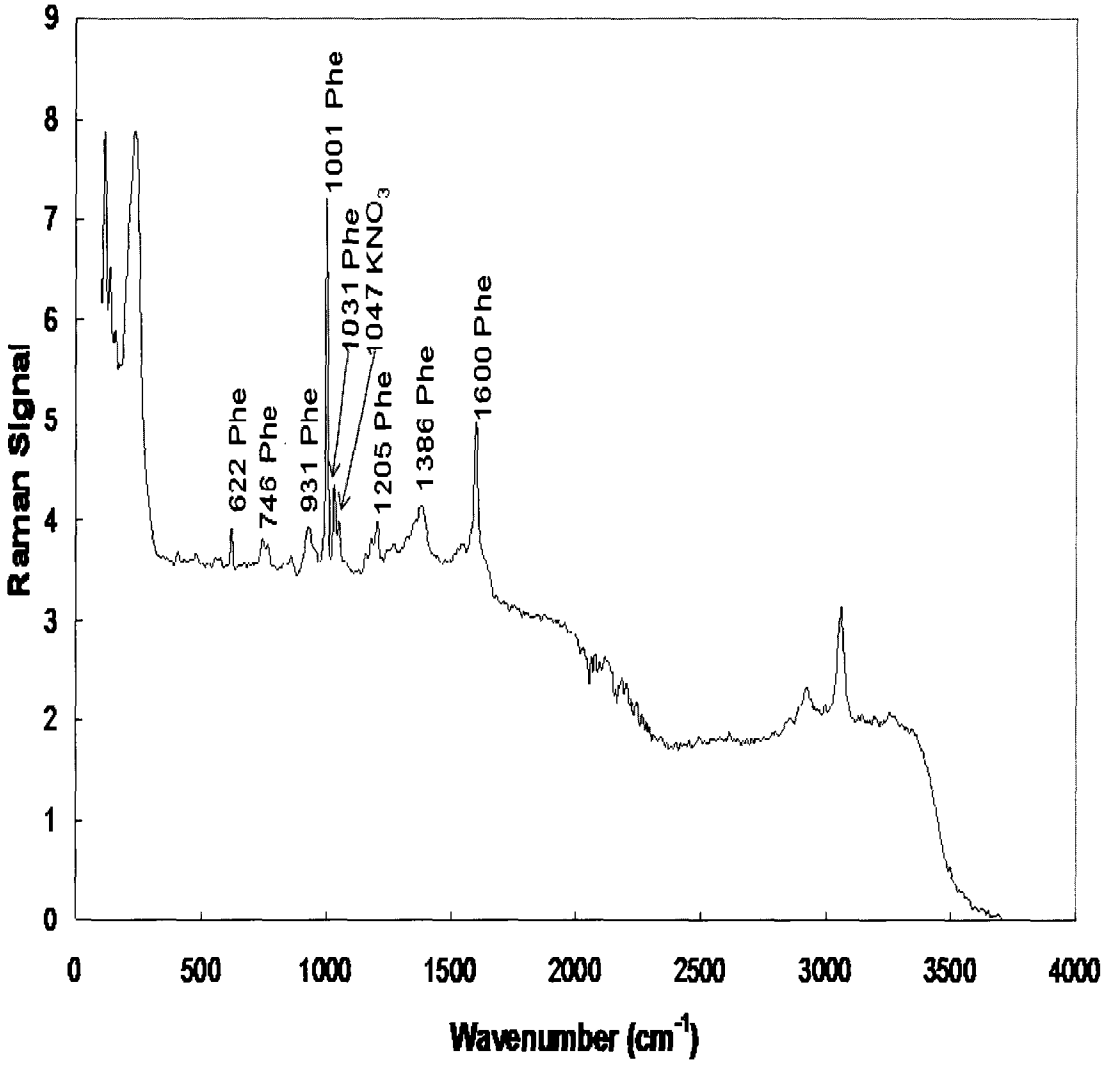

FIG. 36. Average of three SERS spectra of a 2.5 mM phenylalanine + 0.25 M KNO_3 solution (100 µl) adsorbed onto the surface of a silver-coated glass fiber filter (25 mm Whatman GF/A).

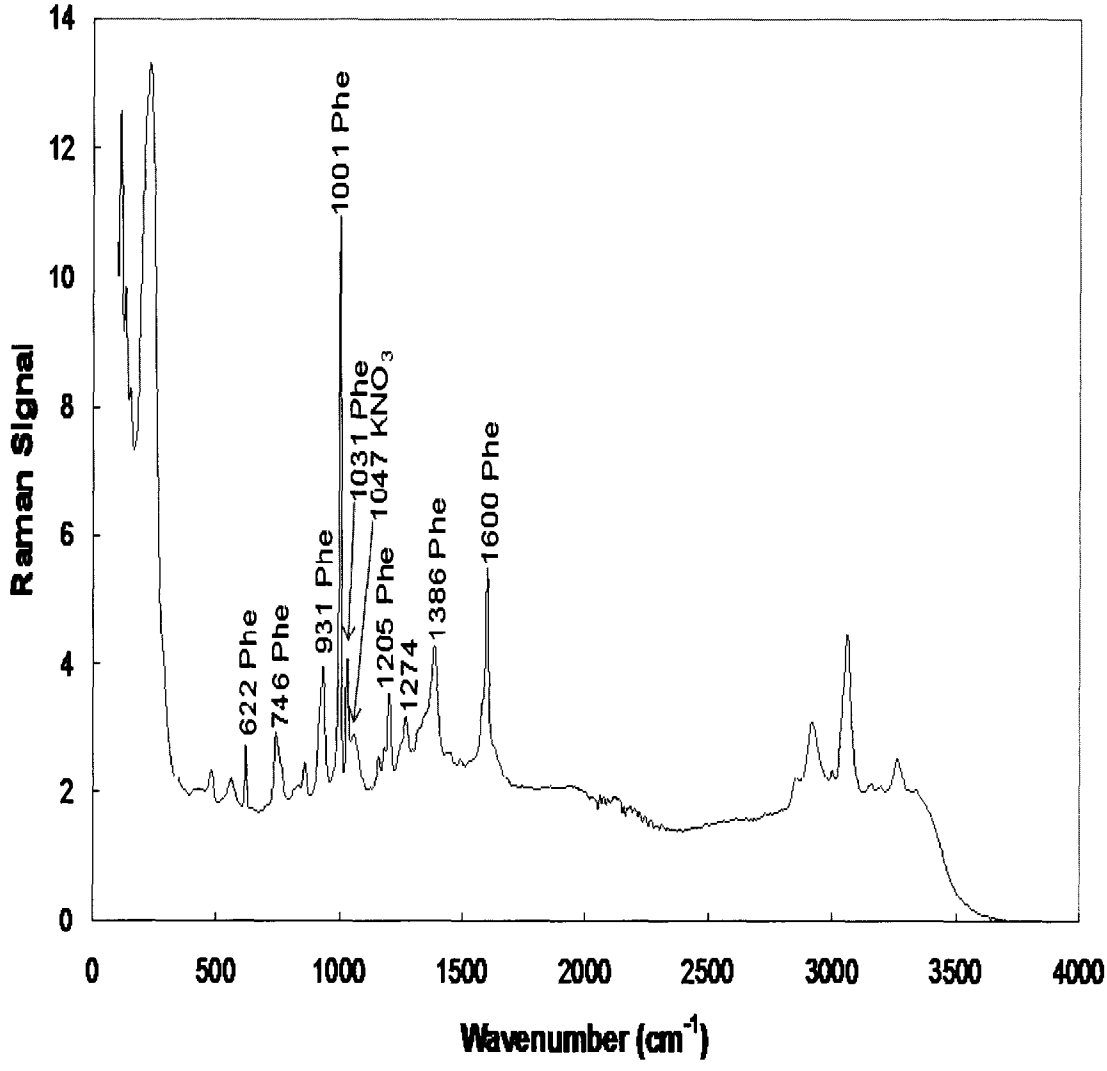

FIG. 37. Average of three SERS spectra of a 5 mM phenylalanine + 0.25 M KNO_3 (100 µl) adsorbed onto the surface of a silver-coated glass fiber filter (25 mm Whatman GF/A).

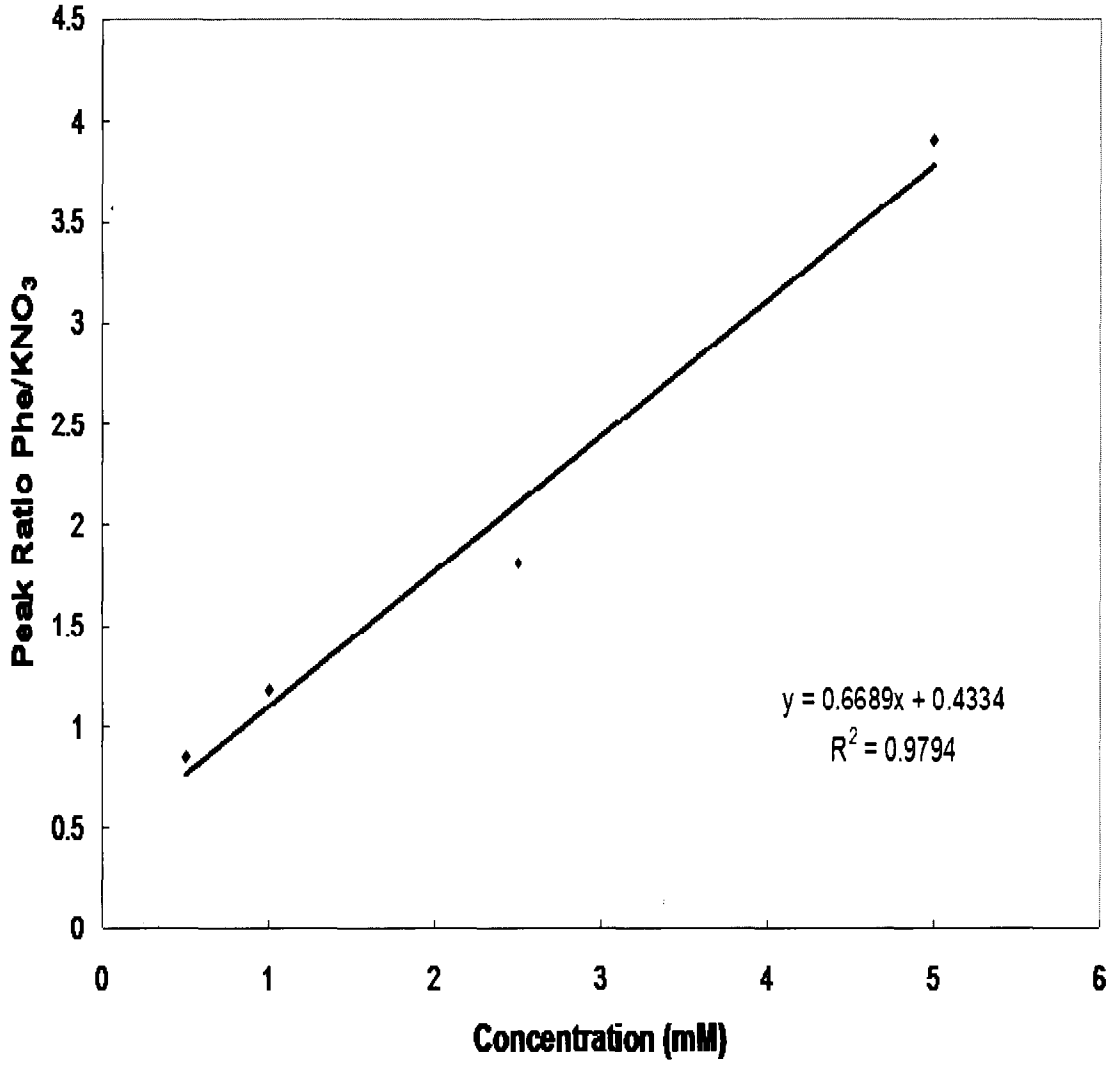

FIG. 38. Ratio of the peak Raman signal of phenylalanine at 1001 cm^{-1} with the peak Raman signal of KNO_3 at 1047 cm^{-1} versus the concentration of phenylalanine (number of replicates (n=3)).

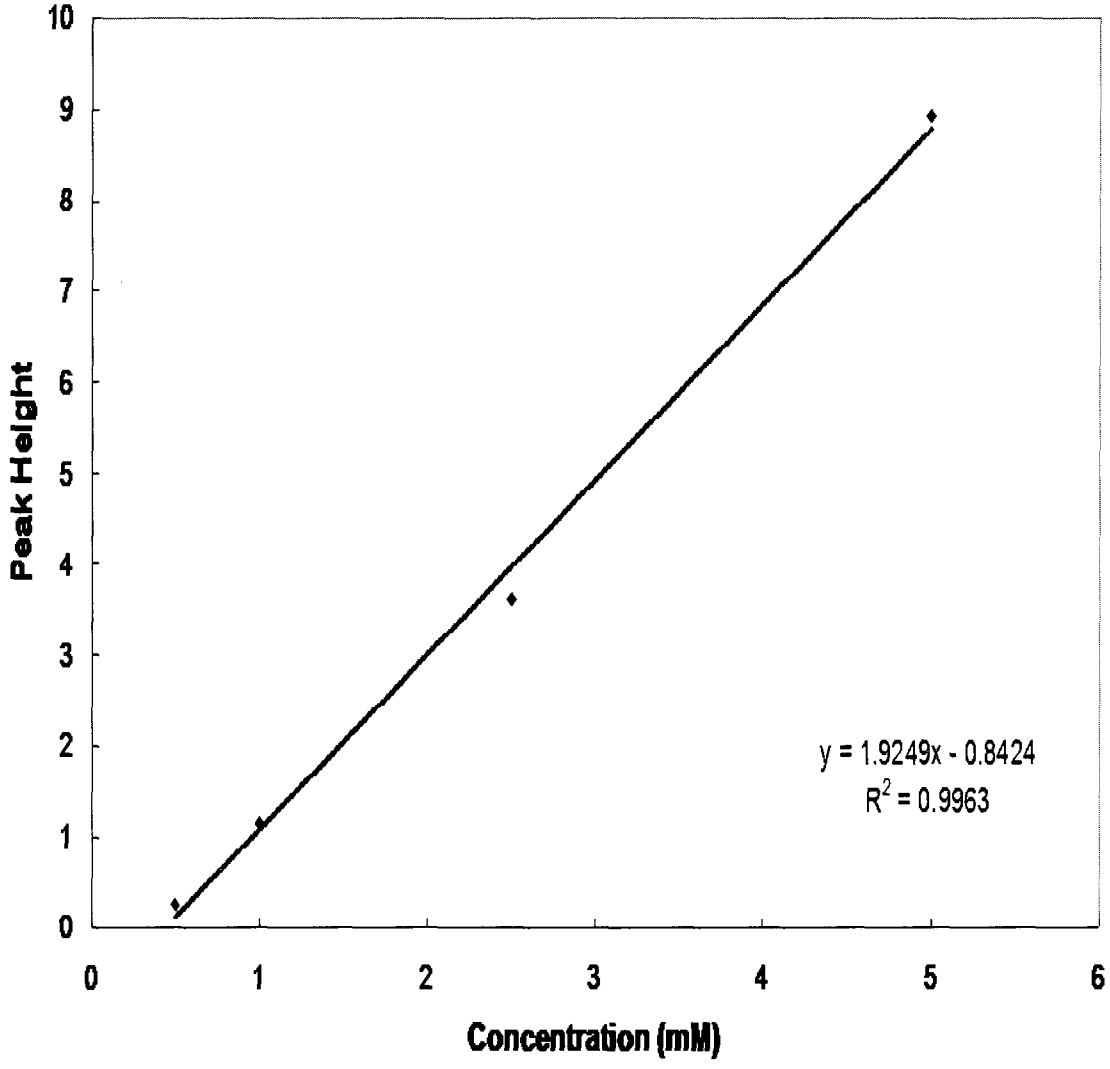

FIG. 39. Peak Raman signal at 1001 cm^{-1} versus concentration of phenylalanine for SERS spectra obtained from silver-coated glass fiber filters (n=3).

The initial experiments were conducted on quartz fiber filters. The filters were coated with silver as described previously and were used to generate SERS spectra on solutions of phenylalanine at several different concentrations. The first set of concentrations consisted of 0.1, 0.5, 1.0, and 5.0 mM phenylalanine solutions. The resulting spectra are given in Figure 40. A plot of the peak Raman signal at 1001 cm^{-1} versus concentration was generated to determine the dependence of the Raman signal on concentration (Figure 41). The peak Raman signal at 1001 cm^{-1} was chosen because it is the strongest peak in the phenylalanine spectrum. The resulting plot shows a sharp jump in the Raman signal as the phenylalanine concentration increases. The Raman signal eventually reaches a maximum value and plateaus. This effect is most likely caused by the orientation of the phenylalanine shifting at higher concentrations. This orientation change can mask the ring stretching mode of the phenylalanine causing a decrease in the intensity of the band at 1001 cm^{-1}. This result demonstrates the ability to elucidate molecular orientation information from the SERS spectra. This is important when considering the analytical analysis of proteins. It appears that the initial increase in the Raman signal is linear between 0.1mM and 1.0mM. This result meant that it was potentially possible to quantify the Raman signal over that range but more data points would need to be taken.

The same experiment was conducted using glass fiber filters instead of quartz. Glass fiber filters are less expensive than quartz and would be an ideal alternative provided that the silver could be deposited on its surface and that a SERS enhancement could be acquired. The silver deposition was carried out successfully using the same procedure as with the quartz filters. Upon visual inspection, no differences in appearance

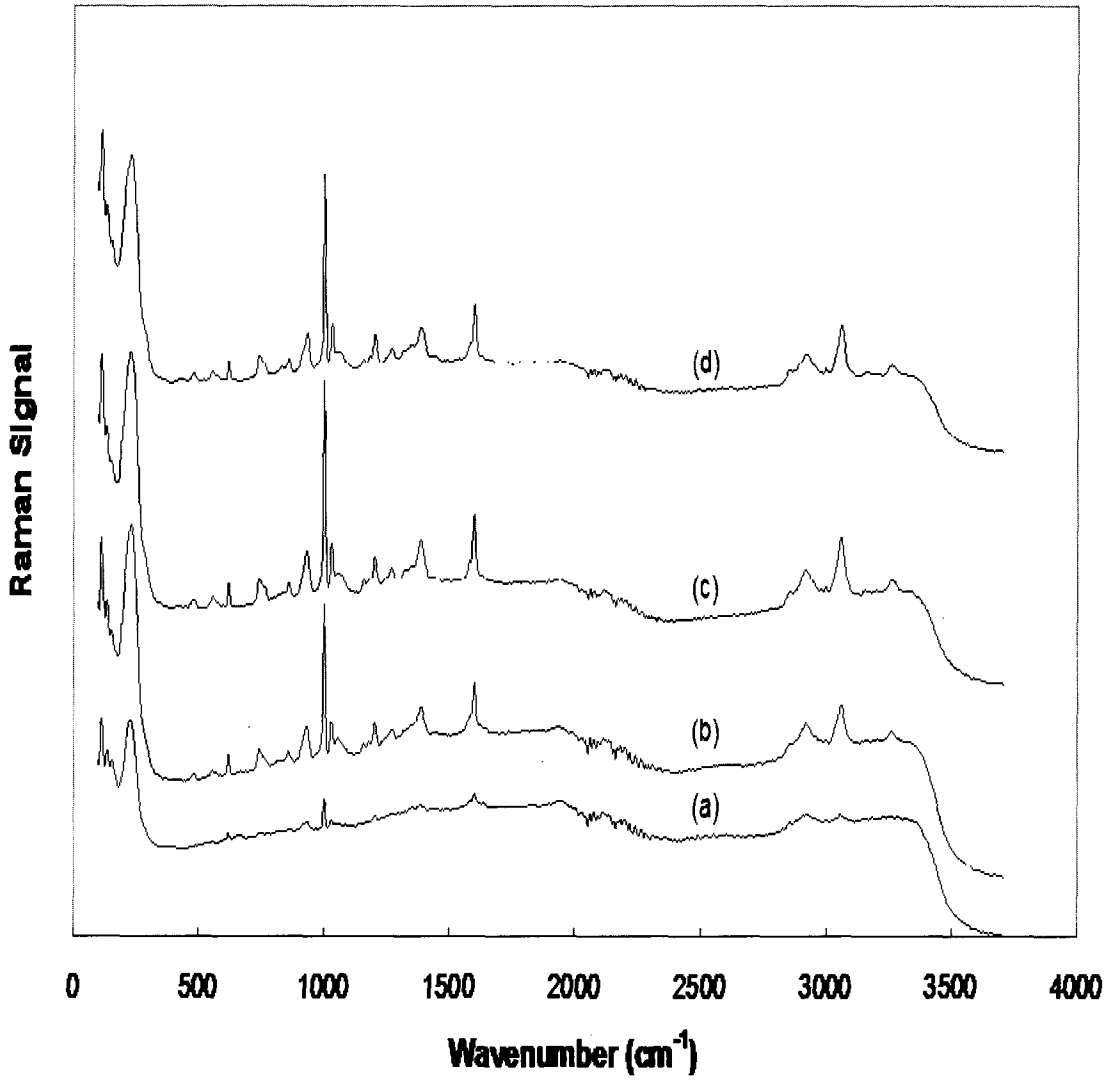

FIG. 40. Average of four SERS spectra of several concentrations of phenylalanine ((a) 0.1 mM, (b) 0.5 mM, (c) 1 mM, and (d) 5mM) (100 μl samples) adsorbed onto the surface of a quartz fiber filter (25 mmWhatman QM-A).

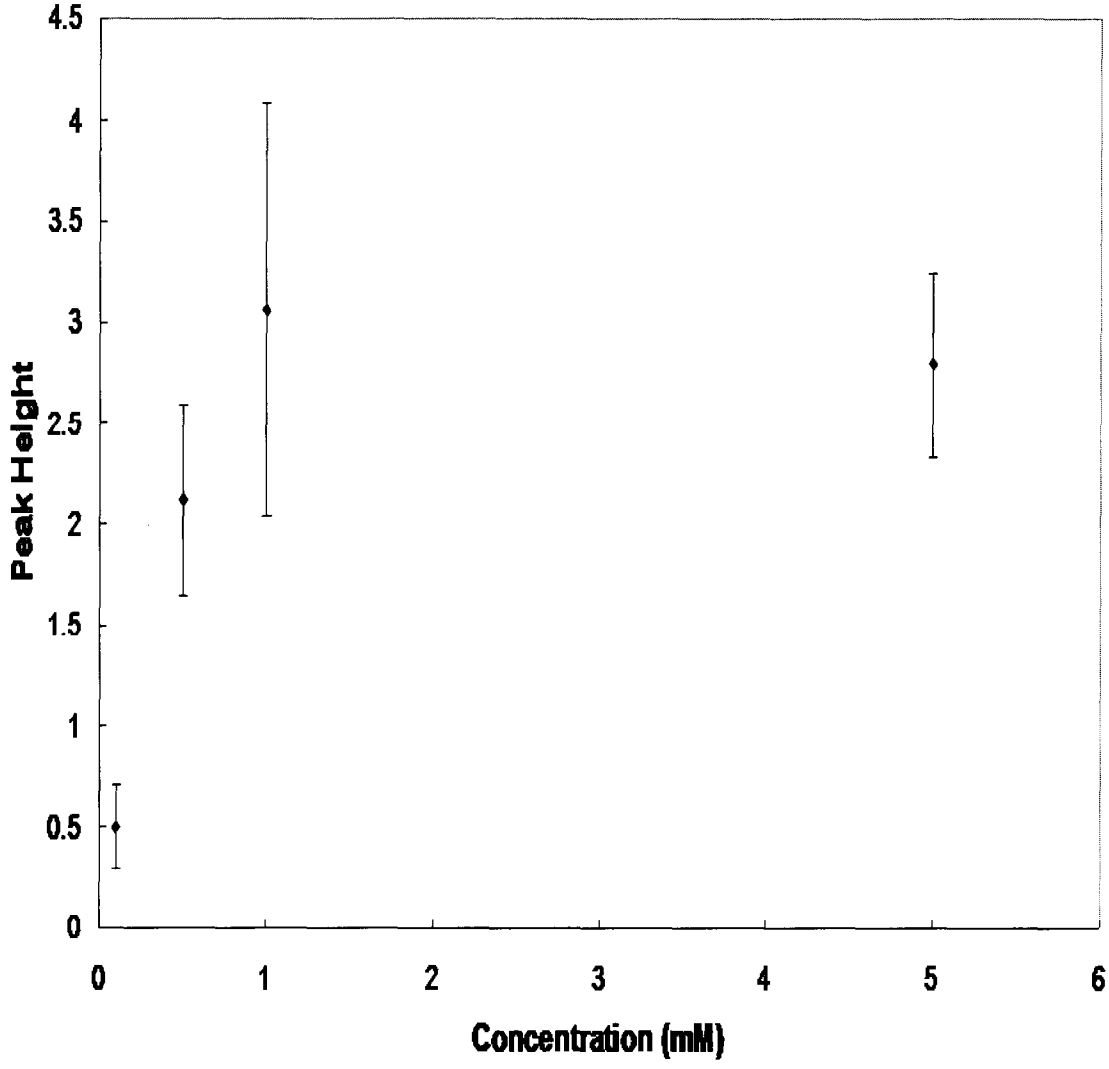

FIG. 41. Average peak Raman signal at 1001 cm^{-1} versus concentration of phenylalanine for SERS spectra obtained from silver-coated quartz fiber filters (n=4).

were observed when compared to the silver-coated quartz filters. SERS spectra were acquired using the filters in the same manner as the quartz using from 1.0, 2.5, and 5.0 mM phenylalanine solutions. The resulting spectra are given in Figure 42. The peak Raman signal at 1001 cm^{-1} was recorded for each concentration and a plot of the resulting data was prepared. This plot is given in Figure 43.

Comparing the peak Raman signal plots of the quartz and glass fiber filters reveals a difference in the intensity of the SERS signal at equal concentrations. The intensity of the SERS signal from the quartz filter is significantly less than the signal from the glass. The rate of increase is also significantly less for the quartz filter. A simple experiment was conducted to compare the SERS signal generated by the quartz and glass filters. Two sets of spectra were acquired from each of the filters. The spectra were taken from 10 mM phenylalanine solutions. The average of the two spectra for each filter type is shown in Figure 44. The average peak Raman signal at 1001 cm^{-1} for the quartz filter is 2.7. This is over half the peak Raman signal of the glass filter which was 6.4. This experiment was repeated using 10 mM tryptophan solutions to see if the same effect would be observed for a different amino acid. The average spectra for both glass and quartz are given in Figure 45. For these spectra we compared the peak Raman signal at 1001 cm^{-1}. The peak Raman signal for the quartz and glass filters was 0.2 and 0.5, respectively. Again, the quartz value was less than half that of the glass filter. This difference in signal was thought to be due to the difference in pore size of the two filters. The glass filters have a pore size of 1.6 μm; the quartz filters have a pore size of 2.2 μm. It is believed that the pore size of the filter may have a large influence on the surface morphology of the deposited silver. It is well known that the magnitude of SERS

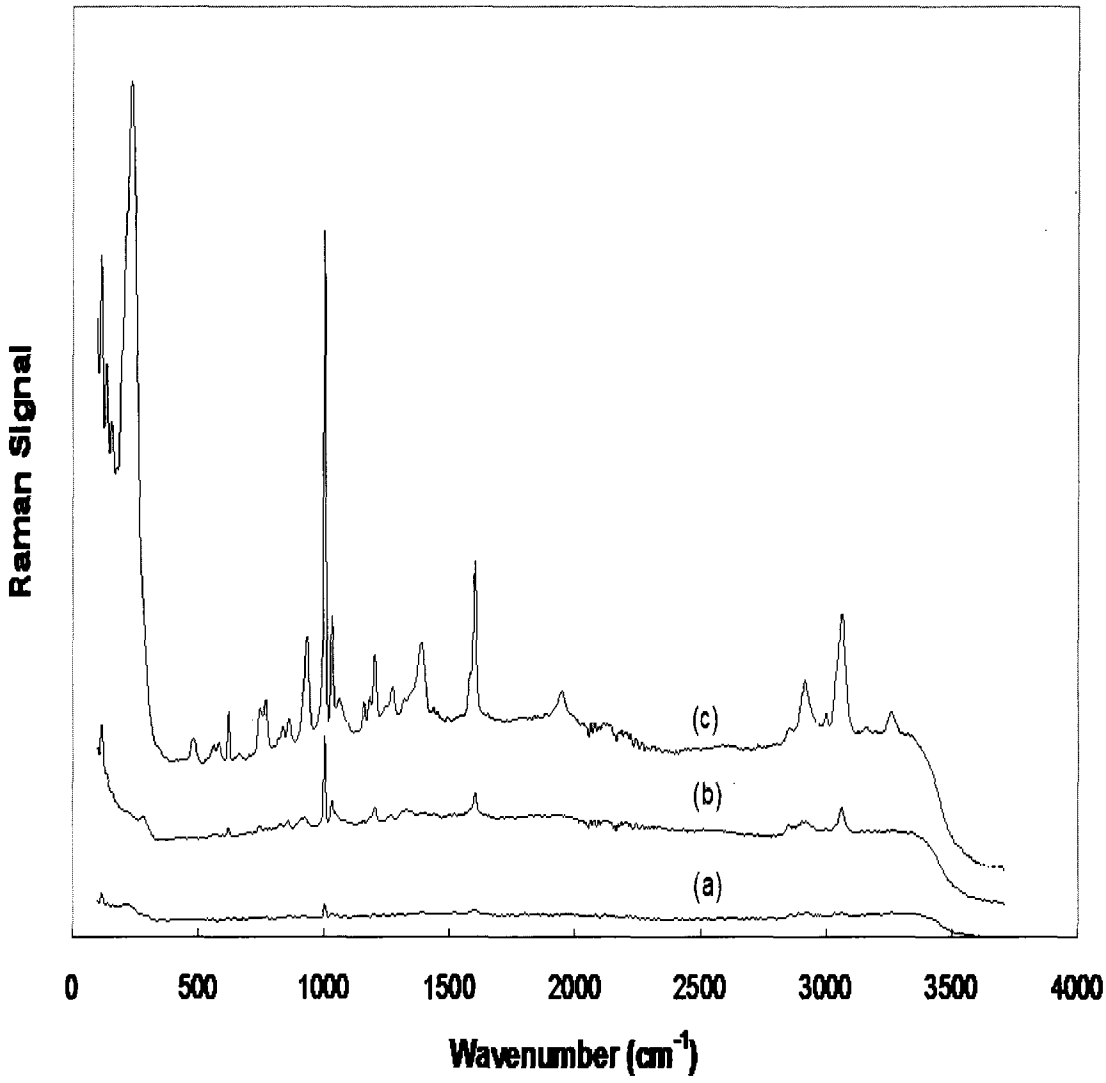

FIG. 42. Average of four SERS spectra of several concentrations of phenylalanine ((a) 1 mM, (b) 2.5 mM, and (c) 5 mM) (100 μl) adsorbed onto the surface of a silver-coated glass fiber filter (25 mm Whatman GF/A).

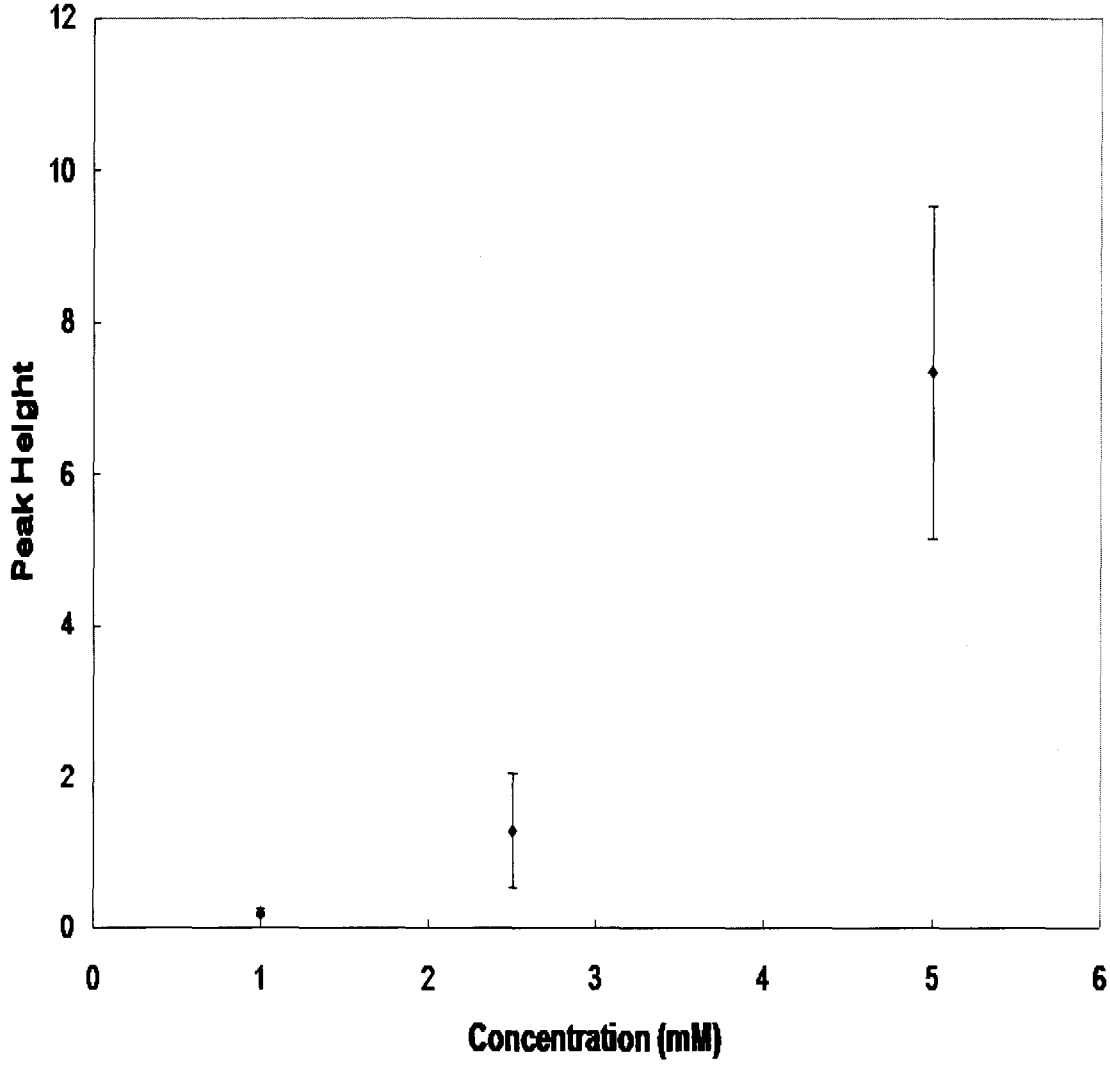

FIG. 43. Average peak Raman signal at 1001 cm^{-1} versus concentration of phenylalanine for SERS spectra obtained from silver-coated glass fiber filters (n=4).

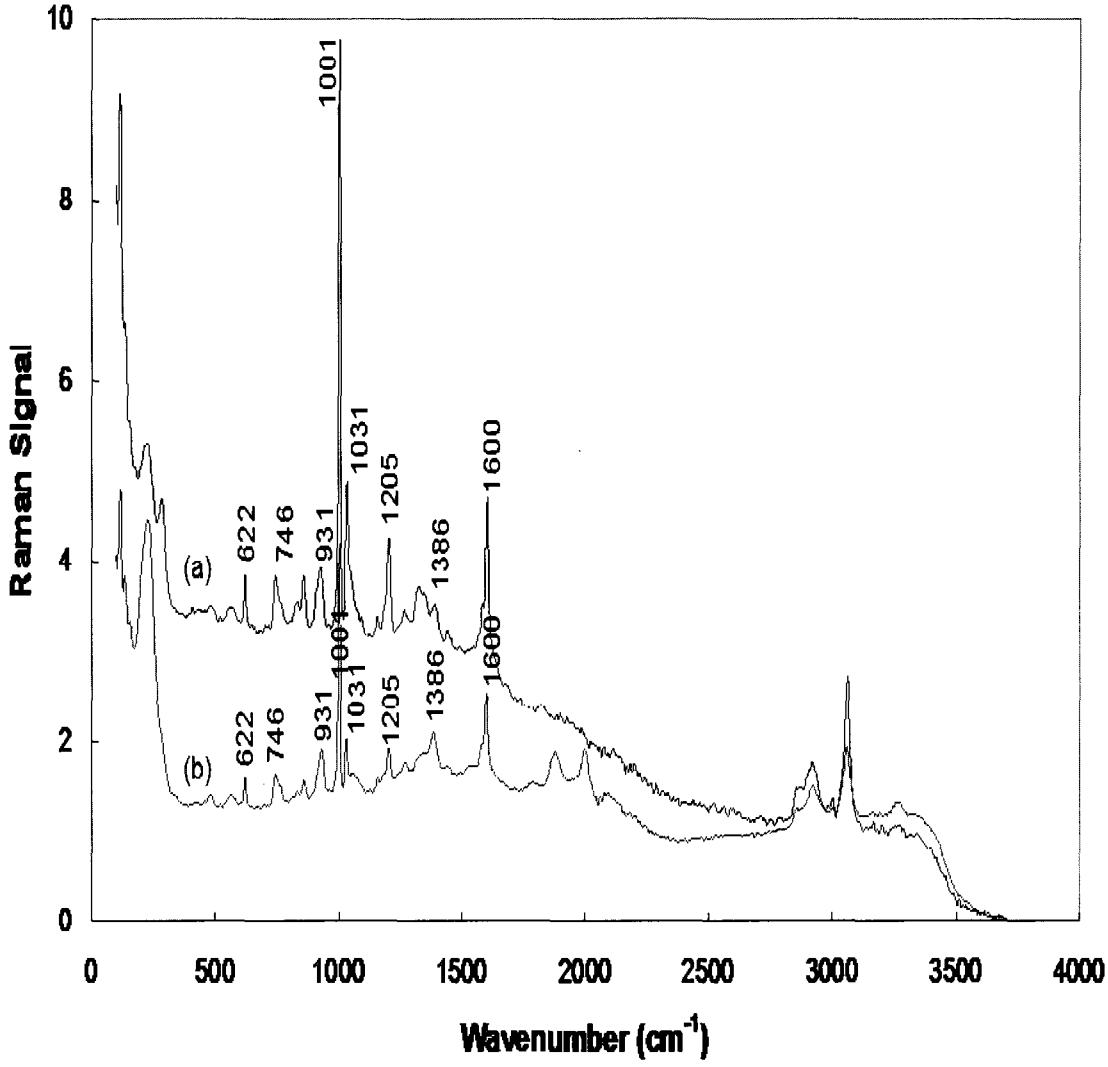

FIG. 44. Avg. SERS spectra of a 10 mM phenylalanine solution (100 μl) taken from both (a) silver-coated glass fiber (25 mm Whatman GF/A) and (b) quartz fiber filters (25 mmWhatman QM-A).

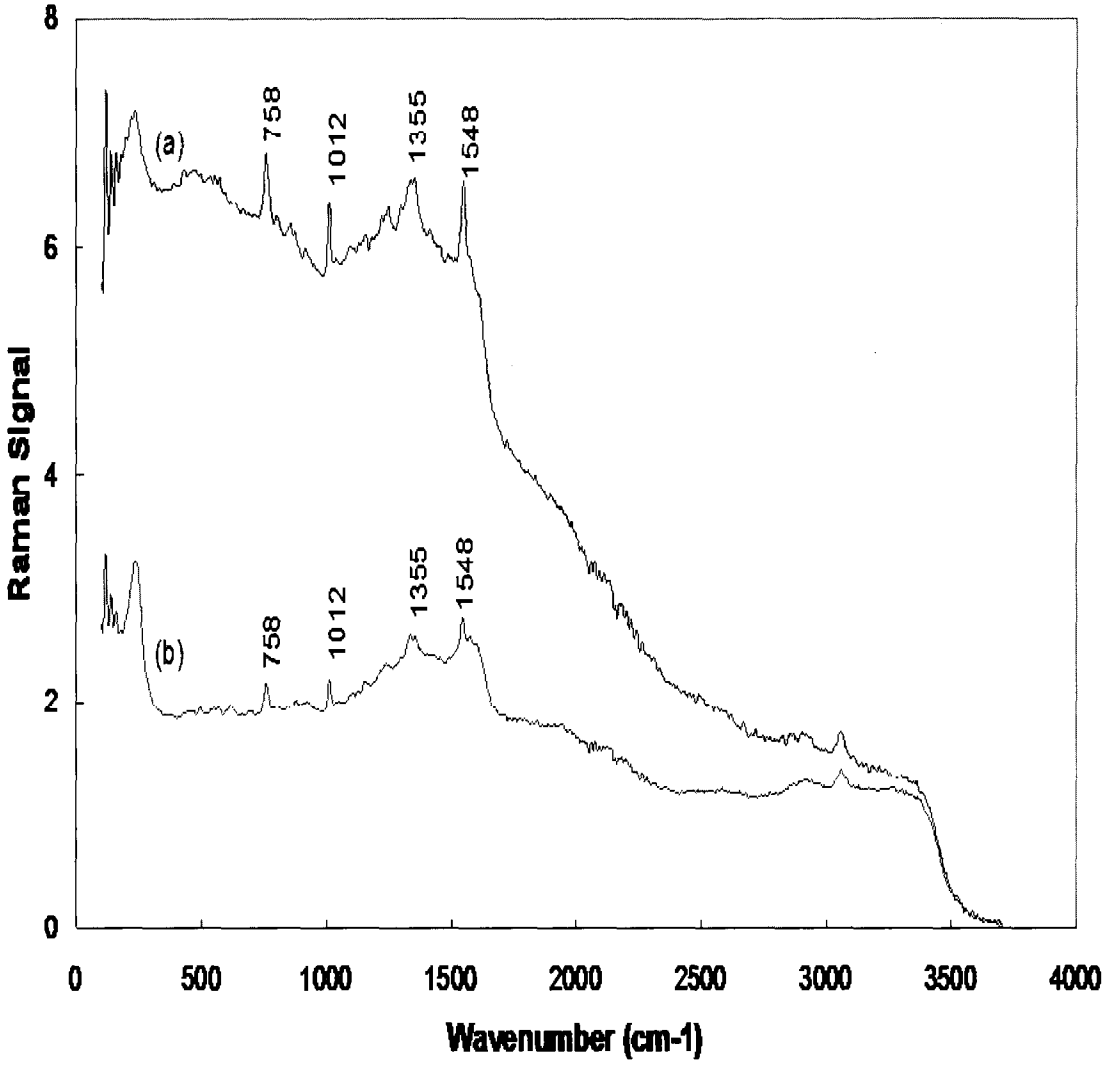

FIG. 45. Avg. SERS spectra of a 10 mM tryptophan solution (100 μl) taken from both (a) silver-coated glass fiber (25 mm Whatman GF/A) and (b) quartz fiber filters (25 mmWhatman QM-A).

enhancement is strongly dependent on the nature of the silver surface.[3] A filter with a smaller pore size could generate smaller silver clusters then a filter with a larger pore size. Smaller clusters would mean that the surface area for adsorption would be less, causing the silver clusters to become saturated with analyte quicker, and therefore the strength of the generated signal will rise at a much greater rate as the concentration of analyte increases. The glass fiber filters have a smaller pore size than the quartz fiber filters. This may explain the differences we have observed between the quartz and glass filters. This observation also suggests that it may be possible to analyze and quantify different concentration ranges by varying the pore size of the filter.

Additional experiments were carried out, using glass fiber filters, in order to establish the linear concentration range and the detection limit of the technique. SERS spectra were acquired from 0.01, 0.05, 0.1, 0.5, and 1 mM phenylalanine solutions. This range of concentrations was selected because it is representative of typical physiological levels.[102] Each spectrum was acquired using the established protocol for SERS measurements. Figure 46 shows the average spectrum for each concentration. Three phenylalanine peaks (1001, 1031, and 1598 cm^{-1}) were chosen for analysis of the spectra. These three peaks represent the strongest peaks in the phenylalanine spectrum. A plot of the peak Raman signal versus concentration for each wavenumber is given in Figures 47-49. The error bars on the plot represent the standard deviation between each individual spectra acquired at that concentration. The resulting plots confirm the previous results from the initial experiments. Each plot shows a sharp increase in the Raman signal from 0.01 mM to 0.5 mM. The plots show no increase in Raman signal between 0.5 and 1 mM. Between these concentrations the signal actually decreases. As stated previously,

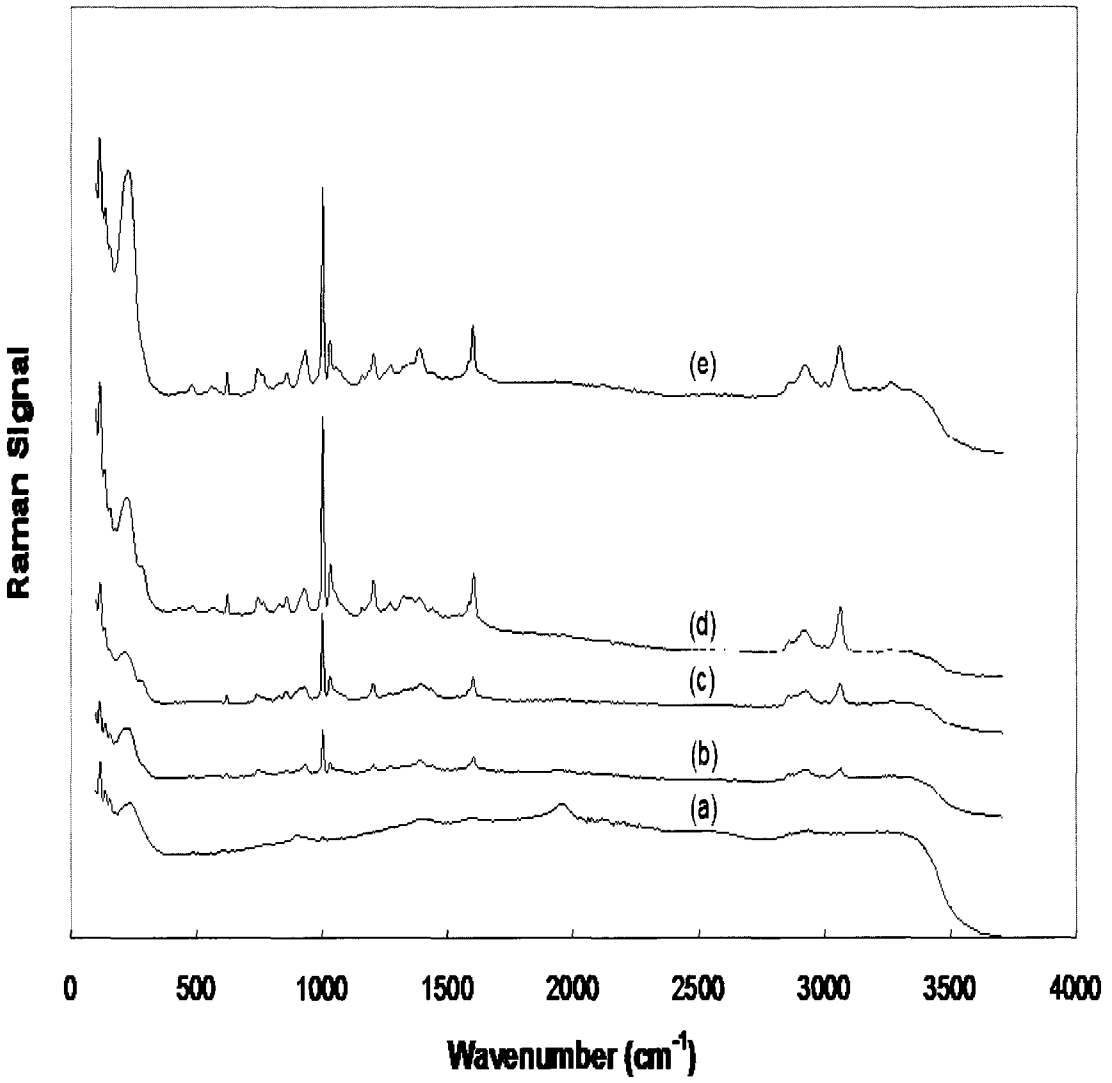

FIG. 46. Average of four SERS spectra of several concentrations of phenylalanine ((a) 0.01 mM, (b) 0.05 mM, (c) 0.1 mM, (d) 0.5mM, and (e) 1 mM) (100 μl) adsorbed onto the surface of a silver-coated glass fiber filter (25 mm Whatman GF/A).

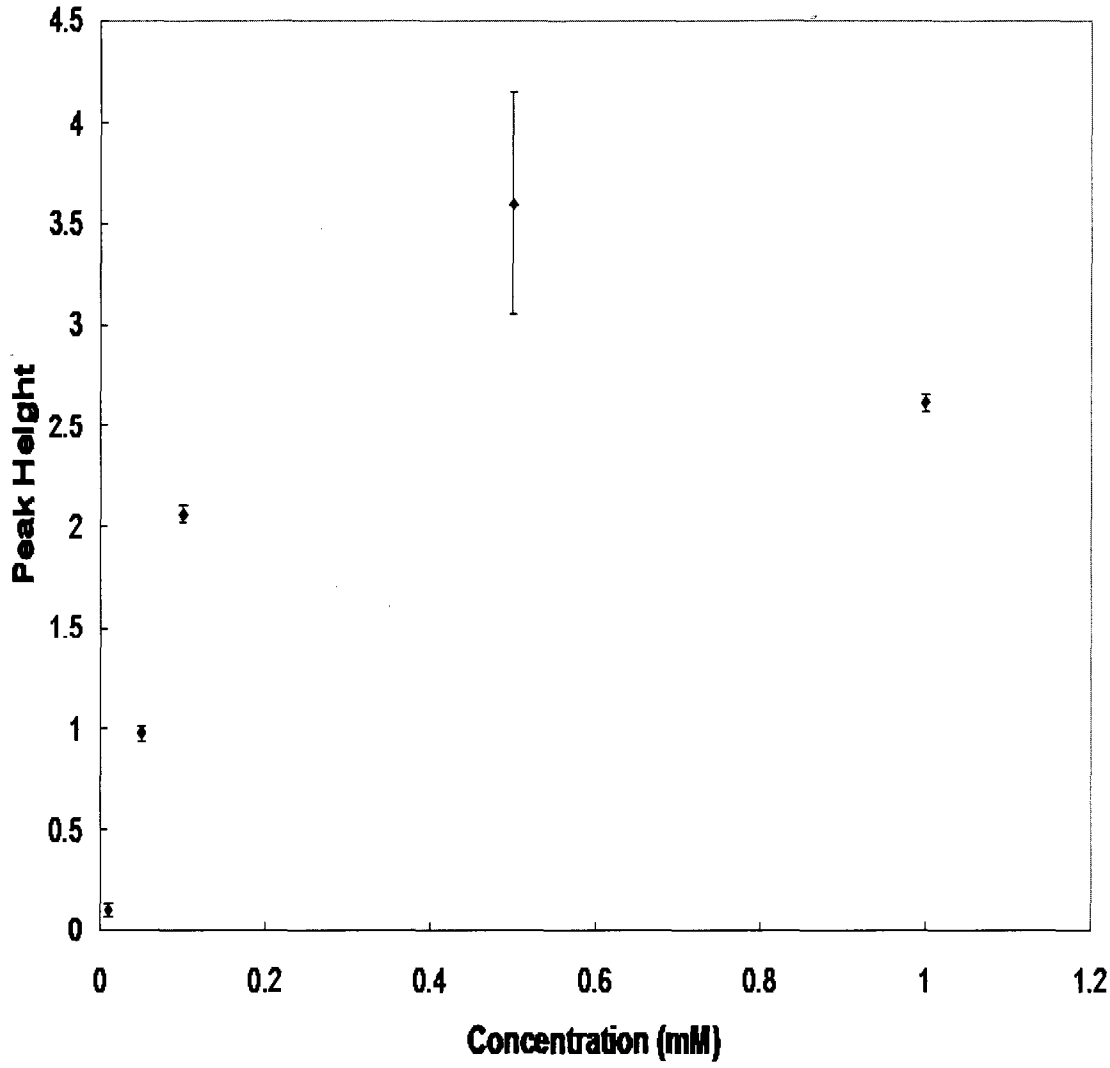

FIG. 47. Average peak Raman signal at 1001 cm^{-1} versus concentration of phenylalanine for SERS spectra obtained from silver-coated glass fiber filters (n=4).

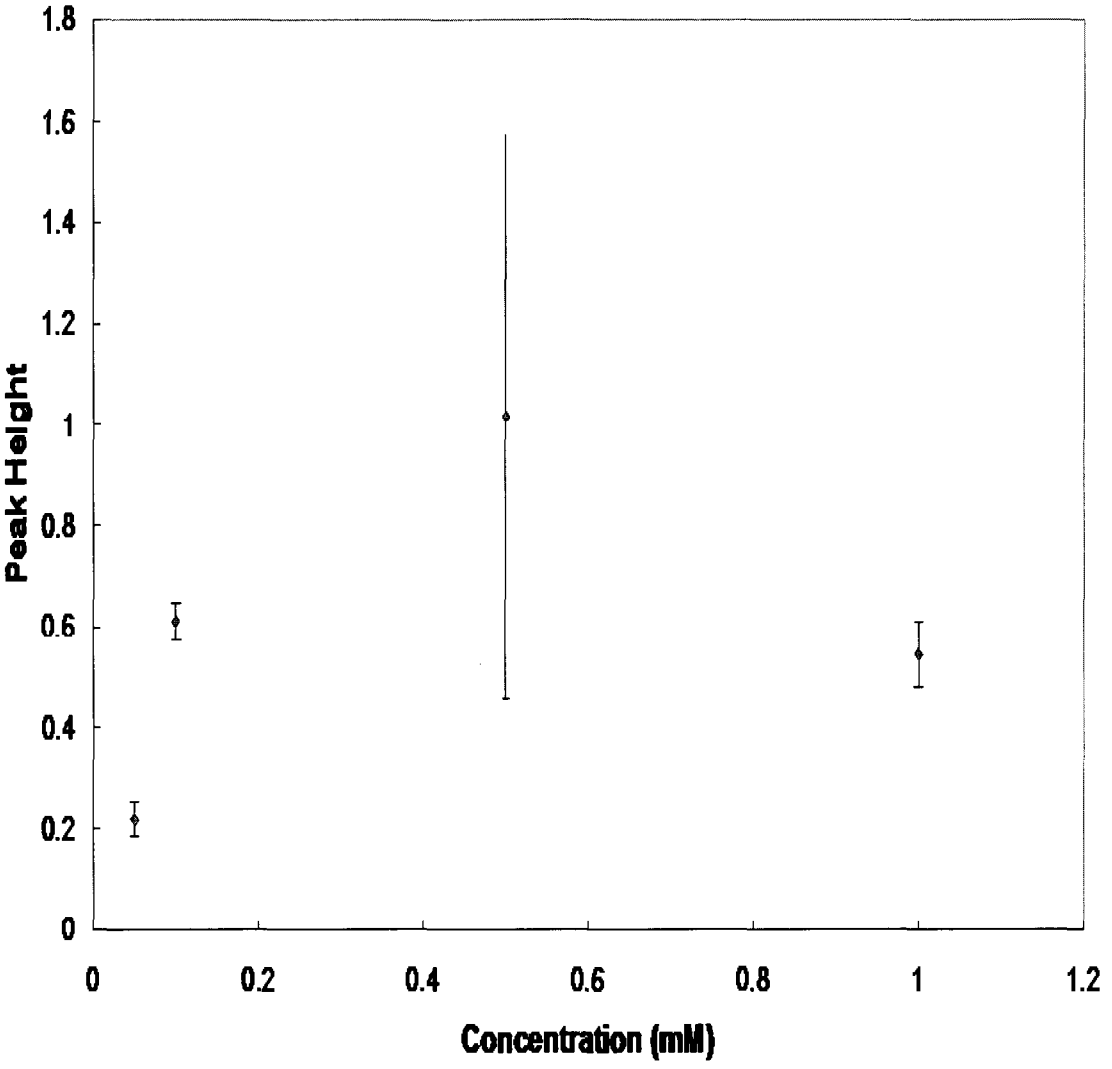

FIG. 48. Average peak Raman signal at 1031 cm^{-1} versus concentration of phenylalanine for SERS spectra obtained from silver-coated glass fiber filters (n=4).

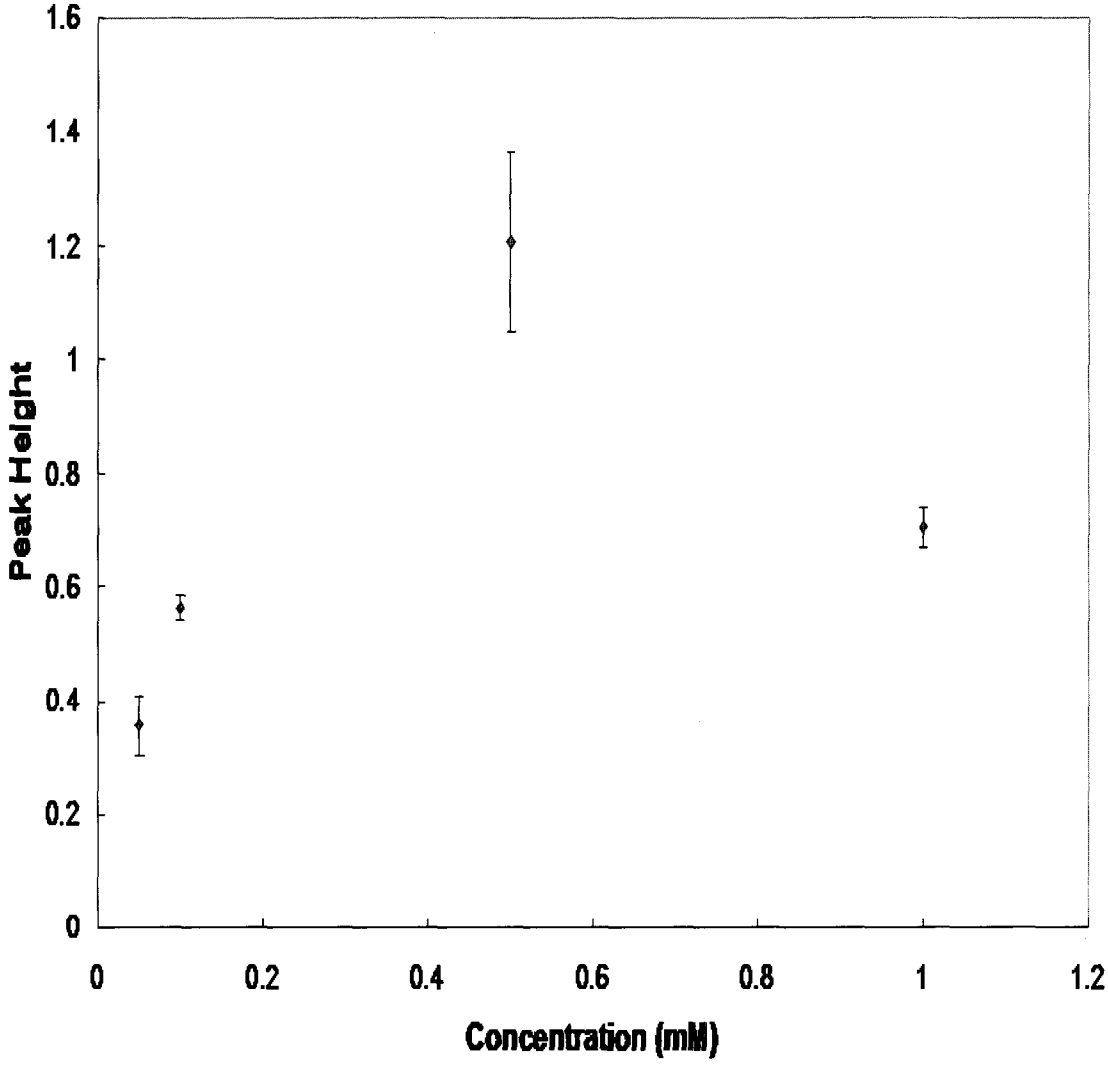

FIG. 49. Average peak Raman signal at 1598 cm^{-1} versus concentration of phenylalanine for SERS spectra obtained from silver-coated glass fiber filters (n=4).

this effect is thought to be caused by the orientation of the phenylalanine shifting at higher concentrations. A comparison of the three plots reveals that the concentration dependence is not the same for the three peaks. The rate of increase of the Raman signal is greater for the peak at 1001 cm^{-1} than the peaks at 1031 and 1598 cm^{-1}. The rate of increase of the Raman signal is similar for the peaks at 1031 and 1598 cm^{-1}. This result agrees with those obtained by M. Sackmann and A. Materny.[84] This implies that there is an inhomogeneous distribution of the intensity versus concentration relationship for different vibrational modes of the adsorbed phenylalanine. The standard deviation of each data point is relatively low for each of the plots with the exception of the point at 0.5 mM. The plots also reveal that there is potentially a linear concentration range somewhere between 0.01 and 0.5 mM. To determine what the actual range of linearity is, more data points need to be collected.

A new series of SERS spectra were acquired using the silver-coated glass fiber filters from the following concentrations: 0.01, 0.05, 0.10, 0.15, 0.25, 0.5, and 1.0 mM. Three sets of data were acquired on three separate days using silver-coated glass fiber filters prepared the previous day. The average spectrum from each of the concentrations for the three data sets is given in Figures 50-52. Plots of the peak Raman signal versus concentration for the three strongest peaks are given in Figures 53-55. The error bars represent the standard deviation between each SERS measurement taken at each point in the data set. The plots from each set of data at 1001 and 1031 cm^{-1} demonstrate a more clearly defined linear concentration range between 0.01 and 0.15 mM. The plots of the peak Raman signal at 1598 cm^{-1} for each data set has a linear range between 0.05 and 0.15 mM. At a phenylalanine concentration of 0.01 mM the peak at 1598 cm^{-1} cannot be

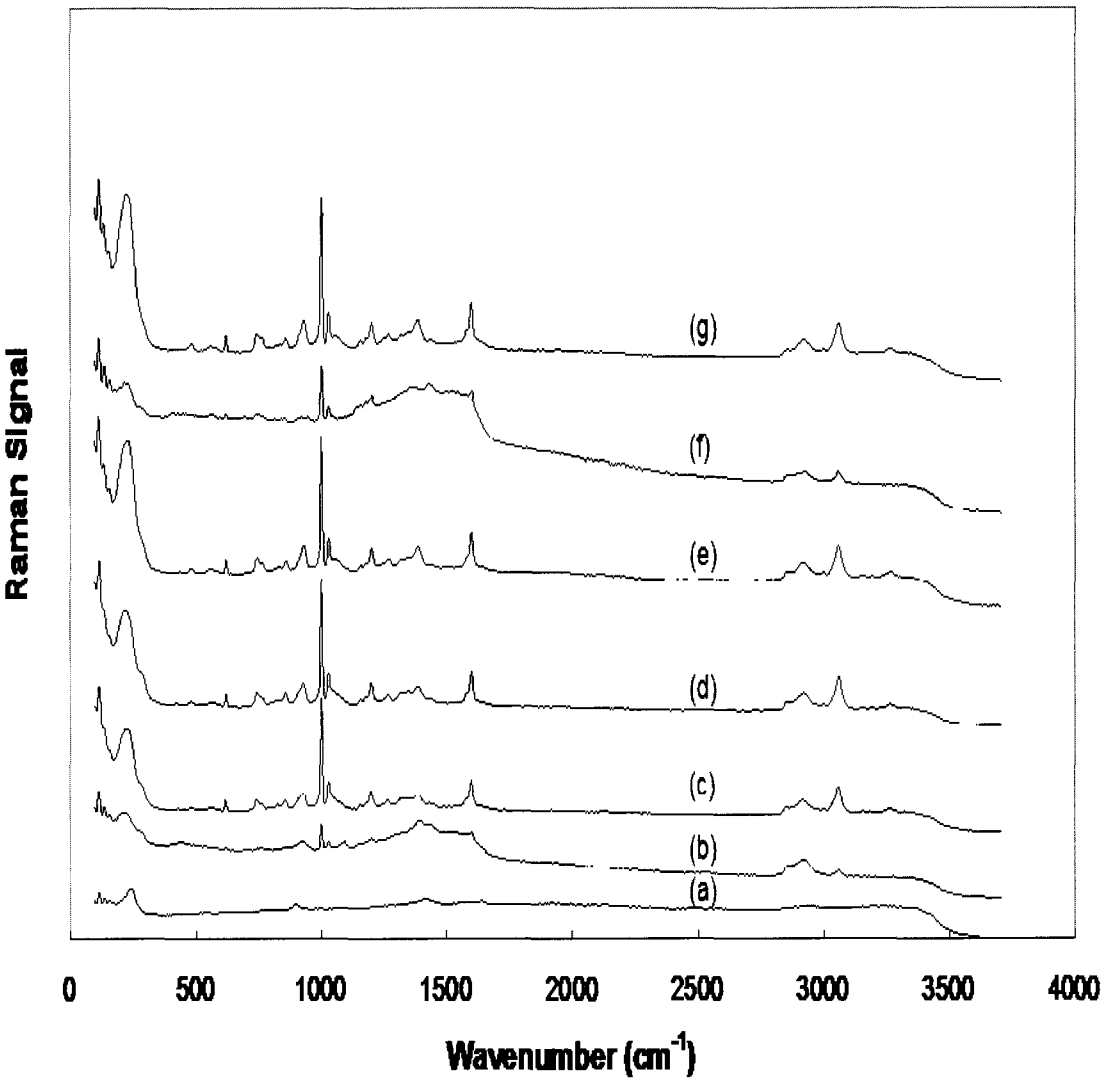

FIG. 50. Average of four SERS spectra of several concentrations of phenylalanine ((a) 0.01 mM, (b) 0.05 mM, (c) 0.1 mM, (d) 0.15 mM, (e) 0.25 mM, (f) 0.5 mM, and (g) 1.0 mM) (100 μl samples) from data set one on silver-coated glass fiber filter (25 mm Whatman GF/A).

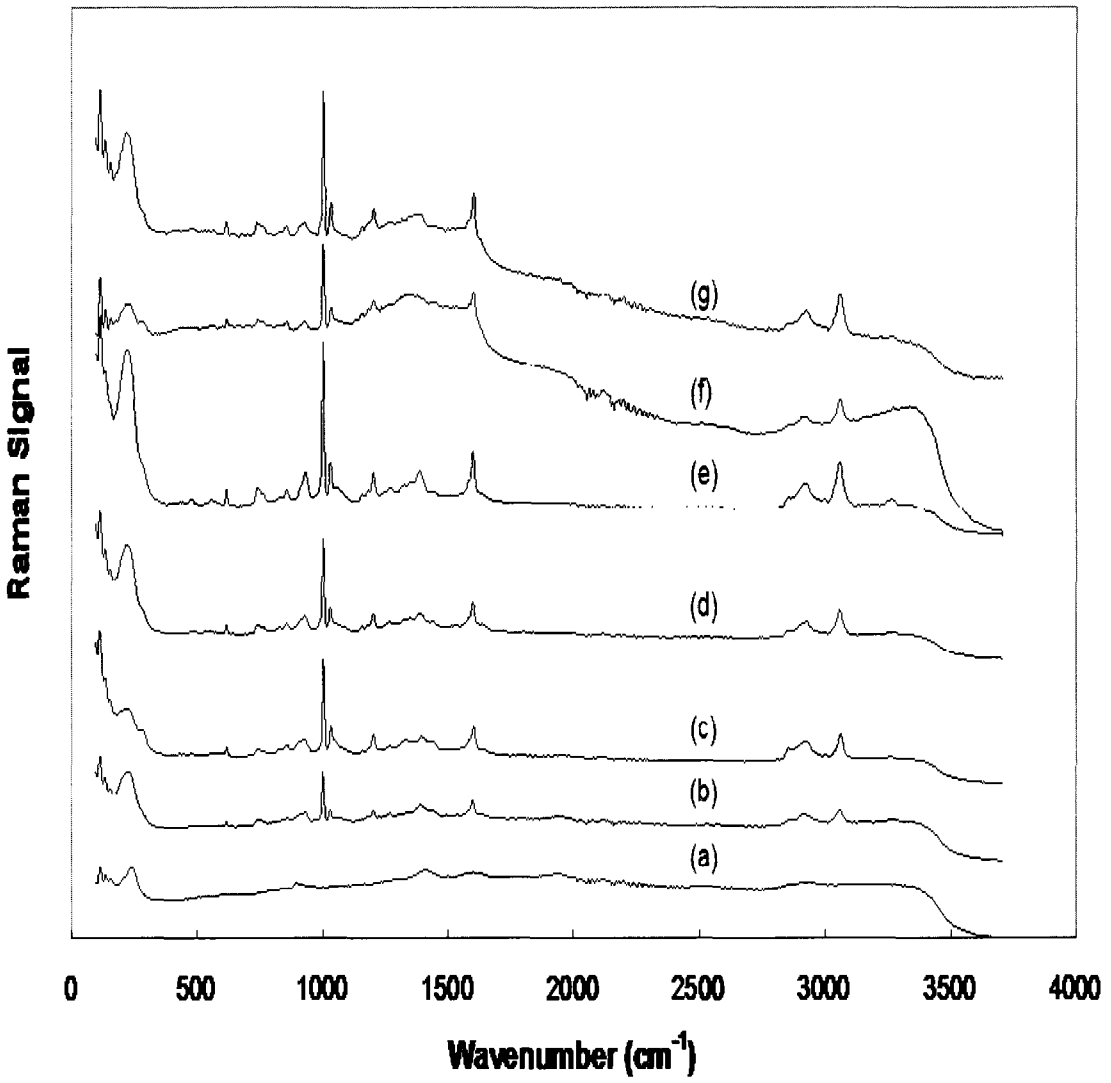

FIG. 51. Average of four SERS spectra of several concentrations of phenylalanine ((a) 0.01 mM, (b) 0.05 mM, (c) 0.1 mM, (d) 0.15 mM, (e) 0.25 mM, (f) 0.5 mM, and (g) 1.0 mM) (100 μl samples) from data set two on silver-coated glass fiber filter (25 mm Whatman GF/A).

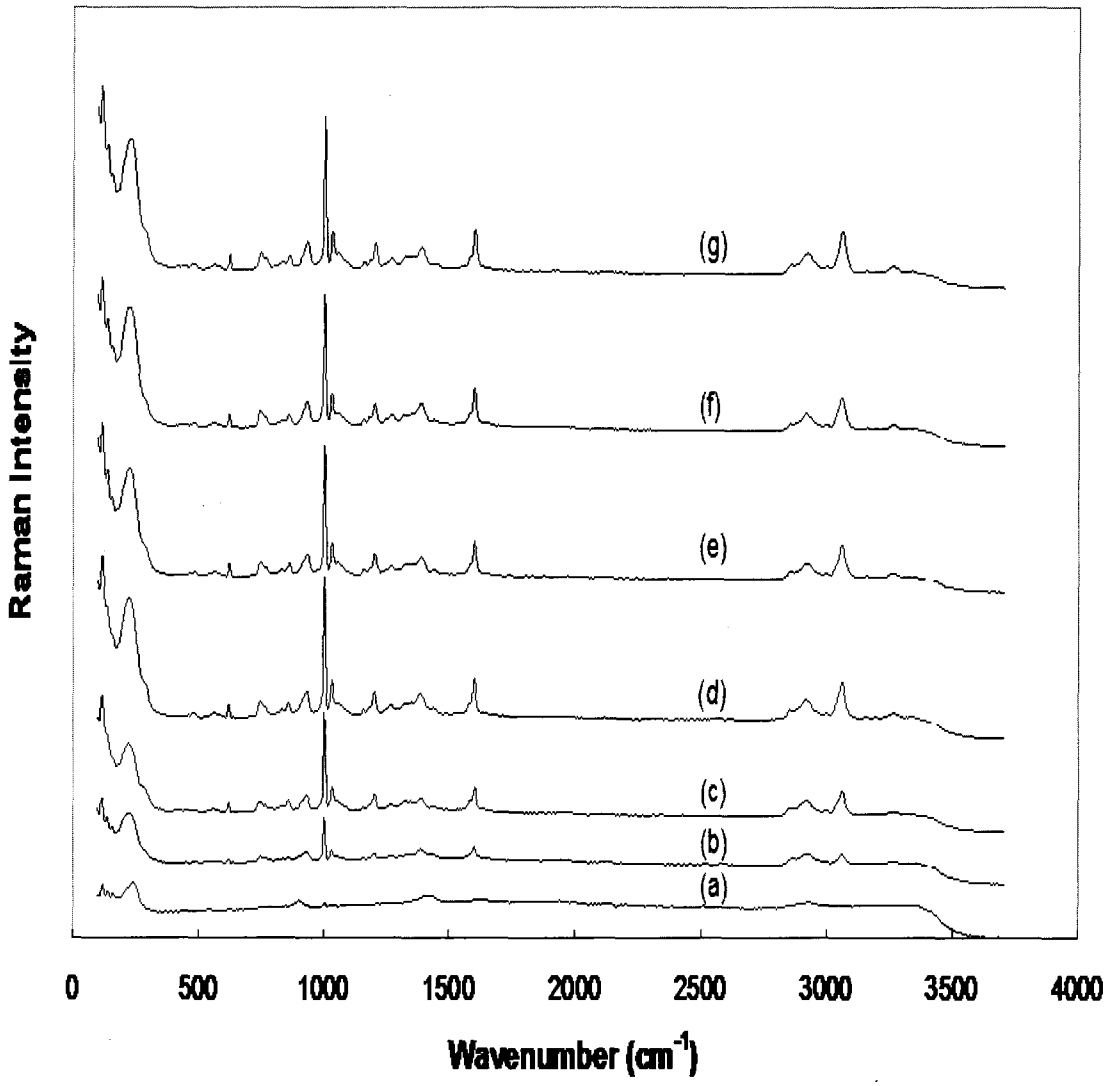

FIG. 52. Average of four SERS spectra of several concentrations of phenylalanine ((a) 0.01 mM, (b) 0.05 mM, (c) 0.1 mM, (d) 0.15 mM, (e) 0.25 mM, (f) 0.5 mM, and (g) 1.0 mM) (100 μl samples) from data set three on silver-coated glass fiber filter (25 mm Whatman GF/A).

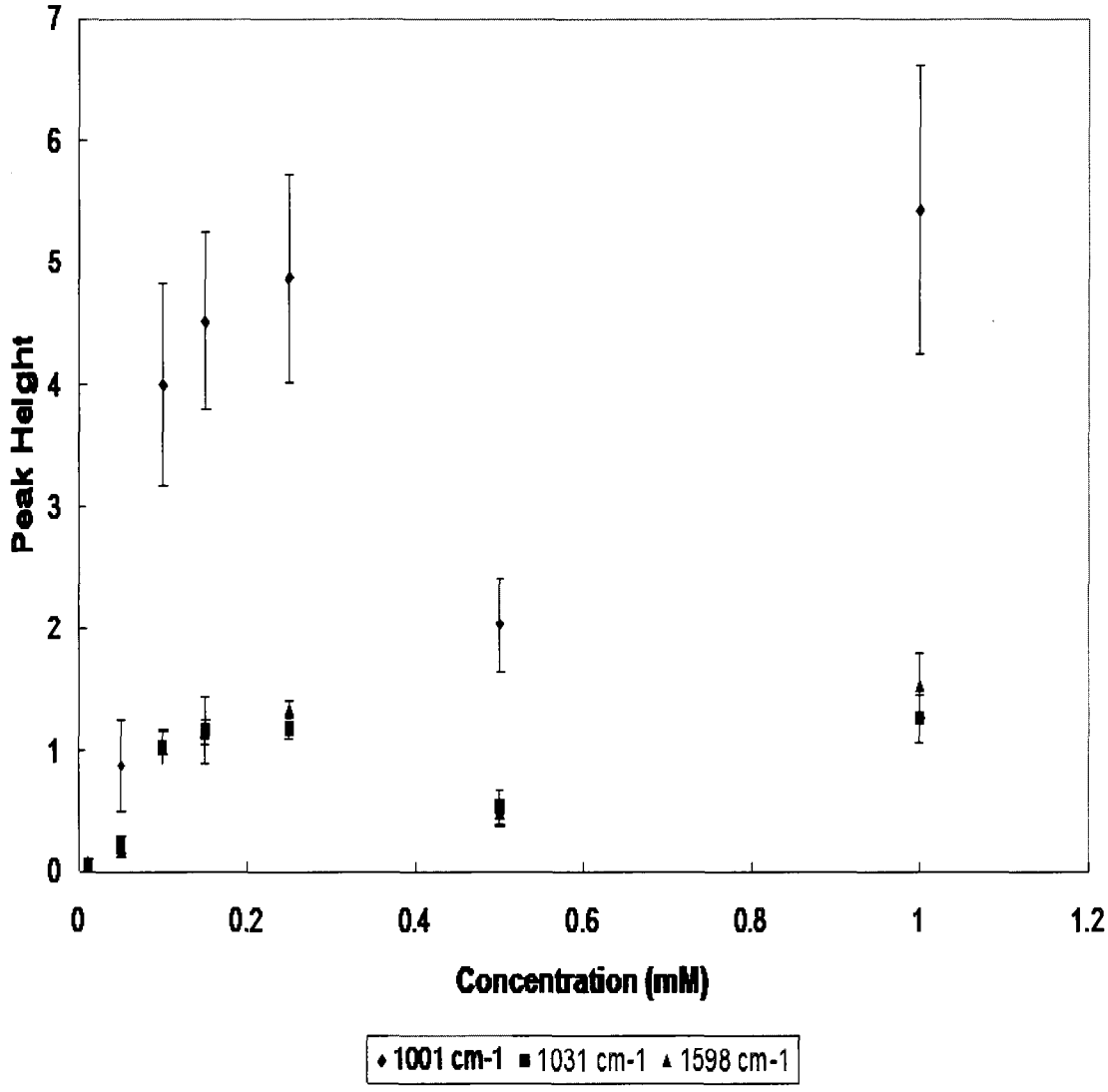

FIG. 53. Average peak Raman signal versus concentration of phenylalanine from data set one for SERS spectra obtained from silver-coated glass fiber filters (n=4).

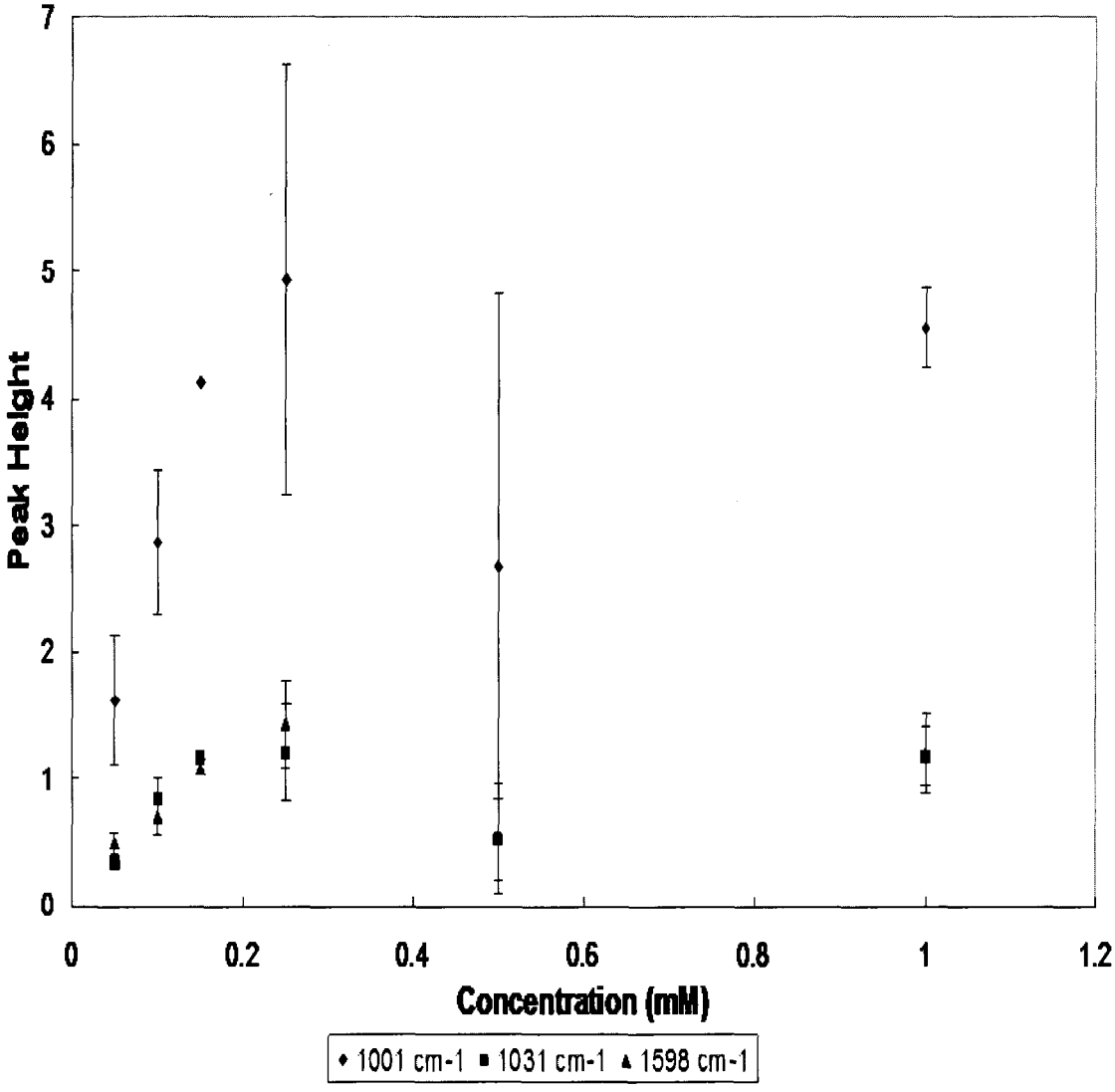

FIG. 54. Average peak Raman signal versus concentration of phenylalanine from data set two for SERS spectra obtained from silver-coated glass fiber filters (n=4).

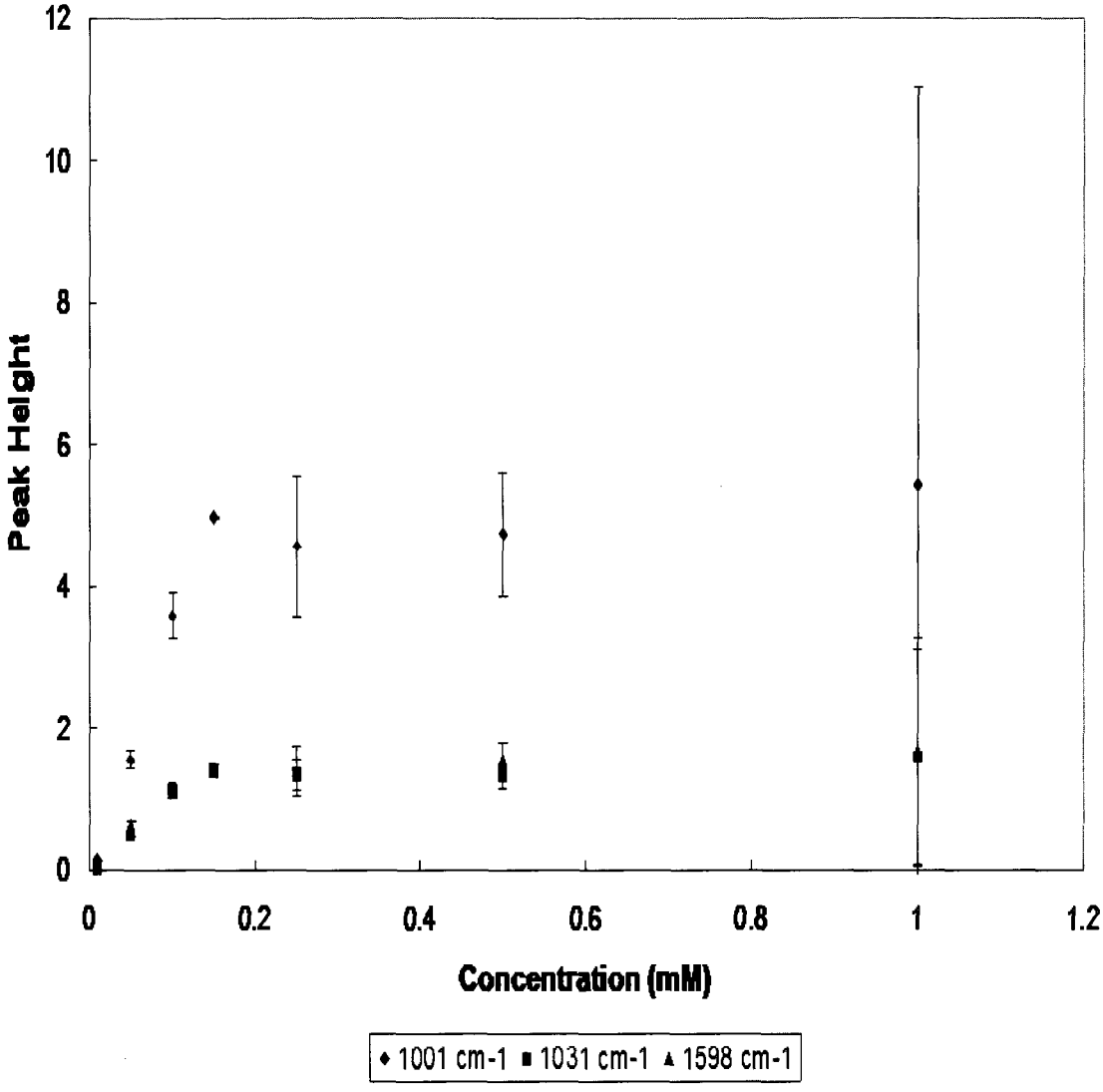

FIG. 55. Average peak Raman signal versus concentration of phenylalanine from data set three for SERS spectra obtained from silver-coated glass fiber filters (n=4).

clearly resolved. Figures 56-64 show the peak Raman signal versus concentration plots again, however, this time they include only the concentration values in the linear range. For Figures 58 and 64, the plots for the peak at 1598 cm^{-1} consist of only three data points due to the inability to clearly resolve the peak height at the 0.1 mM phenylalanine concentration. A linear regression was performed on the data points and is shown in the plots along with the equation of the line and the R^2 value. The error bars represent the standard deviation between each SERS measurement taken at each point in the data set. A summary of the standard deviation for each plot in each data set is given in Tables VII–IX.

Each data set shows a linear response in the SERS intensity over the established concentration range. Data set one was the least linear and had an R^2 value of 0.847 for the peak at 1598 cm^{-1}. The R^2 value for 1001 and 1031 cm^{-1} was 0.9225 and 0.916, respectively. The standard deviation (SD) between points in each plot in data set one varied considerably. The highest SD was ± 50% for 0.01 mM at 1001 cm^{-1} and the lowest SD was ± 5% for 0.25 mM at 1598 cm^{-1}. The R^2 values for data set two were 1.0, 0.9869, and 0.9784 for the peak Raman signal plots of 1001, 1031, and 1598 cm^{-1}, respectively. The highest SD for this data set was ±82% for 0.5 mM at 1598 cm^{-1} and the lowest was ± 7% for 1mM at 1001 cm^{-1}. The R^2 values for data set #3 were 0.9942, 0.97804, and 0.9941 for the peak Raman signal plots of 1001, 1031, and 1598 cm^{-1}, respectively. The highest SD was ± 103% for 1 mM at 1001 cm^{-1} and the lowest SD was ± 0.25% for 0.15 mM at 1001 cm^{-1}. In general, the highest standard deviations were either for data points outside of the linear range 0.5 and 0.1 mM or for the data point at the lowest phenylalanine concentration, 0.01 mM. For each set of data, the SD was never

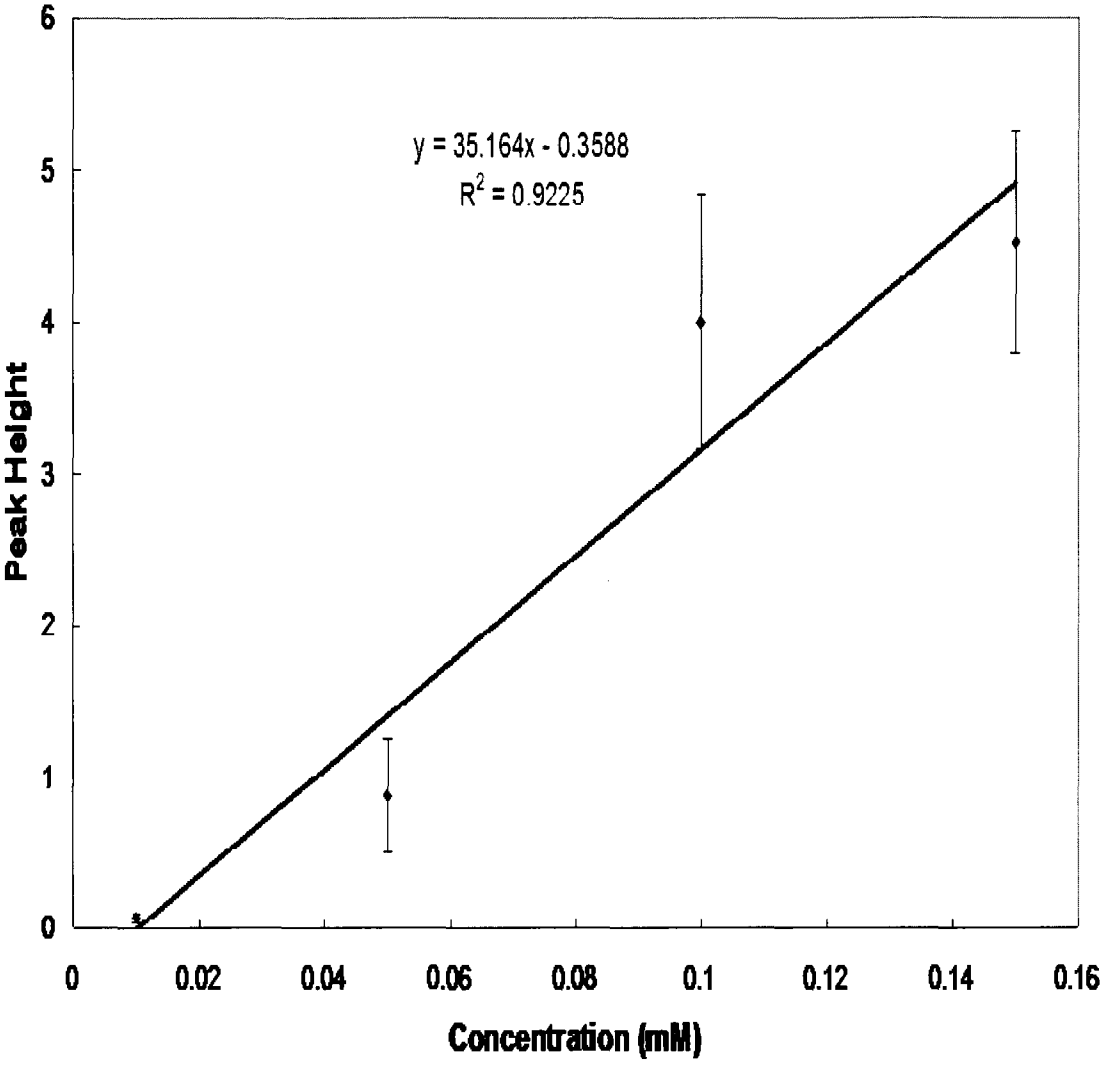

FIG. 56. Average peak Raman signal at 1001 cm^{-1} versus concentration of phenylalanine for data set one showing the range of linearity (n=4).

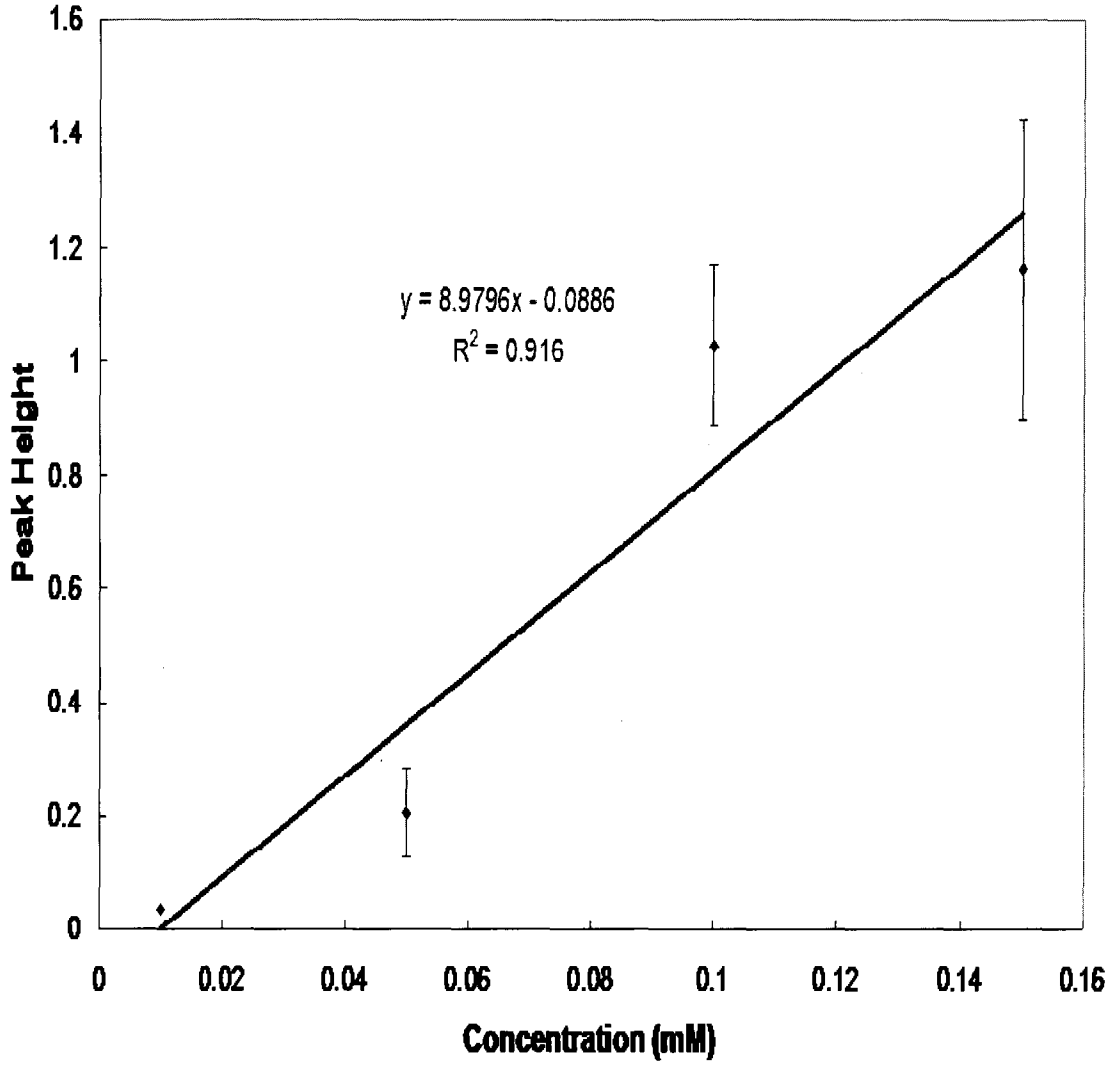

FIG. 57. Average peak Raman signal at 1031 cm^{-1} versus concentration of phenylalanine for data set one showing the range of linearity (n=4).

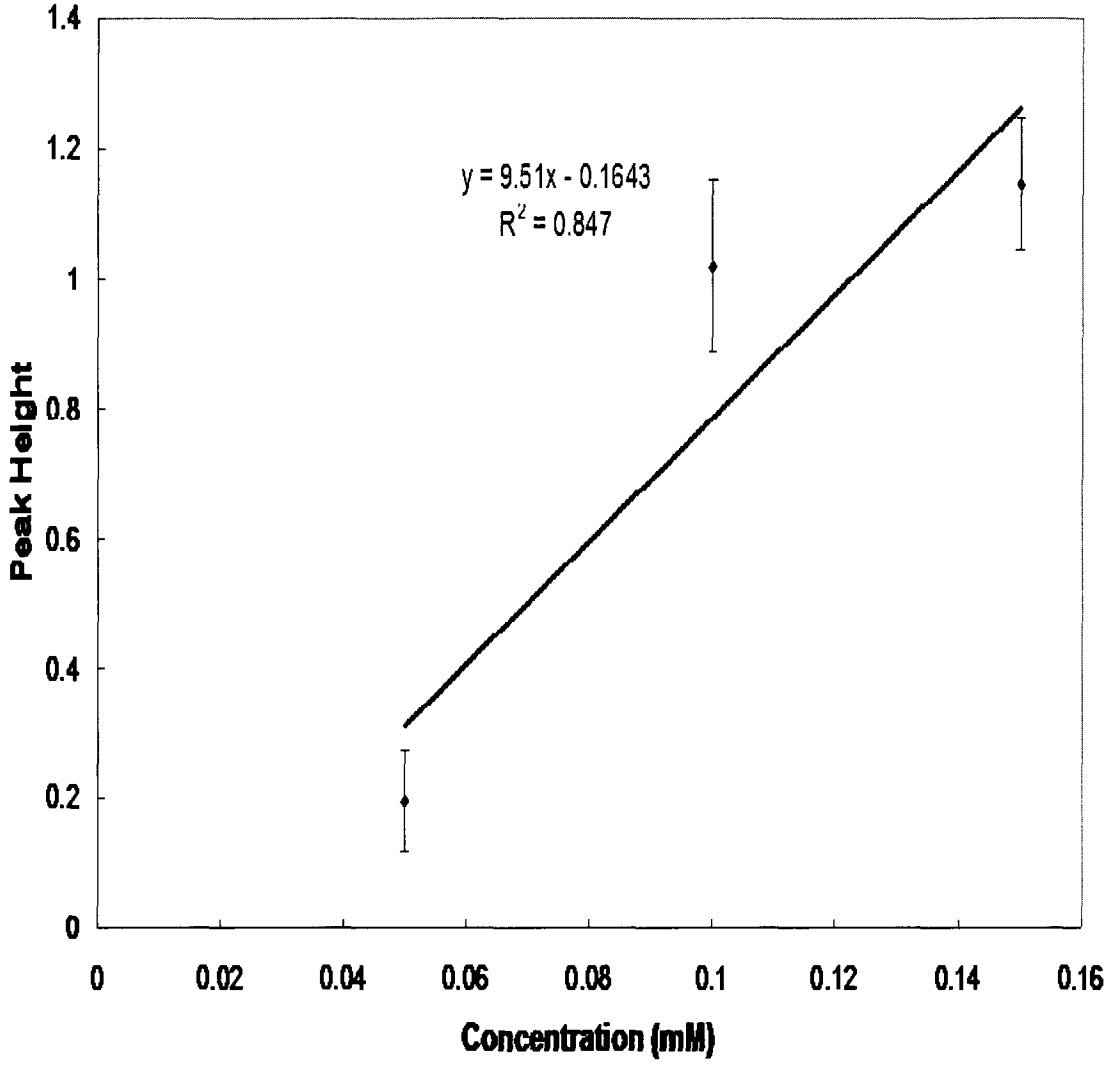

FIG. 58. Average peak Raman signal at 1598 cm^{-1} versus concentration of phenylalanine for data set one showing the range of linearity (n=4).

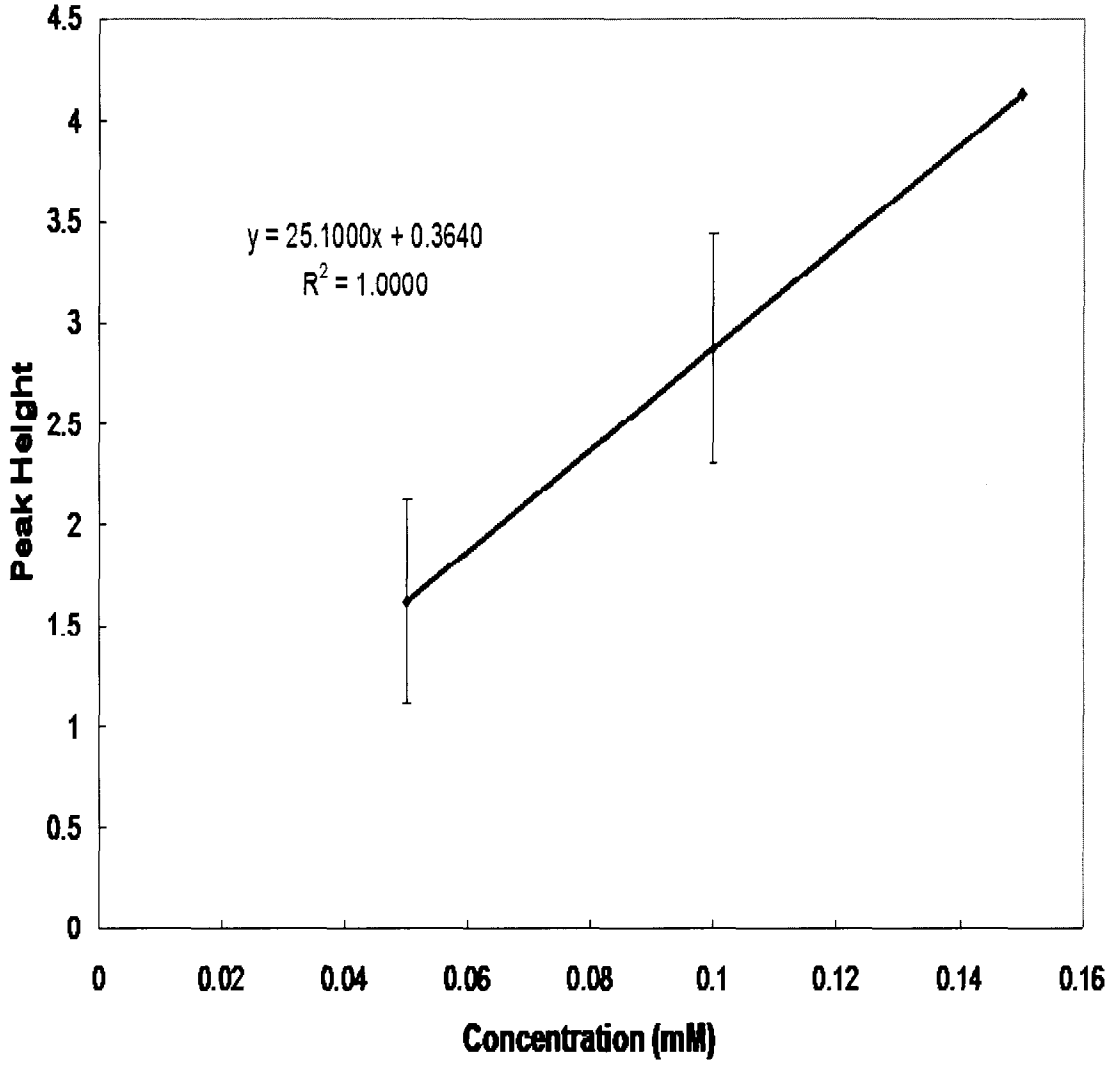

FIG. 59. Average peak Raman signal at 1001 cm^{-1} versus concentration of phenylalanine for data set two showing the range of linearity (n=4).

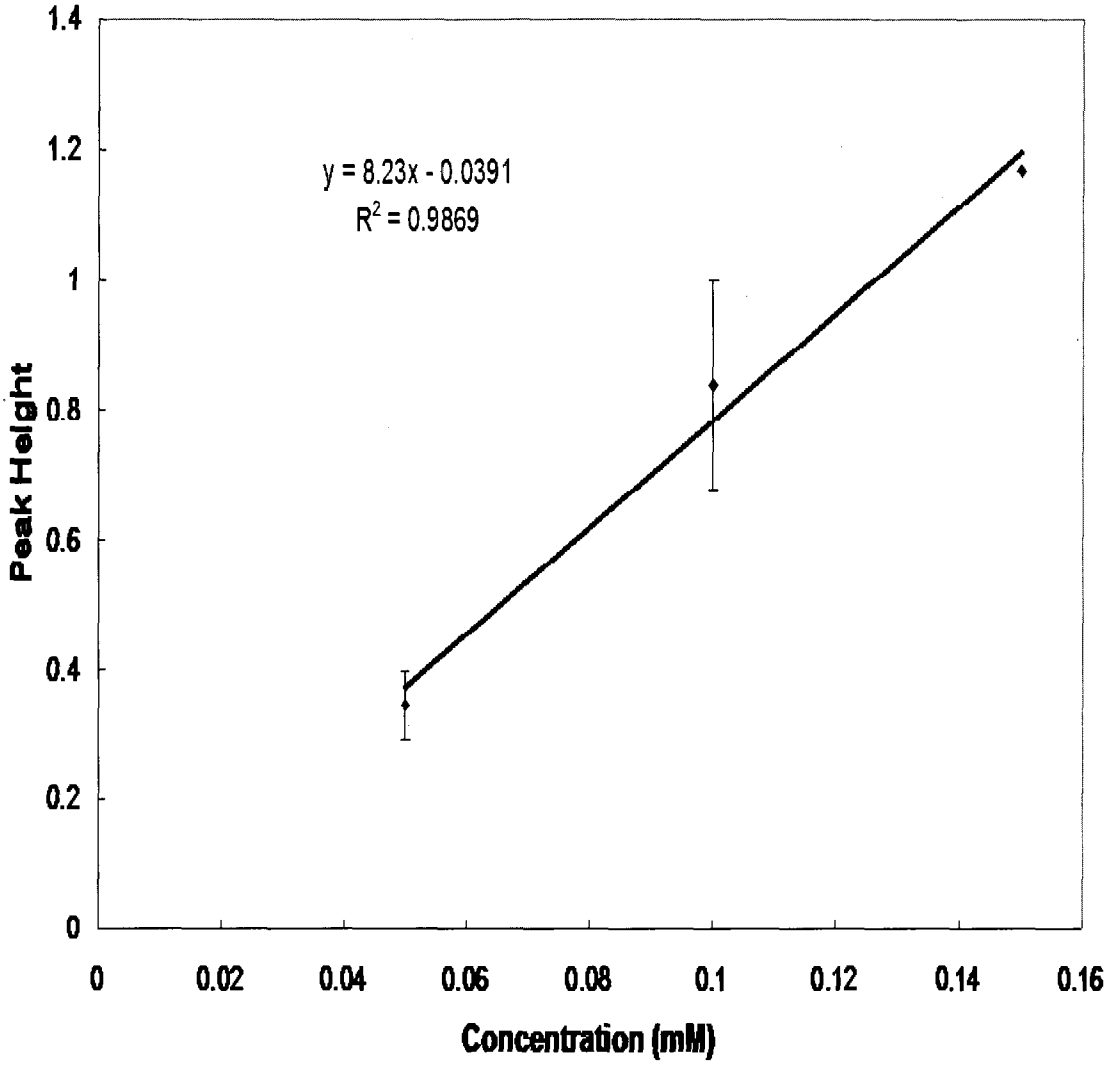

FIG. 60. Average peak Raman signal at 1031 cm^{-1} versus concentration of phenylalanine for data set two showing the range of linearity (n=4).

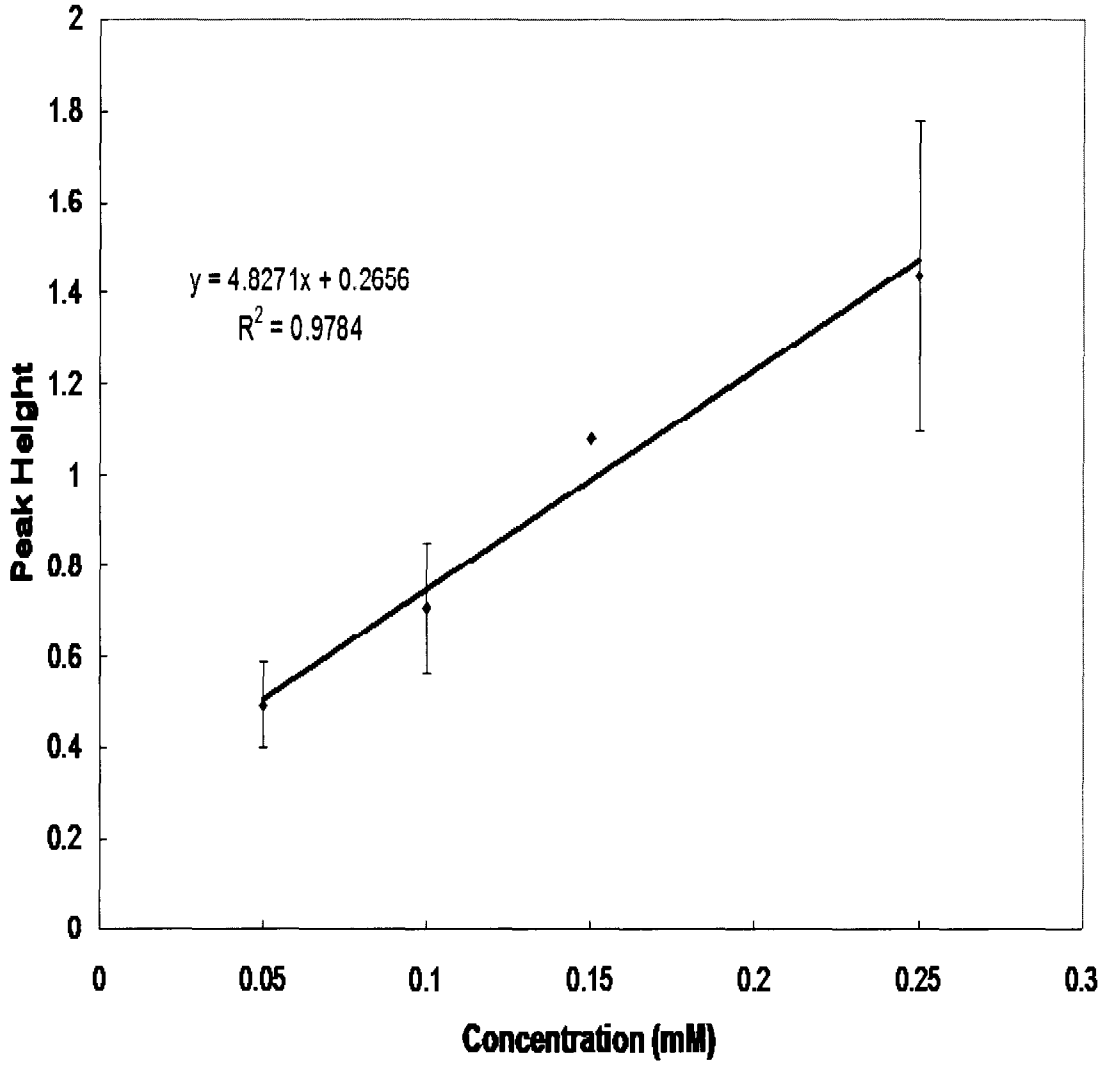

FIG. 61. Average peak Raman signal at 1598 cm^{-1} versus concentration of phenylalanine for data set two showing the range of linearity (n=4).

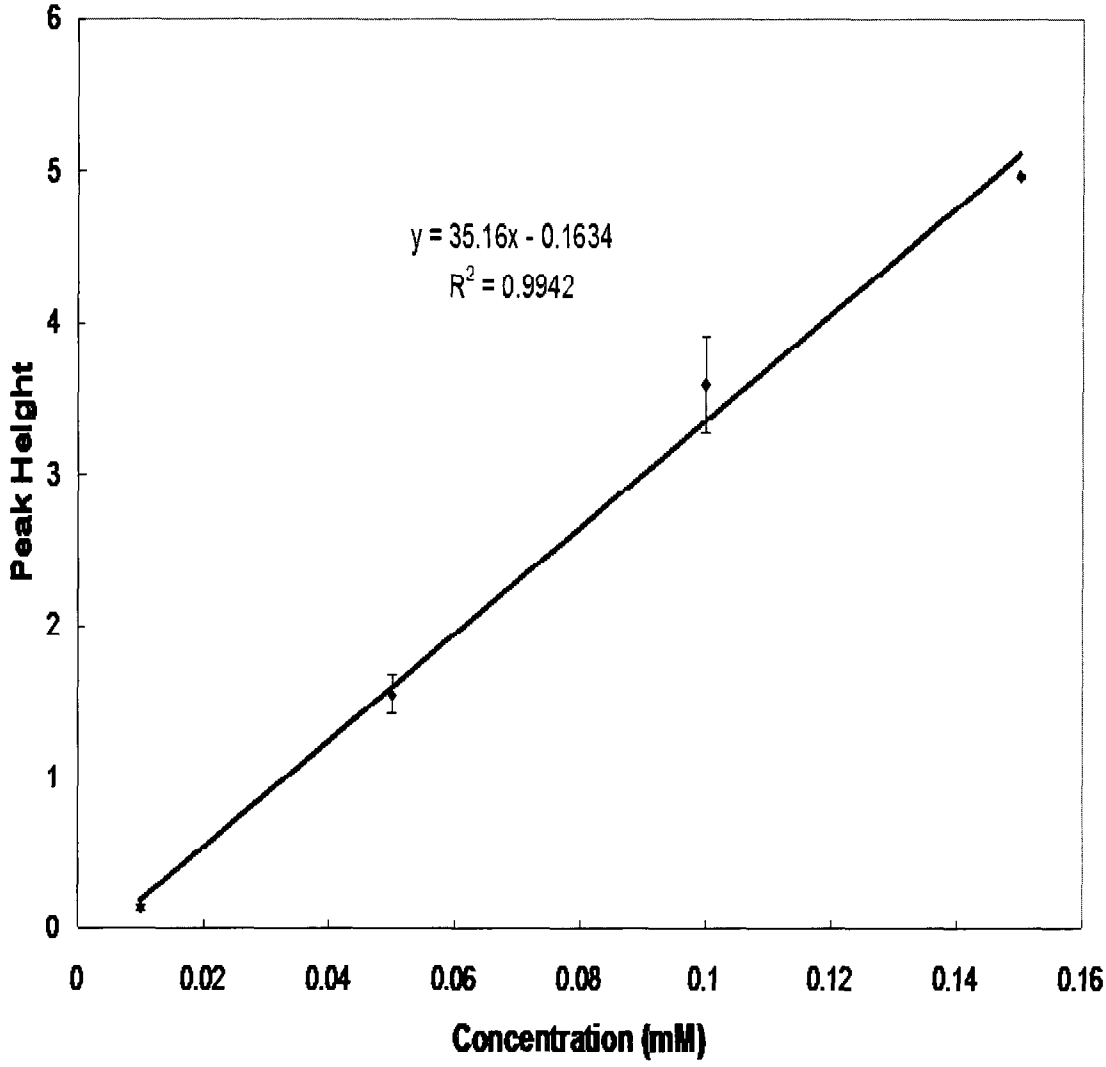

FIG. 62. Average peak Raman signal at 1001 cm^{-1} versus concentration of phenylalanine for data set three showing the range of linearity (n=4).

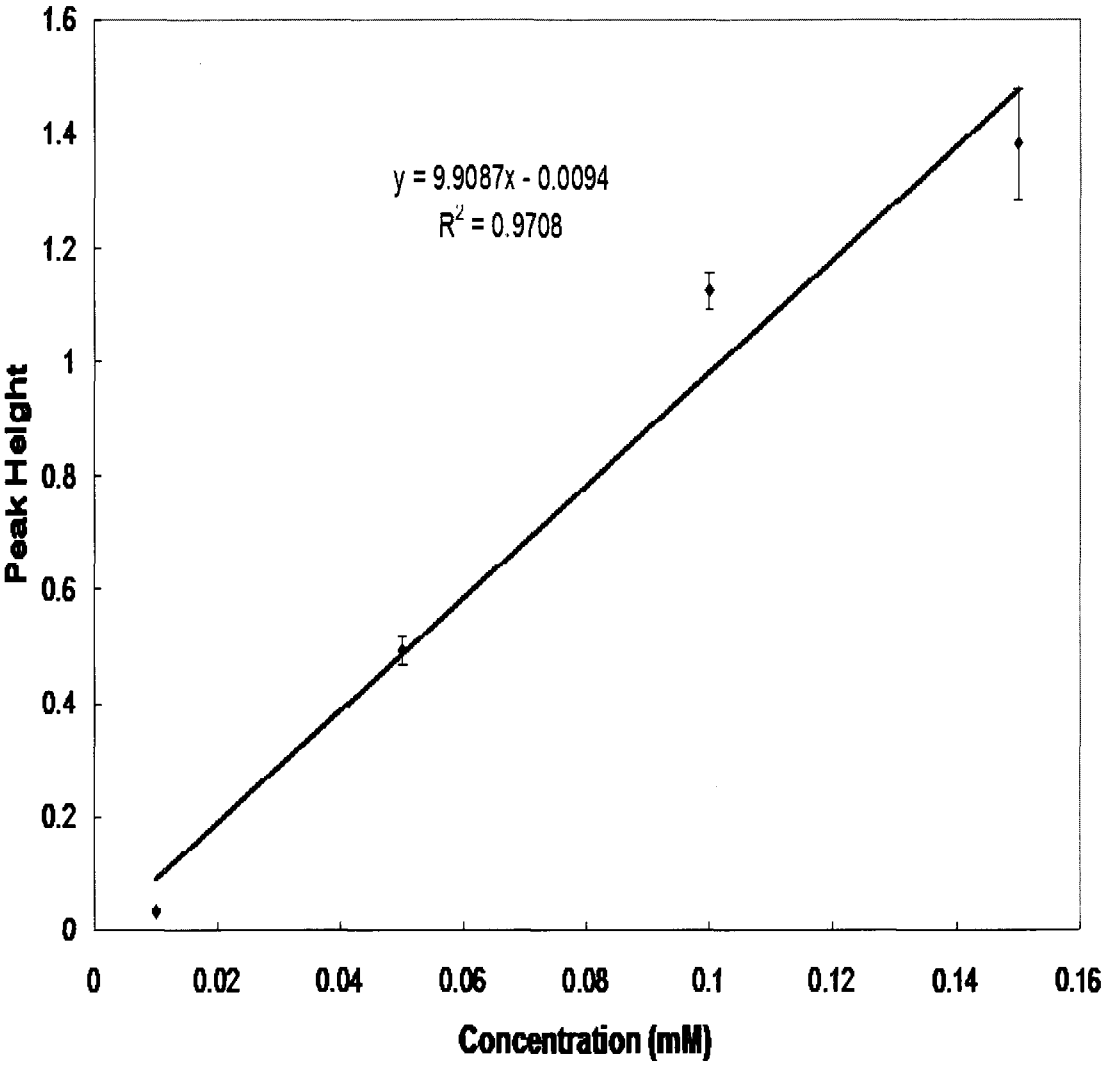

FIG. 63. Average peak Raman signal at 1031 cm^{-1} versus concentration of phenylalanine for data set three showing the range of linearity (n=4).

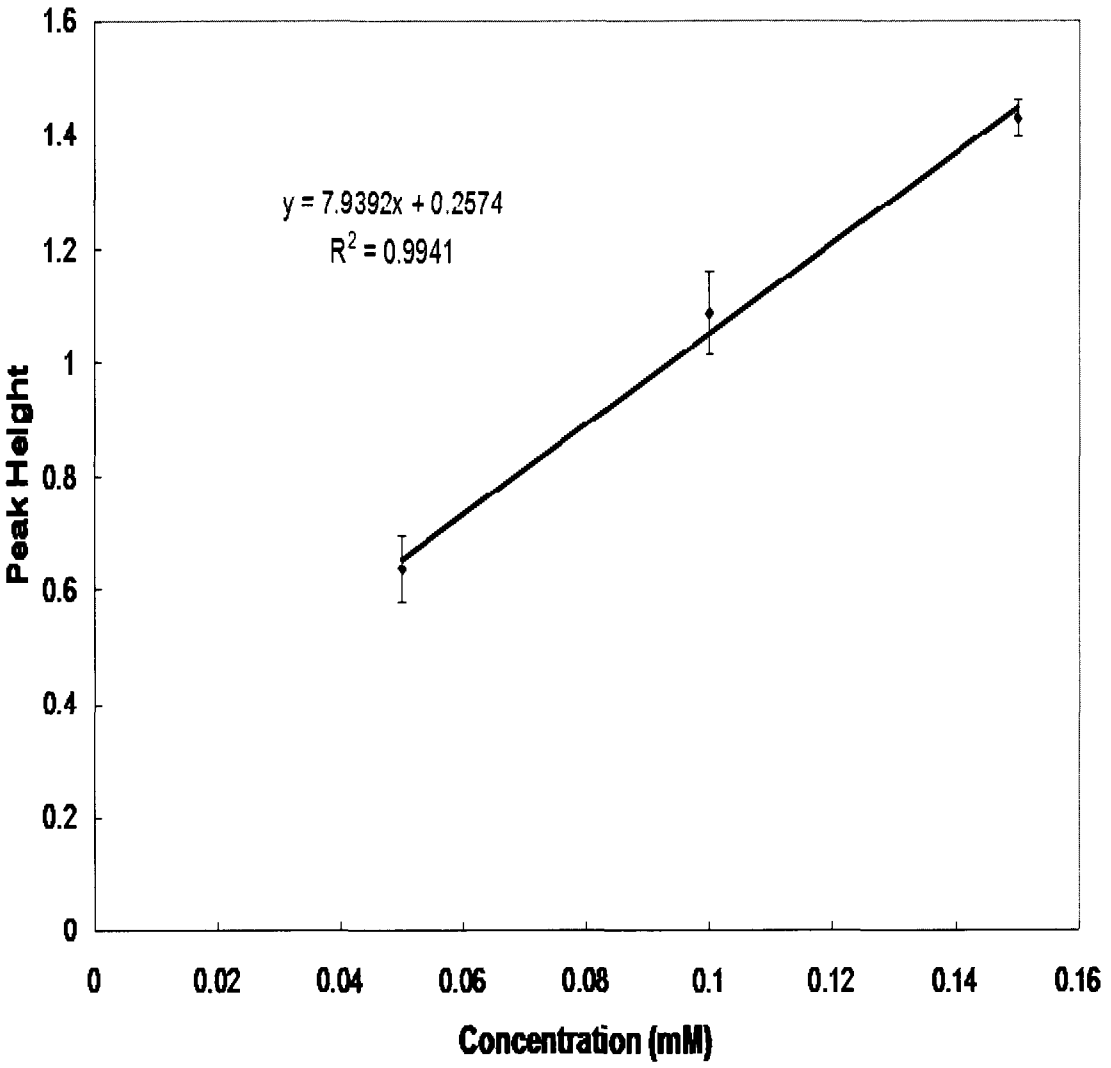

FIG. 64. Average peak Raman signal at 1598 cm^{-1} versus concentration of phenylalanine for data set three showing the range of linearity (n=4).

TABLE VII. Summary of the Standard Deviations for Data Set One Glass.

	1001 cm^{-1}		1031 cm^{-1}		1598 cm^{-1}	
Concentration (mM)	Standard Deviation	% Standard Deviation	Standard Deviation	% Standard Deviation	Standard Deviation	% Standard Deviation
0.010	0.034	50.152	0.001	3.506	-	-
0.050	0.378	43.358	0.078	38.381	0.078	40.354
0.100	0.836	20.887	0.143	13.889	0.134	13.149
0.150	0.732	16.188	0.262	22.562	0.102	8.864
0.250	0.852	17.491	0.067	5.731	0.066	4.928
0.500	0.382	18.810	0.134	25.591	0.106	21.869
1.000	1.184	21.810	0.189	15.049	0.267	17.451

TABLE VIII. Summary of the Standard Deviations for Data Set Two Glass.

	1001 cm^{-1}		1031 cm^{-1}		1598 cm^{-1}	
Concentration (mM)	Standard Deviation	% Standard Deviation	Standard Deviation	% Standard Deviation	Standard Deviation	% Standard Deviation
0.010	0.033	118.324	-	-	-	-
0.050	0.504	31.106	0.053	15.354	0.094	19.151
0.100	0.568	19.794	0.161	19.181	0.143	20.171
0.150	0.000	0.000	0.000	0.000	0.000	0.000
0.250	1.691	34.292	0.381	31.513	0.341	23.706
0.500	2.154	80.616	0.318	60.745	0.429	82.037
1.000	0.311	6.813	0.230	19.607	0.311	26.028

TABLE IX. Summary of the Standard Deviations for Data Set Three Glass.

	1001 cm^{-1}		1031 cm^{-1}		1598 cm^{-1}	
Concentration (mM)	Standard Deviation	% Standard Deviation	Standard Deviation	% Standard Deviation	Standard Deviation	% Standard Deviation
0.010	0.019	13.564	0.004	10.448	-	-
0.050	0.131	8.431	0.025	5.124	0.059	9.221
0.100	0.319	8.900	0.031	2.781	0.074	6.843
0.150	0.012	0.249	0.096	6.945	0.032	2.270
0.250	0.989	21.637	0.221	16.557	0.345	24.912
0.500	0.881	18.566	0.181	13.570	0.239	15.379
1.000	5.604	103.402	1.519	95.725	1.608	96.722

larger than ± 35% for any point within the linear range and only two points were actually greater than ± 35%.

The results from three data sets reveal that the limit of detection for the glass fiber filter is 0.01 mM. The phenylalanine peak at 1001 cm^{-1} could be clearly resolved at this concentration for two of the three data sets. No phenylalanine peak was observed in the spectra for data set two. There was, however, an abnormally high background noise for the spectra at this concentration. This could possibly be due to contamination of the sample or filter surface. It is important to note that none of the other phenylalanine peaks could be resolved for any of the spectra at this concentration. Attempts to obtain spectra at concentrations lower than 0.01 mM revealed only noise and no resolvable peaks.

A comparison of the plots for the three different peaks Raman signals was made to determine any relationships between each peak and to see if one peak gave better results than the others. Several observations were made from the comparison. In general, the plots for the peak at 1001 cm^{-1} were the most linear. Also, the plots for the peak at 100 cm^{-1} had a significantly larger slope than the other two peaks. This meant that the Raman signal for this peak increased its signal strength more than the other two peaks for increasing analyte concentration. The plots from the other two peaks were comparable to one another with the plots for the peak at 1598 cm^{-1} tending to be slightly more linear. The slopes of the lines for the plots at these two peaks were generally close to another. The standard deviations for the plots of the peak at 1001 cm^{-1} were typically higher then for the other two peaks. This could be due to the fact that the peak at 1001 cm^{-1} has the largest peak intensity of the three peaks and also has the largest rate of change of the Raman intensity for increasing analyte concentrations. This will lead to

greater variability between measurements. Also, the largest deviations were observed at the lowest phenylalanine concentration. Since the peak at 1001 cm^{-1} was the only detectable peak at this concentration, its standard deviation was higher. The standard deviations for the other two peaks were almost identical to one another. The results from the comparison suggest that for quantification purposes the peak at 1001 cm^{-1} gave the best results. The fact that it had the most linear plots with the greatest slope value and that its signal was the largest of the three peaks suggest that the results from this peak would be the most reliable. The difference in standard deviations data points at this peak compared to the other two peaks was not great enough to prevent using it for quantification

The results from the three data sets were averaged together and peak Raman signal versus concentration plots for each peak analyzed were prepared and are given in Figure 65-67. Again, Figure 67 consists of only three data points because the peak height for the 0.1 mM phenylalanine concentration at 1598 cm^{-1} could not be clearly resolved. The error bars in these plots represent the standard deviation between each set of data at each data point. A summary of the standard deviation for each plot is given in Table X. The linearity of the combined plots was comparable for each peak Raman signal plot with R^2 values of 0.997, 0.9656, and 0.9987 for 1001, 1031, and 1598 cm^{-1}, respectively. The SD for the combined data set ranged from as high as ± 68% to as low as ± 4%. As with the individual data sets, the combined data set showed the greatest SD at the points outside of the linear range and for the point at the detection limit, with the exception of the data points at 0.05 mM. The SD for the remaining data points within the linear range was less than ± 30%. A comparison of the plots for each peak of the combined data

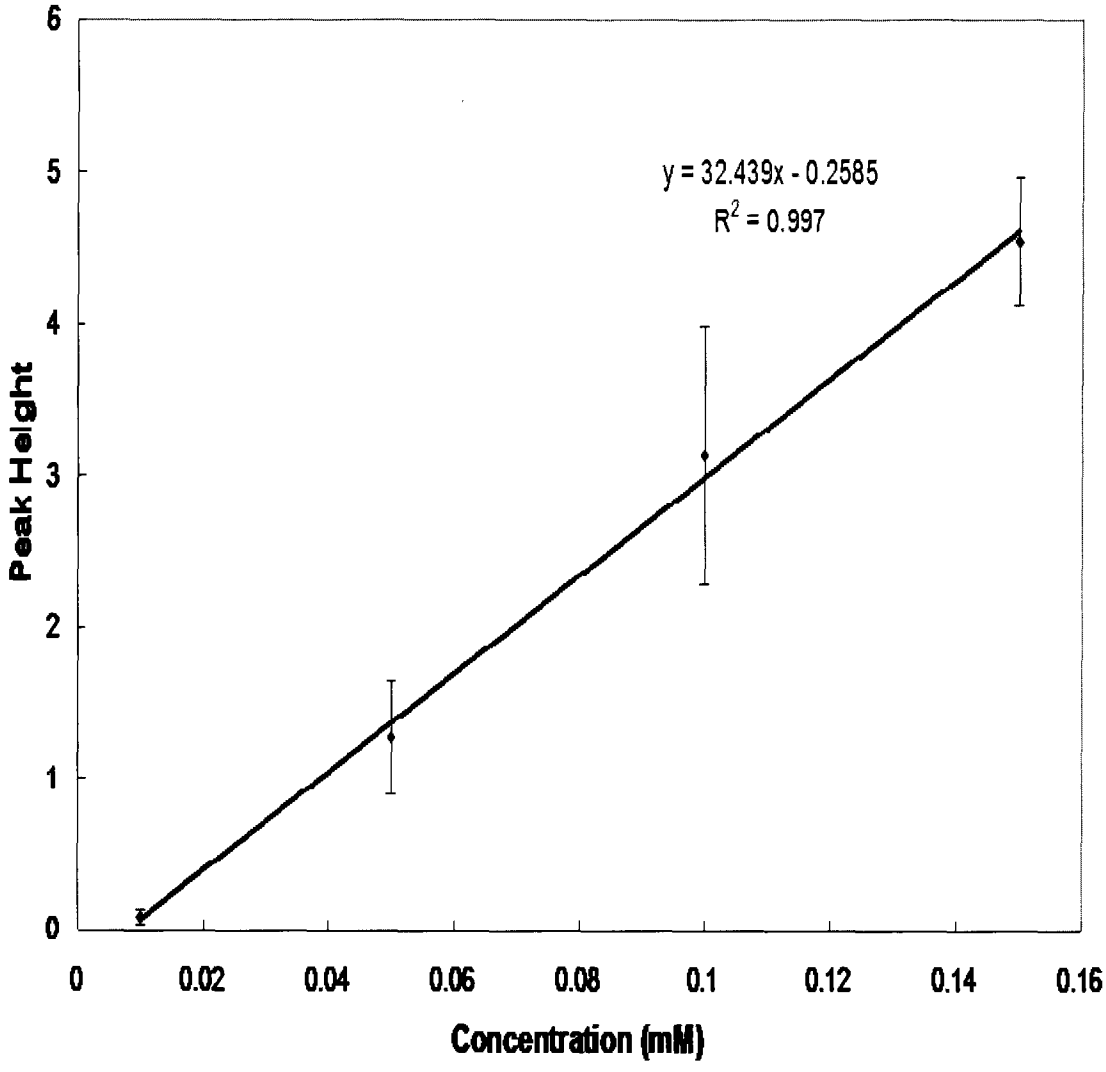

FIG. 65. Average peak Raman signal at 1001 cm^{-1} versus concentration of phenylalanine for the combined data sets showing the range of linearity (n=12).

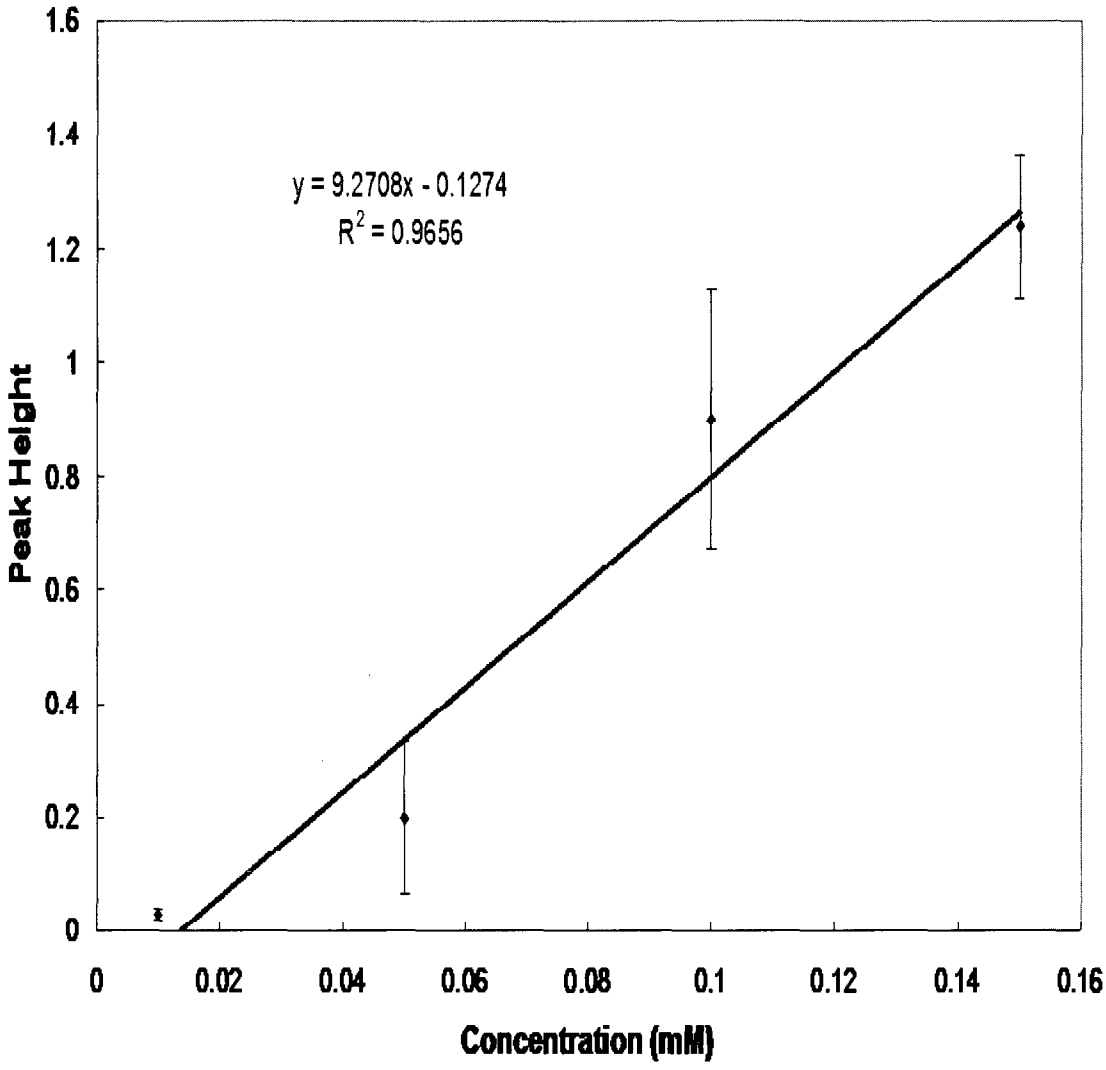

FIG. 66. Average peak Raman signal at 1031 cm^{-1} versus concentration of phenylalanine for the combined data sets showing the range of linearity (n=12).

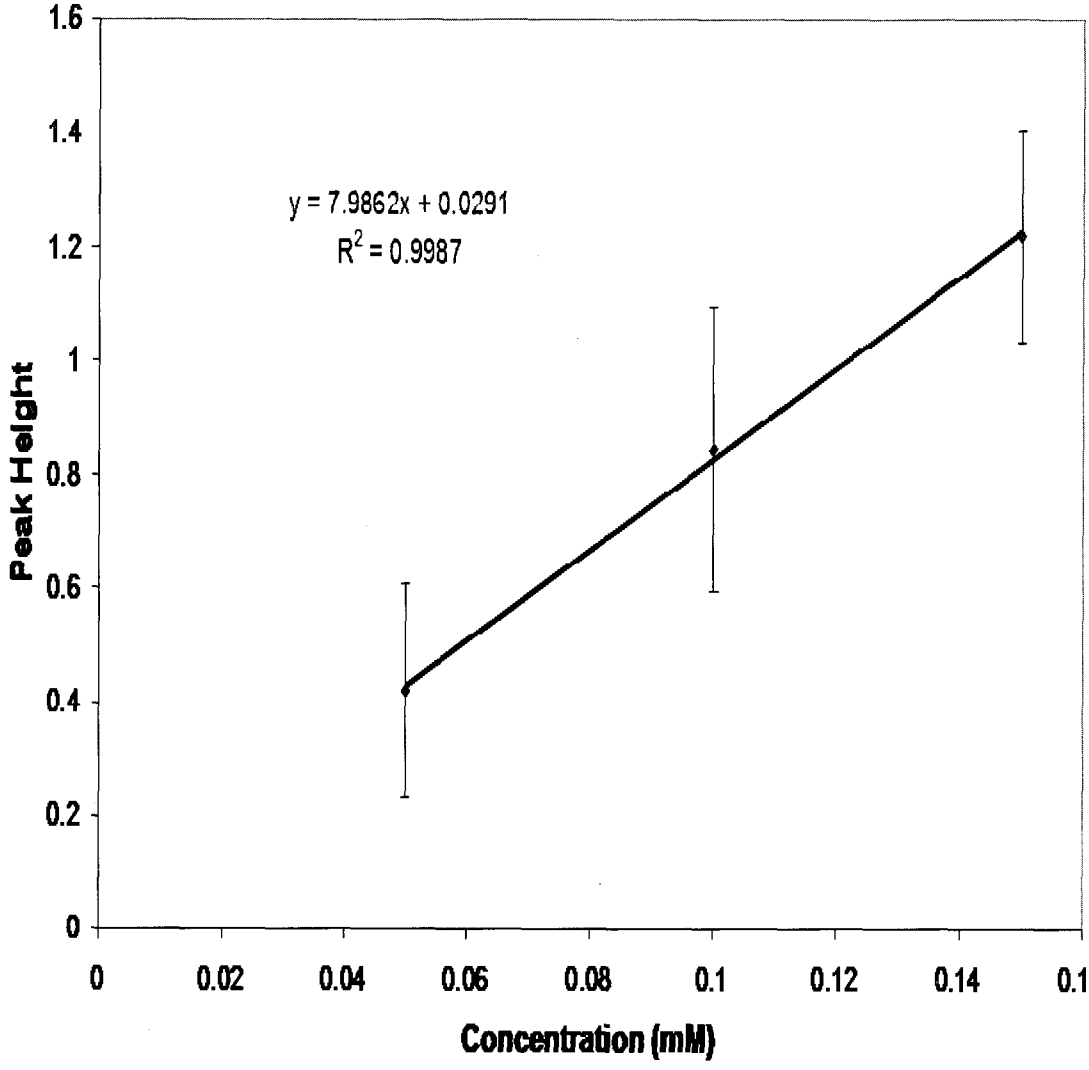

FIG. 67. Average peak Raman signal at 1598 cm^{-1} versus concentration of phenylalanine for the combined data sets showing the range of linearity (n=12).

TABLE X. Summary of the Standard Deviations for the Combined Data Sets Glass.

	1001 cm^{-1}		1031 cm^{-1}		1598 cm^{-1}	
Concentration (mM)	Standard Deviation	% Standard Deviation	Standard Deviation	% Standard Deviation	Standard Deviation	% Standard Deviation
0.010	0.047	55.986	0.010	33.907	-	-
0.050	0.370	29.261	0.133	67.519	0.189	44.975
0.100	0.852	27.219	0.227	25.174	0.250	29.589
0.150	0.421	9.272	0.125	10.131	0.186	15.299
0.250	0.194	4.049	0.086	6.920	0.054	3.883
0.500	1.179	36.171	0.397	46.716	0.526	55.799
1.000	1.322	29.336	0.436	38.163	0.427	33.510

revealed differences from the analysis of the individual data sets. The plots for the peaks at 1001 and 1031 cm^{-1} were the most linear with approximately equal R^2 values. The peak at 1598 cm^{-1} was the least linear. The standard deviation between the sets of data was similar for all three peaks; no specific trend was observed. The slope of the linear regression for all three plots was similar to what they were for the individual data sets.

A new set of experiments was conducted to establish the linear concentration range and the limit of detection for silver-coated quartz fiber filters. Because it was already demonstrated that the linear concentration range of the quartz filters was greater than the linear range of the glass fiber filter, a different set of concentrations was used in the experiments. For these new experiments, SERS measurements were made on 0.2, 0.4, 0.6, and 0.8 mM phenylalanine solutions. Two data sets were acquired using these concentrations. The average spectra from each of the data sets are given in Figures 68 and 69. The spectra were analyzed in the same manner as the spectra acquired using the glass fiber filter. The peak Raman signal for the three strongest peaks (1001, 1031, and 1598 cm^{-1}) was recorded and a plot of the peak Raman signal versus phenylalanine concentration was prepared for each peak in each data set. The resulting plots are given in Figures 70 and 71. The error bars represent the standard deviation of the SERS measurements for each data point. The plots for data set one reveal a linear range between 0.2 and 0.6 mM, while the plots for data set two reveal a linear range between 0.2 and 0.8 mM. New peak Raman signal versus concentration plots were prepared for each data set using the newly defined linear range (Figures 72-77). The new plots contained a linear regression of the data points and displayed the equation of the line and

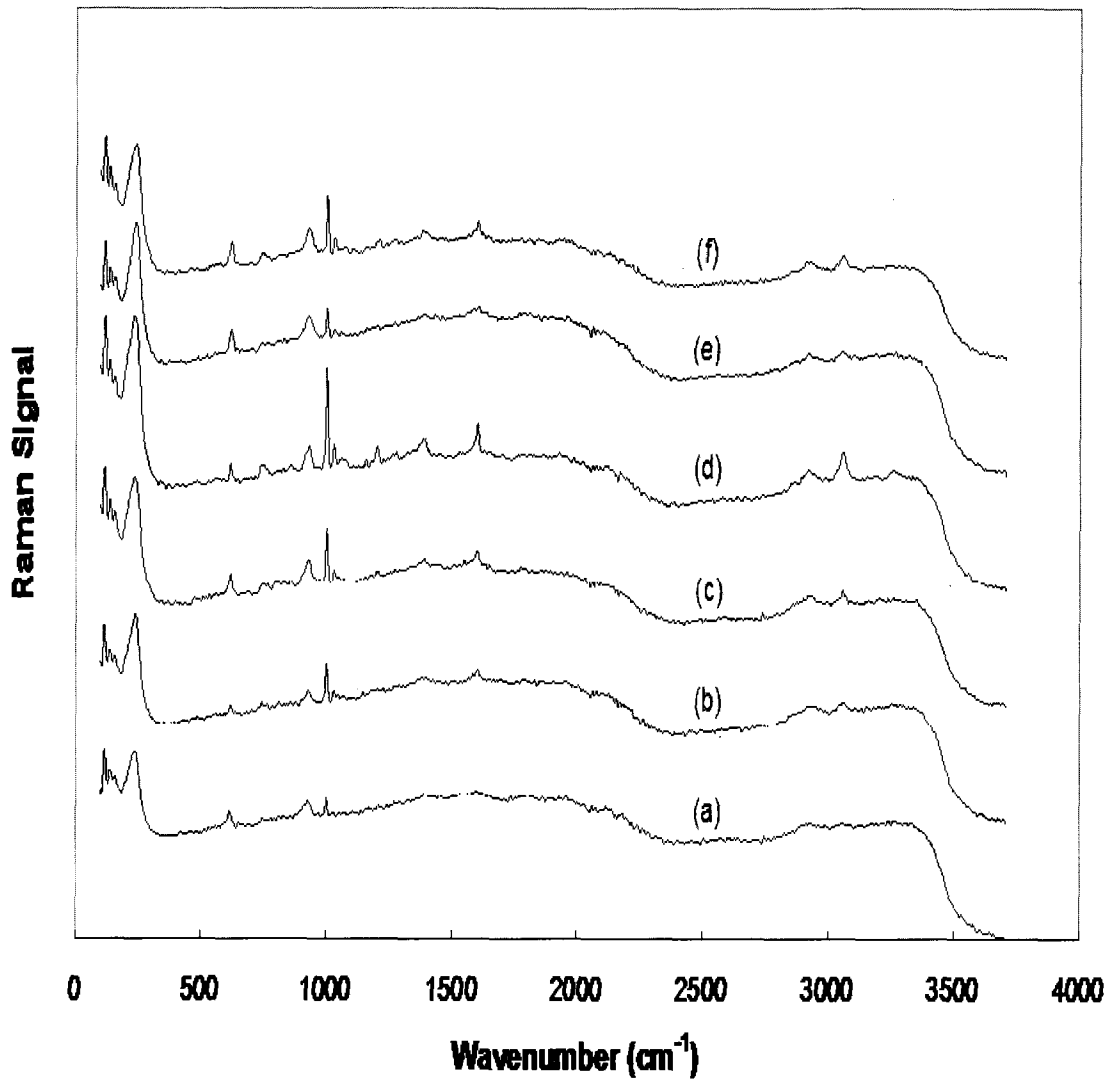

FIG. 68. Average of four SERS spectra of several concentrations of phenylalanine ((a) 0.2 mM, (b) 0.4 mM, (c) 0.5 mM, (d) 0.6 mM, (e) 0.8 mM, and(f) 1.0 mM) (100 μl samples) from data set one on quartz fiber filters (25 mmWhatman QM-A).

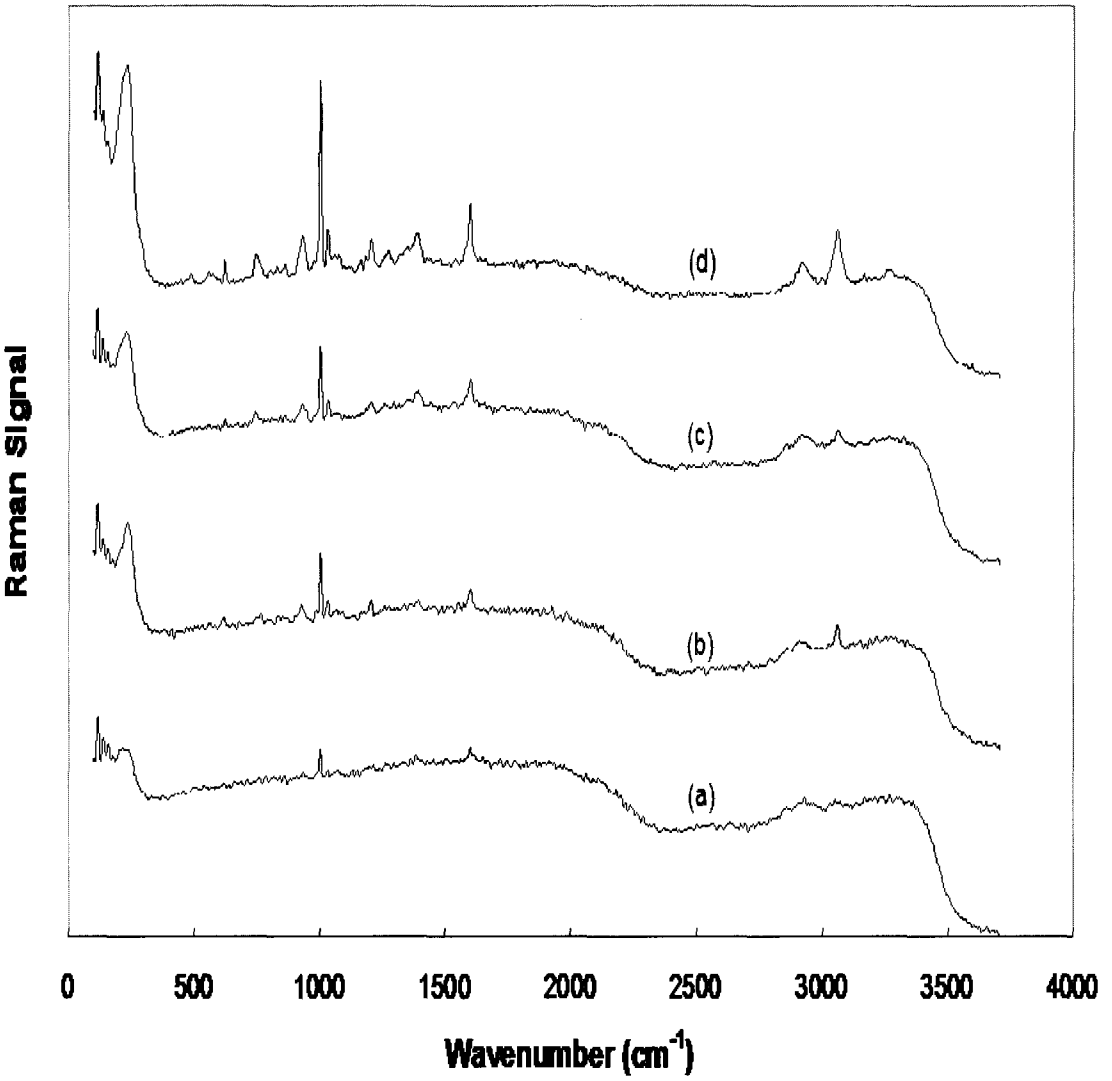

FIG. 69. Average of four SERS spectra of several concentrations of phenylalanine ((a) 0.2 mM, (b) 0.4 mM, (c) 0.6 mM, and (d) 0.8 mM)) (100 μl samples) from data set two on quartz fiber filters (25 mmWhatman QM-A).

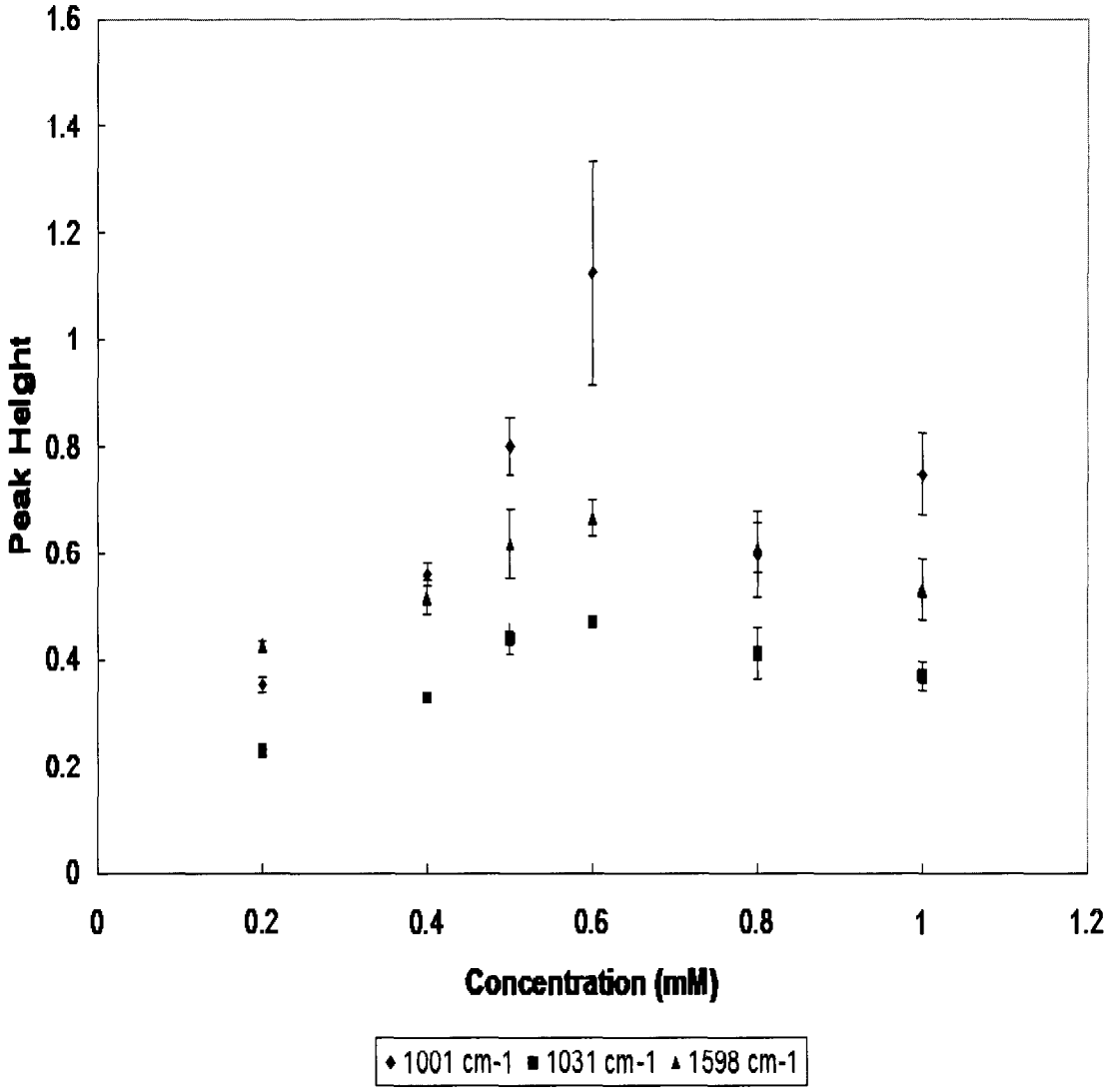

FIG. 70. Average peak Raman signal versus concentration of phenylalanine from data set one for SERS spectra obtained from silver-coated quartz fiber filters (n=4).

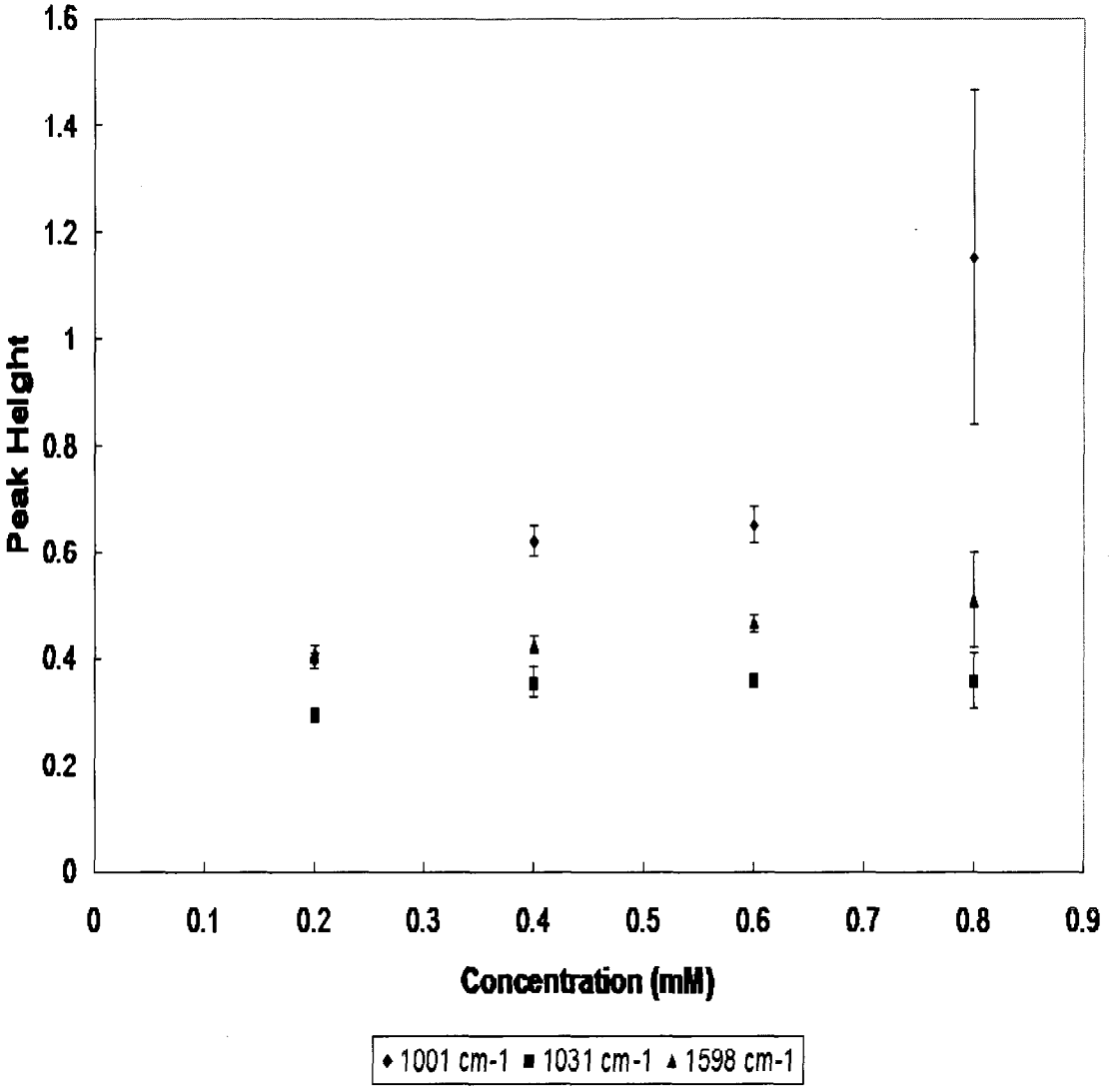

FIG. 71. Average peak Raman signal versus concentration of phenylalanine from data set two for SERS spectra obtained from silver-coated quartz fiber filters (n=4).

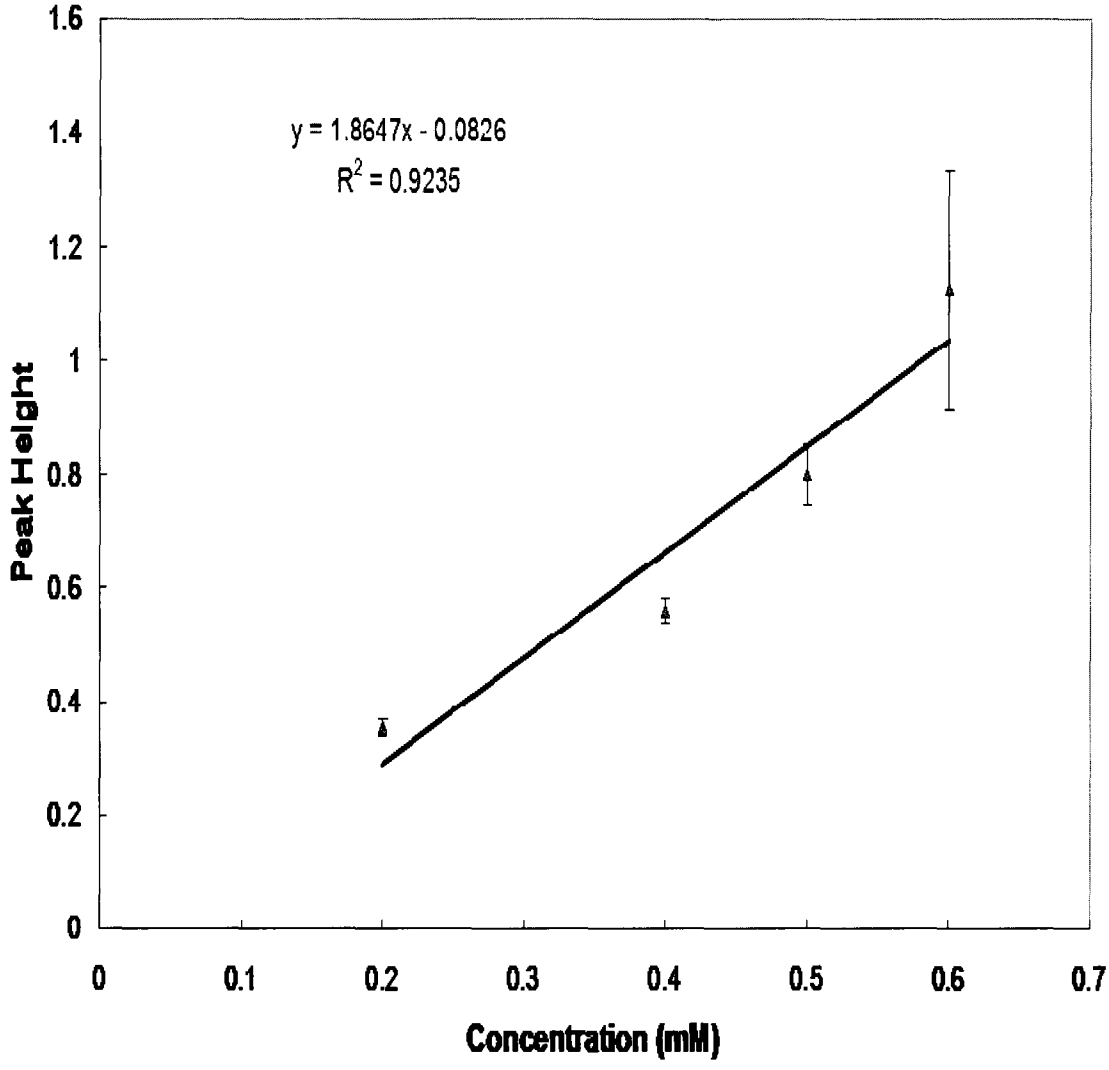

FIG. 72. Average peak Raman signal at 1001 cm^{-1} versus concentration of phenylalanine for data set one from the quartz filters showing the range of linearity (n=4).

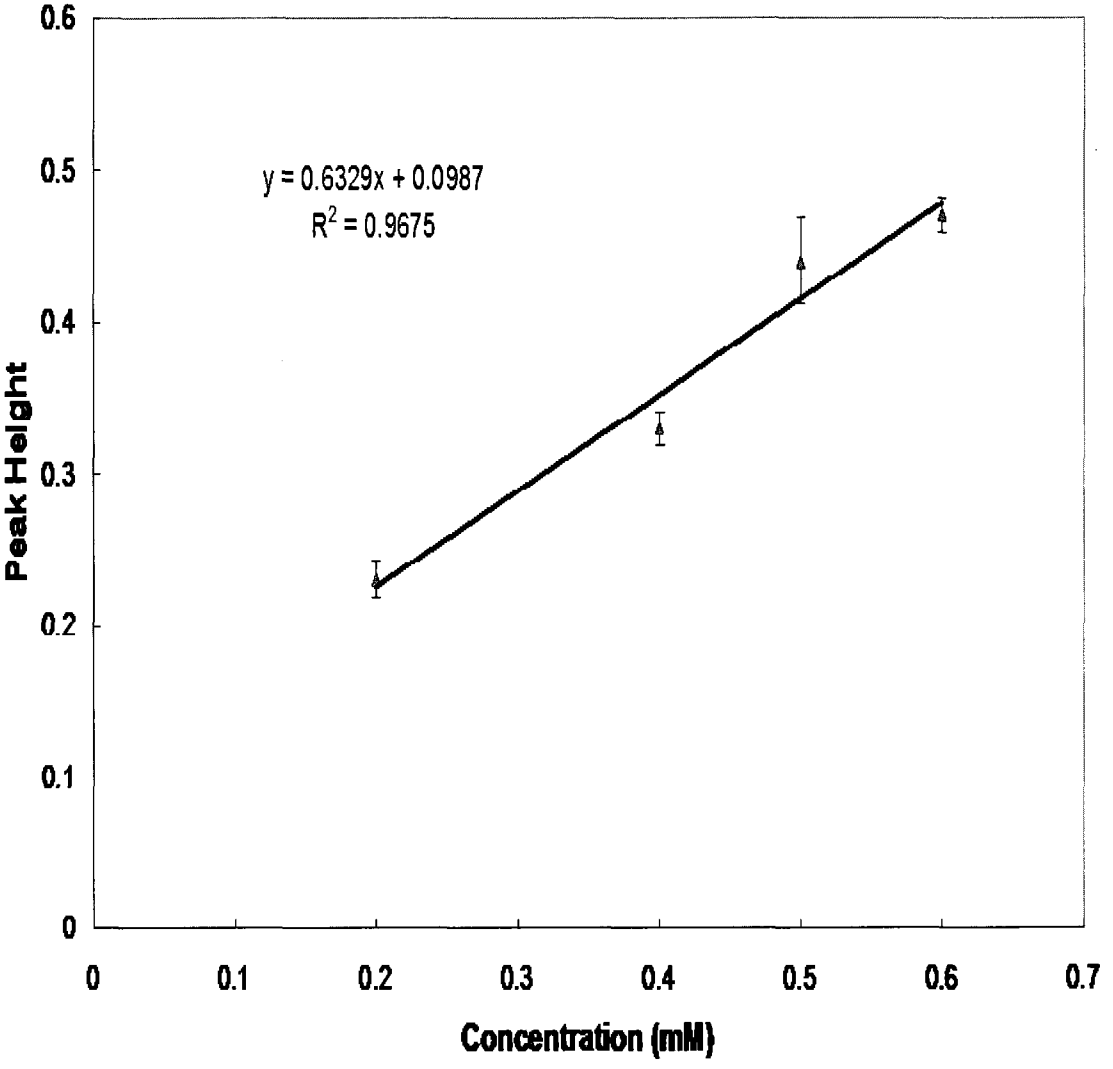

FIG. 73. Average peak Raman signal at 1031 cm^{-1} versus concentration of phenylalanine for data set one from the quartz filters showing the range of linearity (n=4).

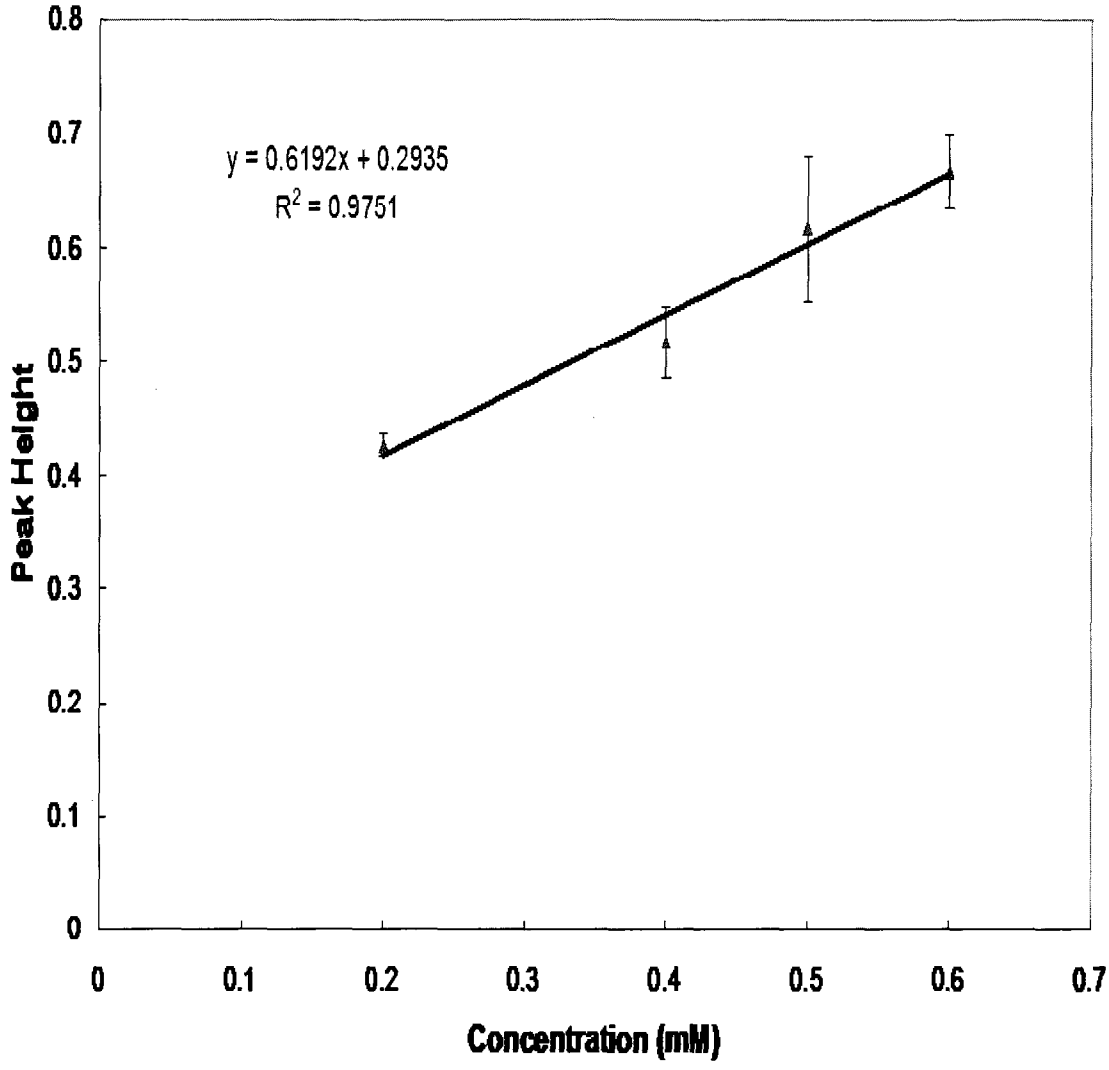

FIG. 74. Average peak Raman signal at 1598 cm^{-1} versus concentration of phenylalanine for data set one from the quartz filters showing the range of linearity (n=4).

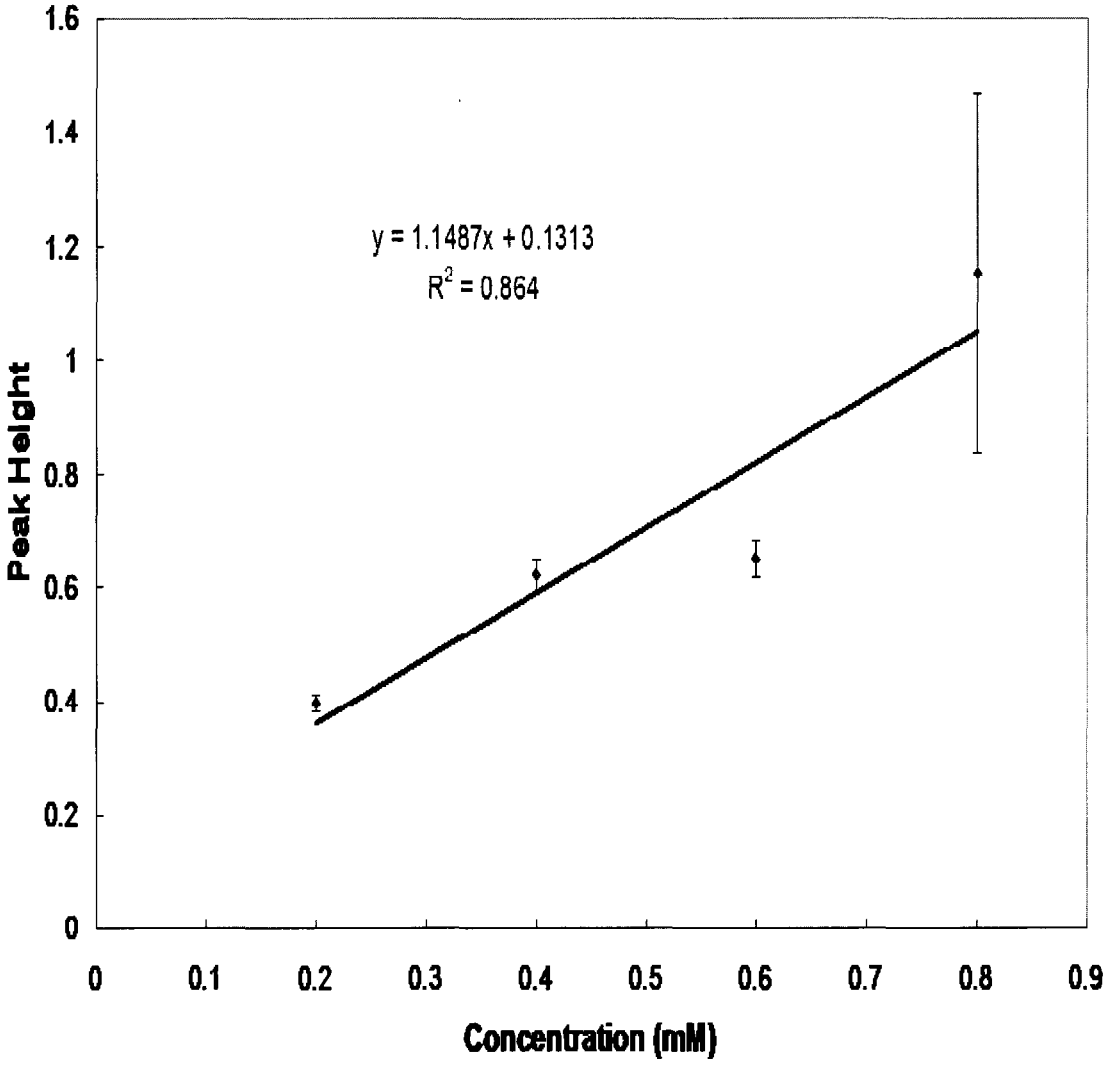

FIG. 75. Average peak Raman signal at 1001 cm^{-1} versus concentration of phenylalanine for data set two from the quartz filters showing the range of linearity (n=4).

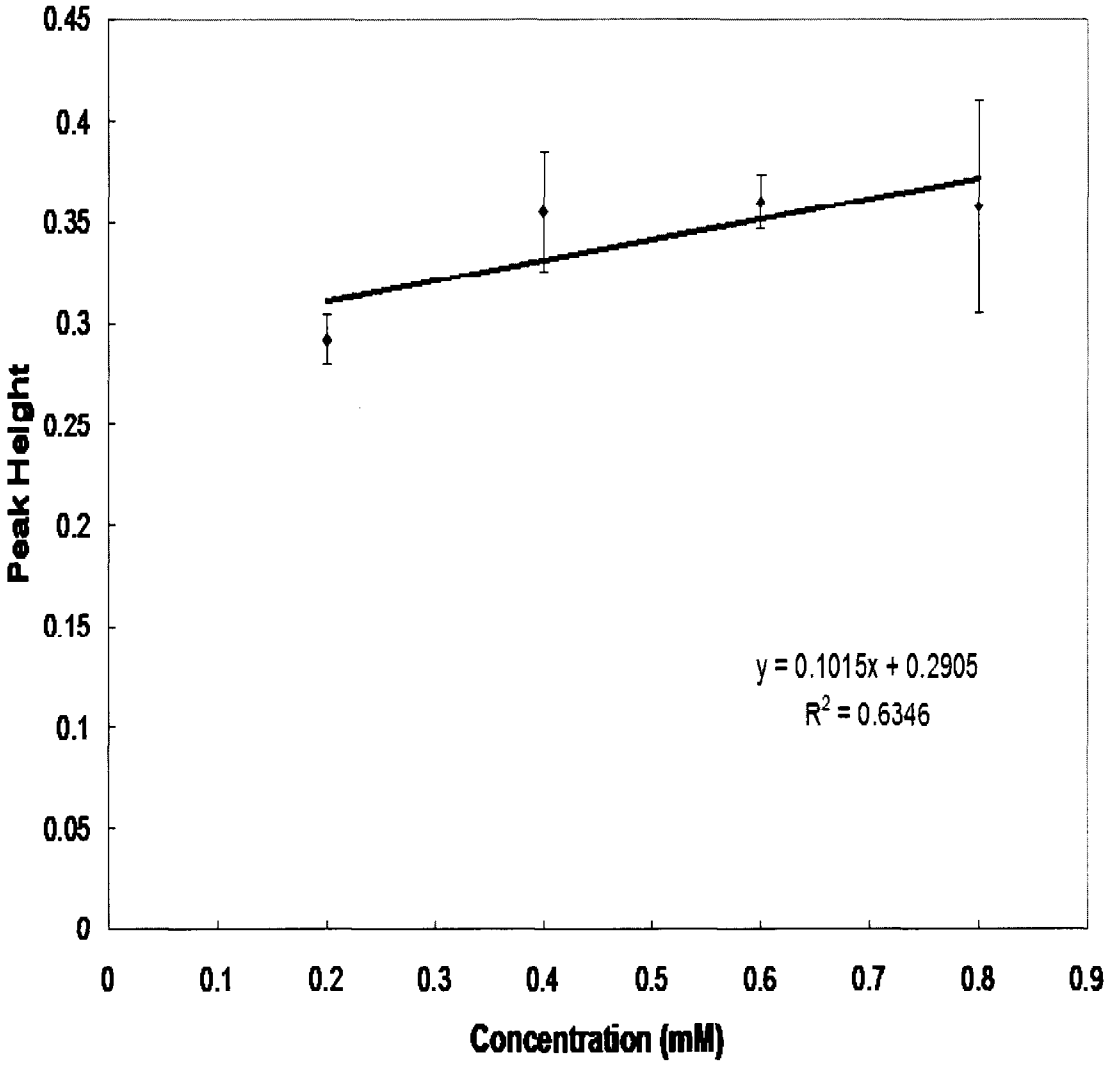

FIG. 76. Average peak Raman signal at 1031 cm^{-1} versus concentration of phenylalanine for data set two from the quartz filters showing the range of linearity (n=4).

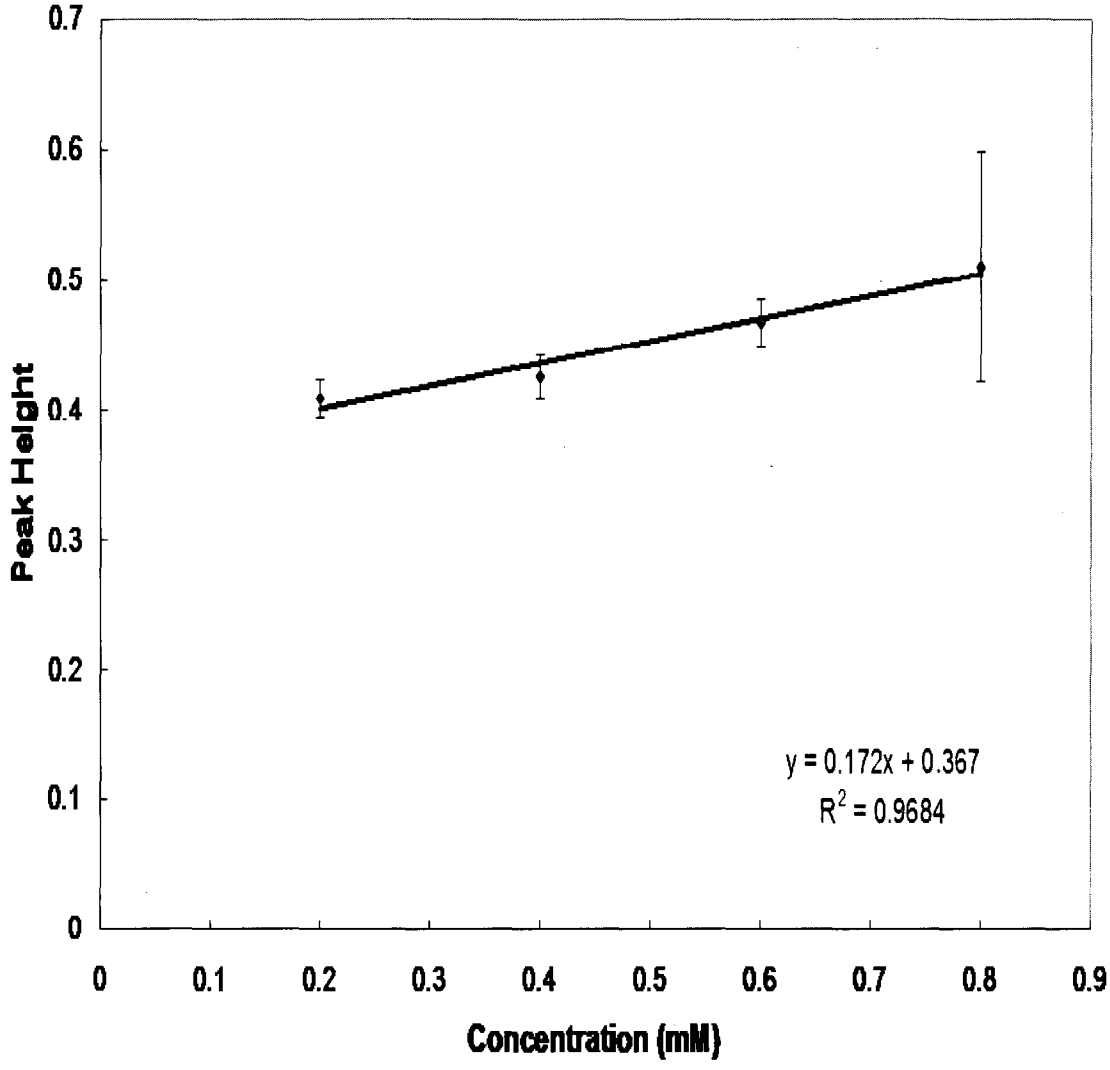

FIG. 77. Average peak Raman signal at 1598 cm^{-1} versus concentration of phenylalanine for data set two from the quartz filters showing the range of linearity (n=4).

TABLE XI. Summary of the Standard Deviations for Data Set One Quartz.

	1001 cm^{-1}		1031 cm^{-1}		1598 cm^{-1}	
Concentration (mM)	Standard Deviation	% Standard Deviation	Standard Deviation	% Standard Deviation	Standard Deviation	% Standard Deviation
0.200	0.015	4.146	0.012	5.310	0.010	2.293
0.400	0.021	3.728	0.011	3.330	0.031	6.083
0.500	0.054	6.712	0.028	6.435	0.064	10.347
0.600	0.210	18.639	0.012	2.474	0.032	4.844
0.800	0.080	13.375	0.047	11.485	0.047	7.616
1.000	0.076	10.141	0.027	7.335	0.056	10.514

TABLE XII. Summary of the Standard Deviations for Data Set Two Quartz.

	1001 cm^{-1}		1031 cm^{-1}		1598 cm^{-1}	
Concentration (mM)	Standard Deviation	% Standard Deviation	Standard Deviation	% Standard Deviation	Standard Deviation	% Standard Deviation
0.200	0.014	3.646	0.013	4.303	0.015	3.640
0.400	0.029	4.672	0.030	8.373	0.016	3.793
0.600	0.033	5.089	0.014	3.766	0.018	3.851
0.800	0.315	27.346	0.052	14.656	0.088	17.242

the R^2 value. A summary of the standard deviation for each point in the plots is given in Tables XI and XII.

The results for data set one were the most promising. All three peaks showed good linearity with R^2 values of 0.92, 0.97, and 0.98 for the peaks at 1001, 1031, and 1598 cm^{-1}, respectively. The largest standard deviation for this set was ± 18.6% for the 0.6 mM data point at 1001 cm^{-1}. The lowest SD was ± 2.29% for the 0.2 mM data point at 1598 cm^{-1}. In general, the standard deviations between peaks were consistent for each phenylalanine concentration. The results of data set two were not as good. The peak Raman signal versus phenylalanine concentration plots showed a large deviation from linearity. The R^2 values of these plots were 0.86, 0.63, and 0.97 for the peaks at 1001, 1031, and 1598 cm^{-1}, respectively. For the peak at 1001 cm^{-1}, the large deviation can be attributed to the low Raman signal observed for the data point at 0.6 mM. The peak Raman signal at this data point was 0.651. This is significantly lower then value of 1.12 observed from the same data point in data set one. The other data points compare favorably between data sets. This low value observed for the 0.6 mM data point in data set two could possibly be attributed to sample contamination. The standard deviations for data set two were similar to that of data set one. The largest standard deviation was ± 27 % for the 0.8 mM data point at 1001 cm^{-1}. The lowest standard deviation was ± 3.64% for the 0.2 mM data point at 1598 cm^{-1}.

A comparison of the peak Raman signal versus phenylalanine concentration plots for each data set to one another suggests that the peak at 1001 cm^{-1} would be the only peak useful for quantitative purposes using quartz fiber filters. The peak Raman signals for the peak at 1031 and 1598 cm^{-1} were too weak causing the overall change in the peak

Raman signal over a range of increasing phenylalanine concentrations to be very small. This can be seen by the low slope values observed from the linear regressions of the plots at these peaks. For this reason, these peaks were not considered to be reliable to use for quantitative purposes. The standard deviations of the data points were similar for each of the data sets with the highest deviations occurring at the higher concentrations.

The results for the plots at 1001 cm^{-1} were averaged together and a new plot of the peak Raman signal versus phenylalanine concentration was prepared. This plot is given in Figure 78. The error bars represent the standard deviation between the two data sets for each data point. A summary of the standard deviation at each point is given in Table XIII. The results from the plots at 1031 and 1598 cm^{-1} were not averaged together because they were considered unreliable due to the weak signal at these peaks. The linearity of the combined plot at 1001 cm^{-1} was good as evidenced by the high R^2 value of 0.99. The standard deviation was high, ± 45% and ± 38%, for the two highest concentrations 0.6 and 0.8 mM, respectively. This result agrees with what was observed in the individual data sets. The two low concentration points, 0.2 and 0.4 mM, had a lower standard deviation, ± 8% and ± 7%.

A comparison of the results from both quartz fiber and glass fiber filters was made to determine if one was more effective than the other. This proved to be difficult because two different phenylalanine concentration ranges were used for each filter type. In general, the glass fiber filters gave higher standard deviations for each data point. This may be attributed to the more intense Raman signals associated with the glass filters. Also, the peak Raman signal versus phenylalanine concentration plots for the glass fiber filters tended to be more linear. This too may be attributed to the higher intensity Raman

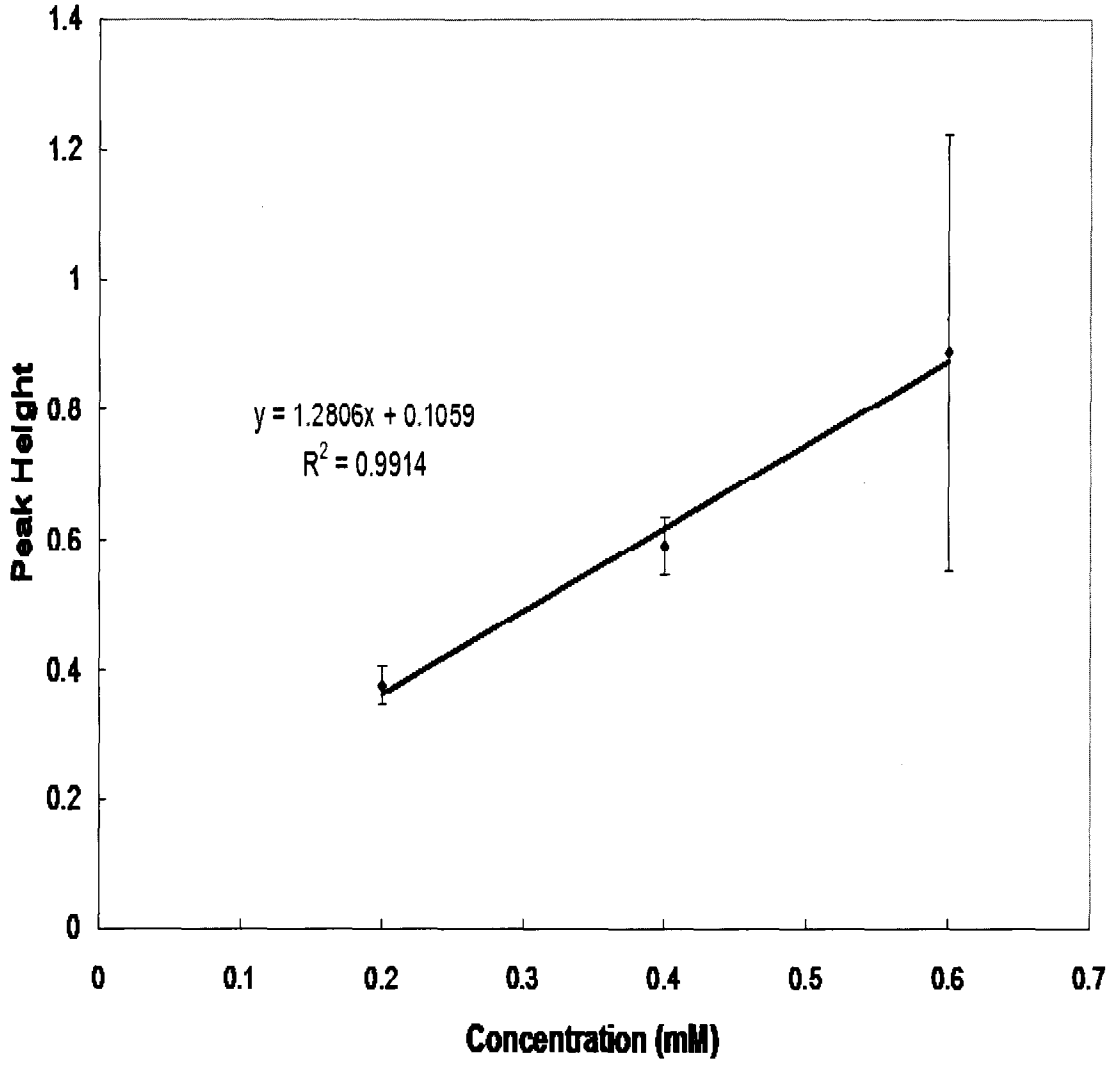

FIG. 78. Average peak Raman signal at 1001 cm^{-1} versus concentration of phenylalanine for the combined data sets from the silver-coated quartz fiber filters showing the range of linearity (n=8).

TABLE XIII. Summary of the Standard Deviations for the Combined Data Sets Quartz.

	1001 cm^{-1}	
Concentration (mM)	Standard Deviation	% Standard Deviation
0.200	0.030	8.00
0.400	0.044	7.44
0.600	0.335	37.72
0.800	0.393	44.89

signals generated by the glass fiber filters. The reason for the difference in intensity between the glass and quarts filters is not clearly understood. The reason is believed to be due to the difference in the pore size (1.6 μm for glass and 2.2 μm for quartz). The range of linearity was also different for both filter types. Again, this difference was thought to be due to the difference in pore size between the filters. This result demonstrates the possibility of tuning the concentration range of the analysis by changing the pore size of the filter. Overall, the glass fiber filters performed better due to the larger Raman signals generated by these filters. The glass fiber filters are also economically more favorable and they are commercially available in a wide range of pore sizes. However, the resulting linearity of the SERS intensity versus analyte concentration from both filter types compare favorably to that found in the literature.[18,77-85]

CHAPTER V

CONCLUSIONS

Raman spectroscopy is an extremely attractive technique for the chemical analysis of biological molecules due to its highly qualitative nature.[1] With the onset of Surface-Enhanced Raman (SERS) techniques, the utility of the Raman method is even greater due to the large increase in analytical sensitivity.[3,4] Furthermore, with the potential for quantitative analysis, this technique would prove to be an invaluable tool in the biomedical sciences. In this present work, three different SERS methods using two different Raman instruments were evaluated for their potential use as a qualitative / quantitative method for biochemical analysis.

The first method evaluated was the electrochemical SERS method. In this thesis, I demonstrated the generation of a SERS signal from pyridine adsorbed to the surface of a roughened silver electrode. The Raman signal was detected utilizing a remote fiber optic probe dispersive Raman instrument. The necessary parameters for generating the optimal SERS signal were established. In fact, when using the correct parameters a significant enhancement of the Raman signal from pyridine was observed such that the instrument's detector became saturated with an integration time of 0.1s. While we were successfully able to optimize the electrochemical conditions and characterize the SERS signal of pyridine, it was determined that because of the need to use cumbersome electrochemical apparatuses, this method of SERS analysis would not be practical for clinical or biomedical applications.

The second method evaluated was the silver colloid method. The synthesis and characterization of silver colloid solutions for the effective use as a SERS active substrate was demonstrated. Two different synthesis methods (laser ablation and chemical reduction) were utilized and the conditions for optimal SERS signal strength were established. SERS signals from solutions of tryptophan were successfully generated and detected using an FT-Raman spectrometer. The use of FT-Raman is significant because it is not commonly used in Raman studies due to its low sensitivity. However, combined with a suitable SERS method, the problem of sensitivity could be overcome. This would allow the FT instruments inherent advantage of low background fluorescence and high spectral resolution to be utilized. Attempts to quantify the SERS signal utilizing an internal standard proved to be unsuccessful. Also, it was demonstrated that due to the complex nature of the colloid aggregation process, it was not possible to generate reproducible SERS signals. For these reasons, the colloid method of SERS enhancement was abandoned and a new method was developed.

The third and final method evaluated involved the development of a novel SERS substrate. In this thesis, I report the successful chemical deposition of a thin, silver film on the surface of a quartz/glass fiber filter for use as a SERS active substrate. The use of this method of silver deposition on glass or quartz fiber filters had not been previously reported in the literature. The necessary conditions for deposition that would give the optimal SERS surface were determined. The successful detection of the SERS signal of solutions of two amino acids, phenylalanine and tryptophan, utilizing the silver-coated filters and a FT-Raman instrument was demonstrated. The ability to detect mixtures of the two amino acids was also demonstrated. Significant progress was made to develop a

quantifiable SERS method utilizing the silver-coated filters. A linear relationship between the SERS signal and the concentration of amino acid was established. Calibration plots were generated from both quartz and glass filters. Large standard deviations were observed from the data collected for both filter types. These large deviations can be attributed to the difficulty in producing reproducible SERS measurements from multiple silver-coated filters at a given amino acid concentration. Two major factors have been identified that could cause variation in the SERS measurement. The first factor identified is the variation in surface features for each individual filter. Because these are fiber filters, the overall pore size is effectively uniform between filters but the surface features are significantly different at the microscale. This dissimilarity between the surface features of the silver films of different filters will cause variability in the SERS signal generated. The second factor leading to the large standard deviations involves slight variations in the data collection process. Before collecting each SERS spectrum, the laser had to be manually focused on the surface of the filter. The time it took to reach the proper focal point varied for each measurement. This meant that some filters were exposed to the laser for a longer period of time prior to taking the SERS measurement than others. This would result in variation in the SERS signal produced as already demonstrated. Both of these factors could be optimized by refining both the silver deposition and the SERS measurement process to generate a more reproducible SERS signal. Although these observed variations in the SERS measurements may suggest that more work is needed to produce a reliable quantitative method, the potential for quantification has been successfully demonstrated. The linearity of the SERS signal versus phenylalanine concentration obtained compares

well to similar quantitative SERS methods reported in the literature.[11-13,18, 77-85] The linear concentration range for each filter type was determined along with the limit of detection. The linear concentration range was different for both filter types. This observation demonstrated the ability to tune the linear concentration range of the analysis by changing the pore size of the filter used. It was shown that the linear concentration range was lower for filters with a smaller pore size.

The silver-coated filter SERS method presented here is a novel and promising method for biochemical analysis. The demonstrated ability to semi-quantitatively detect amino acids and differentiate mixtures of amino acids can be further extended to the detection of other biological molecules such as proteins, tumor markers, and glucose. The use of a FT-Raman instrument combined with this new SERS method allows for a method with both high sensitivity and selectivity. The increased sensitivity is a result of the high intensity signals generated from the SERS substrate. The increased selectivity is a result of the high spectral resolution of a FT instrument. The other advantages of a FT system are also realized: low background fluorescence, decreased laser induced thermal damage, ease of use, and availability. This method is relatively simple and requires no sample preparation prior to analysis. For these reasons, this new method would be a significant benefit to field of bioanalytical chemistry.

REFERENCES

1. G. J. Thomas, Jr., Annu. Rev. Bioph. Biom. **28**, 1 (1999).

2. S. P. Mulvaney and C. D. Keating, Anal. Chem. **72**, 145R (2000).

3. K. Kneipp, H. Kneipp, I. Itzkan, R. C. Dasari, and M. S. Feld, J. Phys-Condens. Mat. **14**, 597 (2002).

4. K. Kneipp, H. Kneipp, I. Itzkan, R. C. Dasari, and M. S. Feld, Chem. Rev. **99**, 2957 (1999).

5. K. Kneipp, H. Kneipp, I. Itzkan, R. C. Dasari, and M. S. Feld, Curr. Sci. India **77**, 7, 915 (1999).

6. G. Ullas, S. S. Nayak, K. Gopalakrishna, J. Jacob, J. Kurien, K. M. Pai, M. Vengal, M. Valiathan, R. J. Lakshmi, K. V. Krishna, K. Raghavendra, and V. B. Kartha, Curr. Sci. India **77**, 7, 908 (1999).

7. A. J. Berger, Y. Wang, and M. S. Feld, Appl. Optics **35**, 1, 209 (1996).

8. A. J. Berger, I. Itzkan, and M. S. Feld, Spectrochim. Acta A **53**, 287 (1997).

9. A. J. Berger, T. W. Koo, I. Itzkan, G. Horowitz, and M. S. Feld, Appl. Optics **38**, 13, 2916 (1999).

10. W. R. Premasiri, R. H. Clark, and M. E. Womble, Laser. Surg. Med. **28**, 330 (2001).

11. T. Wang, H. K. Chiang, H. Lu, and F. Peng, Opt. Quant. Electron. **37**, 1415 (2005).

12. R. Stosch, A. Henrion, D. Schiel, and B. Guttler, Anal. Chem. **77**, 7386 (2005).

13. C. L. Haynes, C. R. Yonzon, X. Zhang, and R. P. Van Duyne, J. Raman Spectrosc. **36**, 471 (2005).

14. X. Y. Xiao, S. G. Sun, J. L. Yao, Q. H. Wu, and Z. Q. Tian, Langmuir **18**, 6274 (2002).

15. X. Dou, Y. M. Jung, H. Yamamoto, S. Doi, and Y. Ozaki, Appl. Spectrosc. **53**, 133 (1999).

16. X. Dou, Y. M. Jung, Z. Cao, S. Doi, and Y. Ozaki, Appl. Spectrosc. **53**, 1440 (1999).

17. A. A. Ooka, K. A. Kuhar, N. Cho, and R. L. Garrell, Biospectroscopy **5**, 9 (1999).

18. S. E. J. Bell, J. N. Mackle, and N. M. S. Sirimuthu, Analyst **130**, 545 (2005).

19. T. Iliescu, D. Maniu, V. Chis, F. D. Irimie, Cs. Paizs, and M. Tosa, Chem. Phys. **310**, 189 (2005).

20. A. Singha, S. Dasgupta, and A. Roy, Biophys. Chem. **120**, 215 (2006).

21. C. V. Raman and K. S. Krishnan, Nature **121**, 501 (1928).

22. C. L. Stevenson and T. Vo-Dinh, "Signal Expressions in Raman Spectroscopy", in *Modern Techniques in Raman Spectroscopy*, J. J. Laserna, Ed. (John Wiley & Sons, Chichester, 1996), Chap. 1, p. 1-38.

23. M. J. Pelletier, "Introduction to Applied Raman Spectroscopy", in *Analytical Applications of Raman Spectroscopy*, M. J. Pelletier, Ed. (Blackwell Science, Oxford, 1999), Chap. 1, p. 1-44.

24. R. L. McCreery, "Instrumentation for Dispersive Raman Spectroscopy", in *Modern Techniques in Raman Spectroscopy*, J. J. Laserna, Ed. (John Wiley & Sons, Chichester, 1996), Chap. 2, p. 41-72.

25. M. C. Fletcher, A. Vivoni, M. M. Moore, J. Lui, J. Cladwell, S. M. Prokes, O. Glembocki, and C. M. Hosten, Surf. Sci. **602**, 1614 (2008).

26. M. V. Canamares and M. Leona, J. Raman Spectrosc. **38**, 1259 (2007).

27. E. Podstawka, A. Kudelski, P. Kafarski, and L. M. Proniewicz, Surf. Sci. **601**, 4586 (2007).

28. E. Podstawka, M. Swiatlowska, E. Borowiec, and L. M. Proniewicz, J. Raman Spectrosc. **38**, 356 (2007).

29. H. Bengter, C. Tengroth, and S. P. Jacobsson, J. Raman Spectrosc. **36**, 1015 (2005).

30. S. Lefrant, M. Baibarac, I. Baltog, C. Godon, J. Y. Mevellec, J. Wery, E. Faulques, L. Mihut, H. Aarab, and O. Chauvet, Synthetic Met. **155**, 666 (2005).

31. A. Rupérez and J. J. Laserna, "Surface-enhanced Raman Spectroscopy", in *Modern Techniques in Raman Spectroscopy*, J. J. Laserna, Ed. (John Wiley & Sons, Chichester, 1996), Chap. 6, p. 227-261.

32. M. Fleischmann, P. J. Hendra, and A. J. Mcquillan, Chem. Phys. Lett. **26**, 163 (1974).

33. A. M. Michaels, M. Nirmal, and L. E. Brus, J. Am. Chem. Soc. **121**, 9932 (1999).

34. S. R. Emory and S. Nie, Anal. Chem. **69**, 2631 (1997).

35. K. Kneipp, Y. Wang, H. Kneipp, I. Itzkan, R. R. Dasari, and M. S. Feld, Phys. Rev. Lett. **76**, 14, 2445 (1996).

36. T. Vo-Dinh, TRAC-Trend. Anal. Chem. **17**, 557 (1998).

37. B. Pergolese, M. Muniz-Miranda, and A. Bigotto, Chem. Phys. Lett. **438**, 290 (2007).

38. Y. Chen, C. Wang, Z. Ma, and Z. Su, Nanotechnology **18**, 325602 (2007).

39. W. Ma and Y. Feng, J. Nanopart. Res. **8**, 761 (2006).

40. Z. Niu and Y. Fang, J. Colloid Interf. Sci. **303**, 224 (2006).

41. Z. Luo and Y. Fang, J. Colloid Interf. Sci. **283**, 459 (2005).

42. Z. Pan, S. H. Morgan, A. Ueda, R. Mu, Y. Cui, M. Guo, A. Burger, and Y. Yeh, J. Raman Spectrosc. **36**, 1082 (2005).

43. P. Douglas, R. J. Stokes, D. Graham, and W. E. Smith, Analyst **133**, 791 (2008).

44. I. Chou, M. Benford, H. T. Beier, G. L. Cote, M. Wang, N. Jing, J. Kameoka, and T. A. Good, Nano Lett. **8**, 1729 (2008).

45. M. D. Porter, R. J. Lipert, L. M. Siperko, G. Wang, and R. Narayanan, Chem. Soc. Rev. **37**, 1001 (2008).

46. B. L. Mitchell, A. J. Patwardhan, S. M. Ngola, S. Chan, and N. Sundararajan, J. Raman Spectrosc. **39**, 380 (2008).

47. I. Pavel, E. McCarney, A. Elkhaled, A. Morrill, K. Plaxco, and M. Moskovits, J. Phys. Chem. C **112**, 4880 (2008).

48. X. M. Qian and S. M. Nie, Chem. Soc. Rev. **37**, 912 (2008).

49. J. Kneipp, H. Kneipp, and K. Kneipp, Chem. Soc. Rev. **37**, 1052 (2008).

50. D. Graham and K. Faulds, Chem. Soc. Rev. **37**, 1042 (2008).

51. C. D. McGuinness, A. M. Macmillan, J. Karolin, W. E. Smith, D. Graham, J. C. Pickup, and D. J. S. Birch, Analyst **132**, 633 (2007).

52. D. H. Murgida and P. Hildebrandt, Chem. Soc. Rev. **37**, 937 (2008).

53. G. Naja, P. Bouvrette, S. Hrapovic, and J. H. T. Luong, Analyst **132**, 679 (2007).

54. X. X. Han, H. Y. Jia, Y. F. Wang, Z. C. Lu, C. X. Wang, W. Q. Xu, B. Zhao, and Y. Ozaki, Anal. Chem. **80**, 2799 (2008).

55. N. Sundararajan, D. Mao, S. Chan, T. Koo, X. Su, L. Sun, J. Zhang, K. Sung, M. Yamakawa, P. R. Gafken, T. Randolph, D. McLerran, Z. Feng, A. A. Berlin, and M. B. Roth, Anal. Chem. **78**, 3543 (2006).

56. C. Johannessen and S. Abdali, Spectroscopy **21**, 143 (2007).

57. Y. Wang, H. Wei, B. Li, W. Ren, S. Guo, S. Dong, and E. Wang, Chem. Commun. **48**, 5220 (2007).

58. J. Moger, P. Gribbon, A. Sewing, and C. P. Winlove, Biochim. Biophys. Acta **1770**, 912 (2007).

59. K. N. Yu, S. Lee, J. Y. Han, H. Park, M. Woo, M. S. Noh, S. Hwang, J. Kwon, H. Jin, Y. Kim, P. J. Hergenrother, D. H. Jeong, Y. Lee, and M. Cho, Bioconjugate Chem. **18**, 1155 (2007).

60. T. Li, L. Guo, and Z. Wang, Biosens. Bioelectron. **23**, 1125 (2008).

61. B. J. Yakes, R. J. Lipert, J. P. Bannantine, and M. D. Porter, Clin. Vaccine Immunol. **15**, 235 (2008).

62. K. J. Jalkanen, V. W. Jurgensen, A. Claussen, A. Rahim, G. M. Jensen, R. C. Wade, F. Nardi, C. Jung, I. M. Degtyarenko, R. M. Nieminen, F. Herrmann, M. Knapp-Mohammady, T. A. Niehaus, K. Frimand, and S. Suhai, Int. J. Quantum Chem. **106**,1160 (2006).

63. S. K. Deb, B. Davis, G. M. Knudsen, R. Gudihal, D. Ben-Amotz, and V. J. Davisson, J. Am. Chem. Soc. **130**, 9624 (2008).

64. M. Feng and H. Tachikawa, J. Am. Chem. Soc. **130**, 7443 (2008).

65. G. V. P. Kumar, S. Shruthi, B. Vibha, A. A. Reddy, T. K. Kundu, and C. Narayana, J. Phys. Chem. C **111**, 4388 (2007).

66. G. V. P. Kumar, R. Selvi, A. H. Kishore, T. K. Kundu, and C. Narayana, J. Phys. Chem. B **112**, 6703 (2008).

67. M. Manimaran and N. R. Jana, J. Raman Spectrosc. **38**, 1326 (2007).

68. A. R. Bizzarri and S. Cannistraro, Nanomedicine-UK **3**, 306 (2007).

69. A. Kaminska, O. Inya-Agha, R. J. Forster, and T. E. Keyes, Phys. Chem. Chem. Phys. **10**, 4172 (2008).

70. F. H. Scholes, A. Bendavid, F. L. Glenn, M. Critchley, T. J. Davis, and B. A. Sexton, J. Raman Spectrosc. **39**, 673 (2008).

71. M. Li, Y. Cui, M. Gao, J. Luo, B. Ren, and Z. Tian, Anal. Chem. **80**, 5118 (2008).

72. S. Habuchi and J. Hofkens, Topics Appl. Phys. **103**, 297 (2006).

73. J. Wessel, J. Opt. Soc. Am. B **2**, 1538 (1985).

74. G. J. Puppels, F. F. M. de Mul, C. Otto, J. Greve, M. Robert-Nicoud, D. J. Arndt-Jovin, and T. M. Jovin, Nature **347**, 301 (1990).

75. R. Diller, S. Maiti, G. C. Walker, B. R. Cowen, R. Pippenger, R. A. Bogomolni, and R. M. Hochstrasser, Chem. Phys. Lett. **241**, 109 (1995).

76. Y. C. Cao, R. Jin, and C. A. Mirkin, Science **297**, 1536 (2002).

77. A. C. Peacock, A. Amezcua-Correa, J. Yang, P. J. A. Sazio, and S. M. Howdle, Appl. Phys. Lett. **92**, 141113 (2008).

78. G. Sabatte, R. Keir, M. Lawlor, M. Black, D. Graham, and W. E. Smith, Anal. Chem. **80**, 2351 (2008).

79. S. E. J. Bell and N. M. S. Sirimuthu, Chem. Soc. Rev. **37**, 1012 (2008).

80. K. R. Ackermann, T. Henkel, and J. Popp, ChemPhysChem **8**, 2665 (2007).

81. J. Moger, P. Gribbon, A. Sewing, and C. P. Winlove, BBA-Gen. Subjects **1770**, 912 (2007).

82. D. Cunningham, R. E. Littleford, W. E. Smith, P. J. Lundahl, I. Khan, D. W. McComb, D. Graham, and N. Laforest, Faraday Discuss. **132**, 135 (2006).

83. J. Jung, J. Choo, D. J. Kim, and S. Lee, B. Kor. Chem. Soc. **27**, 277 (2006).

84. M. Sackmann and A. Materny, J. Raman Spectrosc. **37**, 305 (2006).

85. D. Zhang, Y. Xie, S. K. Deb, V. J. Davison, and D. Ben-Amotz, Anal. Chem. **77**, 3563 (2005).

86. P. C. Lee and D. Meissel, J. Phys. Chem. **86**, 3391 (1982).

87. J. Neddersen, G. Chumanov, and T. M. Cotton, Appl. Spectrosc. **47**, 1959 (1993).

88. F. Mafuné, J. Kohno, Y. Takeda, and T. Kondow, J. Phys. Chem. B **104**, 9111 (2000).

89. F. Mafuné, J. Kohno, Y. Takeda, and T. Kondow, J. Phys. Chem. B **105**, 5114 (2001).

90. F. Mafuné, J. Kohno, Y. Takeda, and T. Kondow, J. Phys. Chem. B **104**, 8333 (2000).

91. Y. Saito, J. J. Wang, D. A. Smith, and D. N. Batchelder, Langmuir **18**, 8, 2959 (2002).

92. D. L. Jeanmaire and R. P. Van Duyne, J. Electroanal. Chem. **84**, 1 (1977).

93. J. A. Creighton, Surf. Sci. **173**, 665 (1986).

94. L. L. Thomas, J. Kim, and T. M. Cotton, J. Am. Chem. Soc. **112**, 9378 (1990).

95. P. Cao, R. Gu, and Z. Tian, J. Phys. Chem. B **107**, 769 (2003).

96. A. Vivoni, S. P. Chen, D. Ejeh, and C. M. Hosten, Langmuir **16**, 3310 (2000).

97. D. D. Tuschel, J. E. Pemberton, and J. E. Cook, Langmuir **2**, 380 (1986).

98. S. Sanchez-Cortez, R. M. Berenguel, A. Madejón, and M. Pérez-Méndez, Biomacromolecules **3**, 655 (2002).

99. C. Zuo and P. W. Jagodzinski, J. Phys. Chem. B **109**, 1788 (2005).

100. E. Podstawka, Y. Ozaki, and L. M. Proniewicz, Appl. Spectrosc. **58**, 570 (2004).

101. W. B. Fischer and H. H. Eysel, Spectrochim. Acta **48A**, 725 (1992).

102. B. Limberg and B. Kommerell, Gut **25**, 1291 (1984).

VITA

ROBERT BUTLER JEFFERS

Department of Chemistry and Biochemistry
Old Dominion University
4541 Hampton Boulevard
Norfolk, VA 23529-0126
Phone: (757) 451-5250
E-mail: rbjeffers@gmail.com

EDUCATION:

1999 ~ Present	OLD DOMINION UNIVERSITY Ph.D. – Chemistry	Norfolk, VA, USA
1997 ~ 99	COLLEGE OF WILLIAM AND MARY Bachelor of Science – Chemistry	Williamsburg, VA, USA
1995 ~ 97	OLD DOMINION UNIVERSITY Bachelor of Science – Chemistry	Norfolk, VA, USA

PUBLICATIONS:

Size and Temperature Dependence of Surface Plasmon Absorption of Gold Nanoparticles Induced by Tris(2,2'-bipyridine)ruthenium(II)
The Journal of Physical Chemistry B, 108 (40): 15543, 2004

Direct measurement of sizes and dynamics of single living membrane transporters using nanooptics
Nano Letters, 2 (3): 175, 2002

Novel solution phase immunoassays for molecular analysis of tumor markers
The Analyst, 126: 1285, 2001

PRESENTATIONS:

Novel Ultrasensitive Solution-Phase Immunoassay of Tumor Markers in Serum Samples Using Electrochemiluminescence
– Oral Presentation at the Pittsburgh Conference meeting in New Orleans, LA – 2001

Biomedical Applications of Nanoparticle Probes
– Oral Presentation at the Pittsburgh Conference meeting in New Orleans, LA – 2001